

Contract NAS8-5046

ANALYTICAL AND EXPERIMENTAL DETERMINATION
OF LIQUID HYDROGEN TEMPERATURE
STRATIFICATION, FINAL REPORT


April 1963

Prepared for George C. Marshal
Space Flight Center
(Control No. TP 2-83504)

Authors

T. Bailey	D. Pedreya
D. Covington	T. Perehoduk
R. Fearn	H. Richards
H. Merrill	

Approved


E. A. Mossman, Manager,
Propulsion Laboratory

MARTIN COMPANY
Denver, Colorado

Aerospace Division of Martin-Marietta Corporation

FOREWORD

This document is submitted under Contract NAS8-5046, Control No. TP 2-83504, Article I.D.3. NASA letter 3-W-07552 (Martin number) indicates approval of preliminary draft of subject document.

CONTENTS

	<u>Page</u>
Foreword	ii
Contents	iii thru viii
Summary	ix
I. Introduction	1
II. Test Equipment and Instrumentation	3
A. Test Equipment	3
B. Instrumentation	7
III. Test Program	36
IV. Test Procedures	39
A. Pretest Checkout	39
B. Purge and Fill	39
C. Instrumentation Calibrations	40
D. Stratification Tests	41
E. Shake Procedure	42
F. Outflow Procedure	42
G. Heat Leak Calibration	43
H. Heat Chamber Calibration	43
V. Test Results	44
A. Data Reduction Methods	44
B. Interpretation of Data	45

VI.	Analytical Model	100
	A. Nomenclature	100
	B. Analytical Model Derivation	103
	C. Description of IBM 1620 Computer Program	107
	D. Comparison of Analytical Model with Test Data	110
VII.	Conclusions	114
	References	115
	Appendix IBM 1620 Digital Computer Program	A-1 thru A-8

Distribution

Figure

1	System Schematic, Mod B	10
2	Inner Tank Lower Dome	11
3	Outer Tank Lower Dome	12
4	Inner Tank	13
5	Test Vessel, Top Dome Removed	14
6	Assembled Test Vessel	15
7	Outer Tank Barrel Section	16
8	Heat Chamber Section	17
9	Vent and Flow Section	18
10	Vacuum Pump and Pressurization Systems	19
11	Pressurization and Vent Lines	20
12	Vent Valve Tree	21
13	LH ₂ and LN ₂ Dewars during Test	22

14	Fill, Throttling, and Dump System	23
15	Inner Tank, View through Manhole	24
16	Hydraulic Actuator	25
17	Liquid Hydrogen Data System Flow Diagram . .	26
18	Control Room during Test	27
19	Thermocouple Locations	28
20	Radial Locations of Thermistors and Thermo- couples	29
21	Thermistors and Thermocouples on Rake No. 1 .	30
22	Instrumentation Rakes Assembly	31
23	Gas Temperature Schematic	32
24	Thermistor Locations	33
25	Thermistor Temperature Schematic	34
26	Tank Wall Temperature Schematic	35
27	Vapor Pressure Curve for Parahydrogen	50
28	Typical Thermistor Calibration Records . . .	51
29	Typical Thermistor Calibration Curves	52
30	Typical Thermistor Oscillograph Record . . .	53
31	Typical Thermistor Recordings during Shake and Outflow	54
32 thru 57	Stratification Temperature Profiles for Var- ious Tests	
32	Test No. 1	55
33	Test No. 1A	56
34	Test No. 2	57

35	Test No. 3	58
36	Test No. 4	59
37	Test No. 5	60
38	Test No. 6	61
39	Test No. 7	62
40	Test No. 8	63
41	Test No. 9	64
42	Test No. 10	65
43	Test No. 10A	66
44	Test No. 11	67
45	Test No. 12	68
46	Test No. 13	69
47	Test No. 14	70
48	Test No. 15	71
49	Test No. 16	72
50	Test No. 17	73
51	Test No. 22	74
52	Test No. 23	75
53	Test No. 24	76
54	Test No. 25	77
55	Test No. E	78
56	Test No. 18, Outflow	79
57	Test No. 19, Outflow	80

58 thru 61	Outflow Thermistor Temperature for Various Tests	
58	Test No. 18	81
59	Test No. 19	82
60	Test No. 20	83
61	Test No. 21	84
62 thru 65	Tank Top Pressure for Various Tests	
62	Test No. 18	85
63	Test No. 19	86
64	Test No. 20	87
65	Test No. 21	88
66 thru 69	Ullage Gas Temperature Profiles for Various Tests	
66	Test No. 18	89
67	Test No. 19	90
68	Test No. 20	91
69	Test No. 21	92
70 thru 73	Liquid Outflow Rate for Various Tests	
70	Test No. 18	93
71	Test No. 19	94
72	Test No. 20	95
73	Test No. 21	96
74	Two-Layer Model	97
75	Heat Flux vs Time for Different Heat Chamber Connections	98

76	Density of Hydrogen and Specific Heat of Parahydrogen vs Temperature	99
----	---	----

Table

1	Electrical System Characteristics	5
2	Revised Test Plan	38

SUMMARY

This report describes the work performed in accordance with Marshall Space Flight Center (MSFC) Contract NAS8-5046 for the analytical and experimental determination of liquid hydrogen temperature stratification in pressurized tanks subjected to heat input along the vertical portions of the tank wall. A total of 28 tests were performed in an 4-ft diameter vacuum-jacketed test vessel of 70 cu ft capacity. During these tests heat flux values ranged from 0.2 to 0.9 Btu/sq ft-sec, and pressures ranged from 24 to 72 psia. Many of the tests were performed with oscillation of the tank at frequencies ranging from 0.5 to 15 cps, including the fundamental sloshing frequency. Four of the tests were performed with liquid outflow either subsequent to or during the heating period. Liquid temperatures were continuously measured throughout each test at a sufficient number of points distributed within the tank to obtain an adequate description of the temperature stratification profiles.

This report describes in detail the test vessel and its associated subsystems, the instrumentation used, the test procedures followed, and the data reduction methods. Graphs are presented of the measured temperature stratification profiles for several times during each test. In addition, some pressurization data are presented for the outflow tests. Finally, an analytical model, which was previously developed and applied successfully to lox and liquid nitrogen data, is described and compared with the test data.

The results of the tests show a pronounced stratification tendency. The agreement with the analytical model was quite good in some tests, but not in others; there is no apparent reason for this inconsistency.

I. INTRODUCTION

One of the primary purposes of a flight vehicle propellant pressurization system is to supply propellant to the engine at the required pressure. For a pump-fed engine, the pressure required is generally that necessary to suppress cavitation in the pump. This pressure is usually specified in terms of a minimum net positive suction head (NPSH) value, which is the difference between total pressure and vapor pressure at the pump inlet.

In the case of cryogenic propellants, vapor pressure is usually a significant portion of the total pressure. Furthermore, aerodynamic heating during flight often results in a considerable increase in vapor pressure. Experience has shown that this vapor pressure increase is not uniform, but has a strong tendency toward stratification. The upper propellant layers show a large increase in vapor pressure and the lower layers show little or no increase. Therefore, the system operating pressure is often determined by the NPSH requirement at stage burnout when the warmest propellant is being consumed. Since both tank structural weight and pressurization system weight are sensitive to design pressure, it is important to be able to predict in the design phase the degree of stratification and the resultant vapor pressure distribution of the propellant.

During the development of Titan I, considerable effort was devoted to the problem of predicting stratification in the lox tanks during flight. An experimental program was conducted, using liquid nitrogen in a full-scale Titan Stage II lox tank, with infrared lamps to simulate aerodynamic heating. Concurrently, an analytical model was developed. Good agreement between the test data and the model encouraged further refinement of the model, which was then used in Titan design studies. A description of the analytical model together with the liquid nitrogen experimental data plus some Titan and Vanguard flight test data, are presented in Ref 1.

A small test vessel 2 ft in diameter was used in the first attempt to obtain experimental stratification data with liquid hydrogen. Although definite similarities to the lox-liquid nitrogen data and to the analytical model were observed, a large and uncontrolled heat leak in the test vessel made the results difficult to interpret quantitatively. A brief description of this program and some of the data obtained are presented in Ref 2.

The liquid hydrogen stratification test program described in this report was undertaken to overcome the deficiencies of the first experimental effort, to provide data from a larger size test vessel, and to investigate the effects of liquid oscillation and sloshing on the stratification phenomenon.

II. TEST EQUIPMENT AND INSTRUMENTATION

This chapter describes the test equipment and instrumentation used in the stratification test program.

A. TEST EQUIPMENT

The stratification test program was conducted at the Martin-Denver Hydrogen Research Laboratory. A 60 cu ft vacuum-jacketed test vessel was designed specifically for liquid hydrogen propellant feed and pressurization system tests. The test vessel was equipped with subsystems (shown schematically in Fig. 1) to provide capabilities for:

- 1) Purging;
- 2) Fill and drain;
- 3) Pressurization with either helium or hydrogen gas to 150 psig;
- 4) Throttled venting;
- 5) Wall heating rates to 0.8 Btu/sq ft-sec;
- 6) Controlled shake to 15 cps.

1. Test Vessel

The test vessel has a 4-ft diameter stainless steel inner tank with standard ASME domes, and a 63-in. barrel section (Ref Drawing 1049, Cryogenic Engineering Co., Denver, Colorado). The tank is designed to withstand working pressures of 150 psig at liquid hydrogen temperatures. The liquid enters and leaves the tank from the bottom, which has a cross-shaped vortex suppressor baffle as shown in Fig. 2.

The inner tank is supported vertically by four legs (Fig. 3), and horizontally by tie rods connected to the upper and lower domes, as shown in Fig. 4. These supports are designed to provide a long heat path to minimize heat leak, and to withstand $2\frac{1}{2}$ g of horizontal acceleration.

A 14-in. manhole provides access to the inner tank (Fig. 4 and 5). This manhole is sealed by compressing a 0.010-in. thick Mylar gasket between the two flanges, one of which has a slight serration on it.

Both domes of the inner tank are covered with a 1 in. thickness of multilayer insulation to shield against radiation from the outer tank.

The outer tank, shown in Fig. 6, is 6 ft in diameter. This tank provides a 1-ft vacuum annulus around the inner tank. This tank has standard ASME domes connected to the barrel section by flanged connections (Fig. 7). An O-ring provides the vacuum seal between the domes and barrel. There are four 1-ft diameter access ports equally spaced around the barrel midsection. These ports provide access for wiring the heat chambers to the external feedthroughs. There are O-ring seals around all the access ports.

2. Heat Chamber

Heat is applied to the inner tank by radiation from 1000 watt General Electric infrared T-3 quartz lamps. These lamps are mounted vertically in four rows around the tank. For improved efficiency, the lamps are mounted within an electrolytically polished aluminum heat chamber of very low emissivity. One quadrant of the lamps is shown in Fig. 8. The lamps are supported by copper bus bars attached to the aluminum by ceramic standoffs. These bus bars also supply current to the lamps, and are arranged to allow several circuit configurations for different heating rates, as required. Baffles on the top and bottom of each quadrant minimize the heat leak from the ends of the chamber, and improve the uniformity of heat flux to the tank wall.

3. Electrical Power

Power to the heat lamps is supplied from a remotely located 480-volt 3-phase substation (Fig. 9). Current is fed to the heat lamps through hermetically sealed ceramic feedthroughs in the outer tank wall. The heat flux applied to the inner tank can be varied from test to test by wiring the lamps with either 4, 6, 8, 10, 12, or 16, in series across the 480-volt lines. The approximate electrical power consumption associated with each of these wiring configurations is shown in Table 1. The values in the table are based on a total of 304 lamps, and an assumed constant voltage of 480.

Table 1 Electrical System Characteristics

Wiring Configuration		Voltage/ Lamp	Amp/ Lamp	KW/ Lamp	Total KW	Total Q Btu/sec
Designation	Lamps in Series					
A	4	120	3.1	0.35	108	102
B	6	80	2.6	0.21	66	63
C	8	60	2.2	0.14	44	42
	10	48	2.0	0.08	25	24
D	12	40	1.7	0.07	21	20
E	16	30	1.6	0.06	18	17

4. Vacuum System

The space between the inner and outer tanks is evacuated with a Kinney KS-47 roughing pump, through a $1\frac{1}{2}$ -in. line (Fig. 10). Because of the location of the test vessel in a pit, the vacuum pump had to be placed about 20 ft from the tank, which prevented the pump from operating at maximum efficiency. When the test vessel is warm, it cannot be readily pumped down to a pressure less than about $5(10)^{-2}$ mm Hg. When liquid hydrogen is admitted to the tank, however, cryopumping action will reduce the pressure to approximately $2(10)^{-5}$ mm Hg in about 15 min. Getter bags, containing activated charcoal, are wrapped around the inner tank just above and below the heated zone to absorb residual gases, which may be outgassed during extended heating runs.

5. Purging Provisions

The purging operations that precede each series of tests extract all oxygen and condensable gases from the test vessel. The system is sweep purged, first with nitrogen, and then with hydrogen gas. The purge gas enters the liquid transfer line and goes in through the bottom of the tank and out through the vent line. The instrumentation feedthrough line and the power and instrumentation junction boxes are also purged with nitrogen gas to assure a non-explosive atmosphere. Purge gas is fed through a valve manifold located in the corner of the test cell.

The test vessel is vented through a 2-in. aluminum line (Fig. 11) that runs to the valve tree (Fig. 12), and then into the facility vent system that exhausts the gas to the atmosphere through a 40-ft vent stack. The valve tree consists of a 2-in. vent valve that is used during fill and fast venting, a Domotor throttling valve that permits throttling of the vent gas to control the rate of venting, and a 2-in. burst disk which is set for 175 psig. The facility vent system has a 6-in. main shutoff valve in parallel with a 2-in. flow measuring section containing another shutoff valve, as shown in Fig. 9. The flow measuring section can be equipped with different sized sharp-edged orifices for measuring vent gas flowrate. The entire vent system is continuously purged with nitrogen gas whenever there is liquid hydrogen in the test vessel. A flapper valve on top of the vent stack maintains about 1 psig backpressure in the system, thus preventing any air from being drawn into the system.

6. Fill and Drain System

The test vessel is filled through 2-in. vacuum-jacketed transfer lines. The fill line enters the bottom of the tank through a 4-ft section of flex hose that is a permanent part of the test vessel. The remainder of the transfer line is connected together by bayonet-type fittings. The liquid nitrogen which is used for precooling and checkout is supplied from a 600-gal. dewar, and the liquid hydrogen is supplied from a 1500-gal. dewar. Both dewars are shown in Fig. 13.

The three valves shown in Fig. 14 control the liquid flow. The fill and dump valves are remotely controlled, and the throttling valve is manually operated. The dump valve is only used in case of an emergency dump, when there would be insufficient time to back-transfer the liquid into the storage dewar. The fill valve has the capability of remote filling of the test vessel. However, this valve has not been used because manual control of the fill operation is satisfactory.

7. Pressurization System

The pressurization system provides either hydrogen or helium as the pressurizing gas. The gas may be admitted into the test vessel either through a straight pipe or through the diffuser screen shown in Fig. 15. The hydrogen gas is supplied from a cascade trailer, the helium gas from a manifold of six K-bottles. The other system components, shown in Fig. 10, include a two-way high-pressure selector valve for selecting either helium or hydrogen gas, a servodome regulator for controlling the flow metering

nozzle upstream pressure, a 5 cu ft accumulator that smooths out pressure fluctuations downstream of the regulator, a main shutoff valve, and a flow metering nozzle that controls the rate of gas flow. Five nozzles ranging from 0.05- to 0.25-in. throat diameter are available for installation, depending on the rate of flow anticipated.

8. Shaker System

The shaker system has the capability of oscillating the tank back and forth about a pivot point at a maximum rate of 15 cps and a maximum double amplitude of $1\frac{1}{2}$ in. The test vessel is mounted on a platform connected to the base fixture through two pivot pins. The base fixture is imbedded in a block of concrete of sufficient mass to absorb any reaction loads resulting from the oscillation of the test vessel.

A Moog Model 1725 hydraulic servoactuator pin connected between the base fixture and a grip-ring on the test vessel (Fig. 16), is used to oscillate the tank back and forth. Pressure to operate the actuator is supplied through hoses from a hydraulic pumping unit located away from the test vessel.

The amplitude and frequency of the actuator are controlled by a Hewlett-Packard Model 202A low-frequency function generator. The output of this function generator is fed into a magnetic servoamplifier, which in turn drives the hydraulic actuator.

B. INSTRUMENTATION

The instrumentation system at the Hydrogen Research Laboratory, shown schematically in Fig. 17, was designed to accurately handle the requirements of a variety of test programs to be conducted in the test cells. All data channels are brought into the main control center patch system, which provides maximum flexibility of equipment selection. The control center, shown in Fig. 18, is used for remote control operation, signal conditioning, and data recording for all tests.

1. Temperature Measurement

Gas Temperatures - The test vessel contains 24 thermocouples, located as shown in Fig. 19 and 20 for measuring ullage gas temperatures. These thermocouples are made of 30-gage copper-constantan thermocouple wire, and are supported in 1/8-inch diameter stainless steel tubes attached to the instrumentation rakes as shown in Fig. 21 and 22. The measuring junction extends approximately 1/8 in. beyond the end of the supporting tube. An ice bath is used for the reference junctions, with continuous lengths of thermocouple wire between each measuring junction and its reference junction. A schematic diagram of the thermocouple circuit is shown in Fig. 23.

Tank Wall Temperatures - Ten tank wall temperature measurements are provided by 36-gage iron-constantan thermocouples, located as shown in Fig. 19. Each wire of a thermocouple pair is individually spot welded to the tank wall. The reference junctions are located in an external liquid hydrogen bath. A schematic of this thermocouple circuit is shown in Fig. 26. Because of the low signal level of this measurement (50 μ v. for full-scale deflection), it was necessary to filter the amplifier output to reduce the noise level.

Liquid Temperatures - Seventy-two thermistors (Keystone Carbon Company Model L0904), located as shown in Fig. 20 and 24, measure liquid temperatures in the test vessel. The thermistors are supported by two-hole ceramic tubes attached to the instrumentation rakes as shown in Fig. 21 and 22. Two 24-gage Teflon-insulated wires are connected to each thermistor and brought out of the test vessel through hermetically sealed plugs. Figure 25 is a schematic of the thermistor bridge used for these measurements. Each of these bridges has its own voltage source -- Microdot Model PB-290 adjustable power supplies. The supply voltage was chosen to provide adequate sensitivity, and yet minimize the thermistor self-heating error. The 1.5-volt value chosen provides an overall sensitivity of approximately 0.2 in. of galvanometer deflection per degree Rankine, with a self-heating error of less than 0.05°R. The calibration stability of this circuit is directly proportional to the stability of the power supply voltage. For the Microdot units used, this stability is within $\pm 0.05\%$.

2. Liquid Level

The liquid hydrogen liquid level for all the tests is monitored by a differential pressure slant tube manometer. Copper tubing of 1/4 in. diameter connects the top and bottom of the test vessel to the manometer located in the control room. Unity oil (specific gravity of 1) is used as the fluid in the manometer. The manometer can be read with a precision of 0.01 in. water. For some tests, thermistor point level sensors were used to establish calibration points for the manometer liquid level gage. Although there are some uncertainties in the use of a differential pressure liquid level measurement, it is estimated that these data are reliable to $\pm 1/2$ in., which is adequate for the purposes of this study.

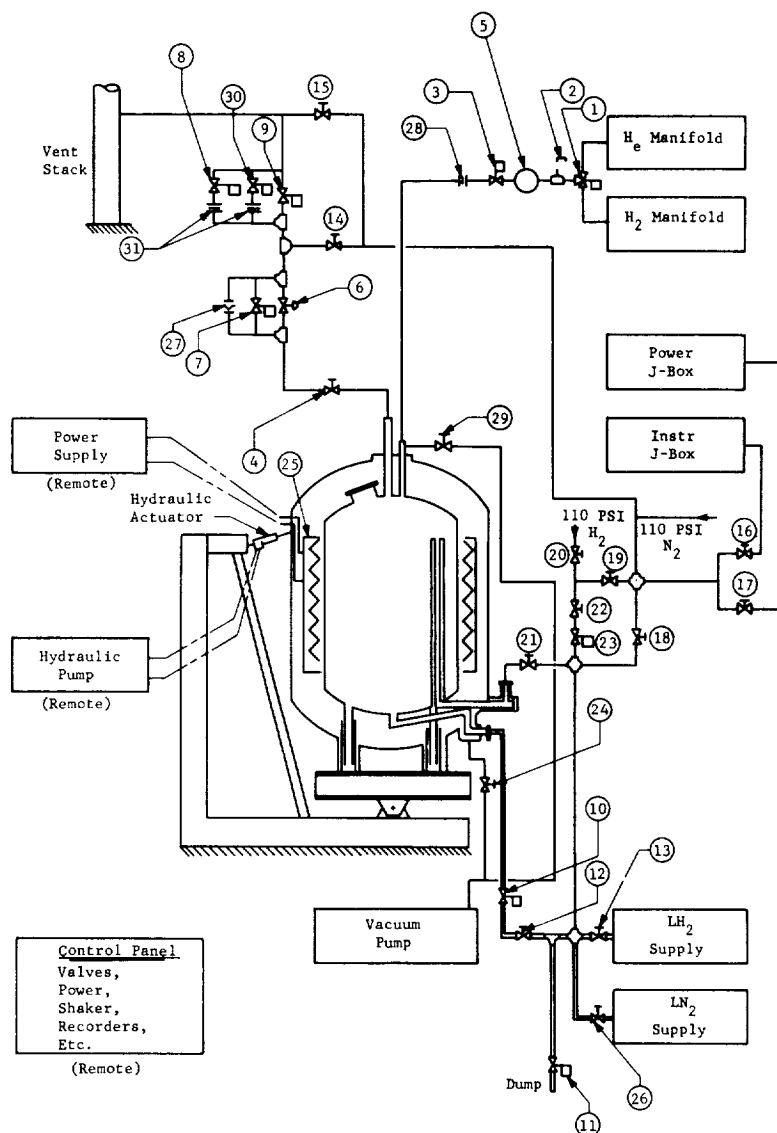
3. Pressures

All test pressure measurements are made with Statham pressure transducers. The combined error due to nonlinearity and hysteresis is less than $\pm 1.0\%$.

4. Voltage and Current

Current - The total heat lamp current is measured by Weston Model 461 current transformers installed in each power line. The secondary of each of these transformers is connected to a Weston rectifier-converter that provides a 0 to 50 mv dc signal to Bristol strip chart recorders.

Voltage - A stepdown voltage transformer and full-wave rectifier are connected across each power phase to provide a dc input to a Bristol stripchart recorder. Only one such voltage, selected by means of a manually operated switch, is recorded at a time.



- | | |
|---|---|
| 1. He - H ₂ pressurization gas selector valve (remote) | 17. Gaseous nitrogen purge valve for power J-box |
| 2. Pressure regulator (remote) | 18. Bypass valve for gaseous nitrogen purge |
| 3. Pressurization shut-off valve (remote) | 19. Block off valve between N ₂ and H ₂ purge systems |
| 4. 2" manual vent valve | 20. Shut-off valve for H ₂ gaseous purge |
| 5. Accumulator | 21. Gaseous purge line to instrumentation feedthrough |
| 6. 2" Vent throttling valve (remote) | 22. Control valve for gaseous purge through tank |
| 7. Emergency vent and cool down valve (remote) | 23. Solenoid valve for emergency purging with N ₂ gas |
| 8. 2" Vent flow section shut-off valve (remote) | 24. Vacuum shut-off valve on tank |
| 9. Vent gas flow section bypass valve (remote) | 25. Heat chambers |
| 10. Liquid fill valve (remote) | 26. LN ₂ Dewar transfer valve |
| 11. Liquid dump valve (remote) | 27. Vent line burst disk |
| 12. Dump throttling valve (manual) | 28. Pressurization gas flow orifice |
| 13. LH ₂ Dewar transfer valve (manual) | 29. Shut-off valve for vacuum purge on inner tank |
| 14. Vent line purge valve for nitrogen gas | 30. 1/2" vent flow section shut-off valve (remote) |
| 15. Vent stack purge valve for nitrogen gas | 31. Vent flow section orifices |
| 16. Gaseous nitrogen purge valve for instrumentation J-box | |

Fig. 1 System Schematic, Mod B



Fig. 2 Inner Tank Lower Dome



Fig. 3 Outer Tank Lower Dome

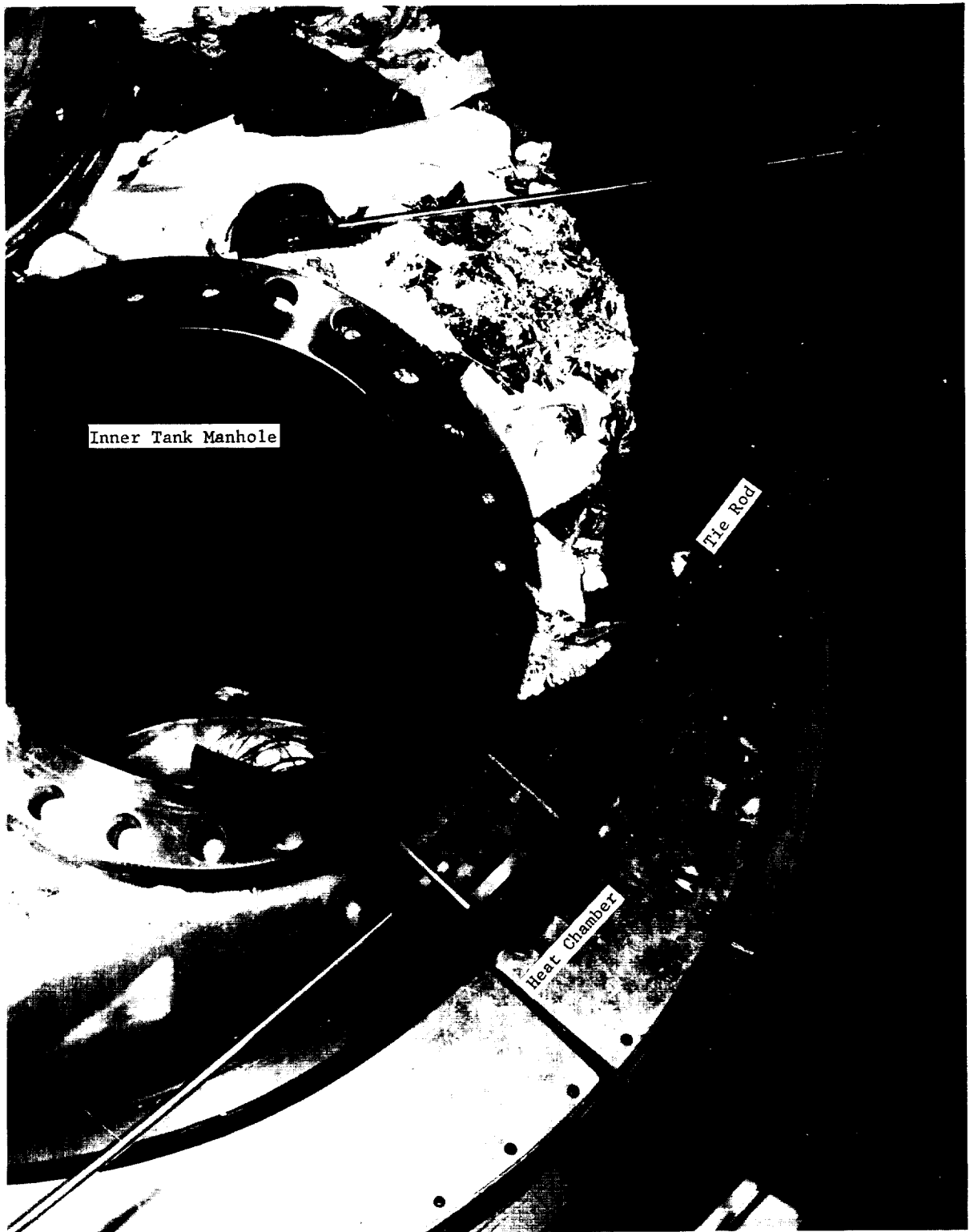


Fig. 4 Inner Tank

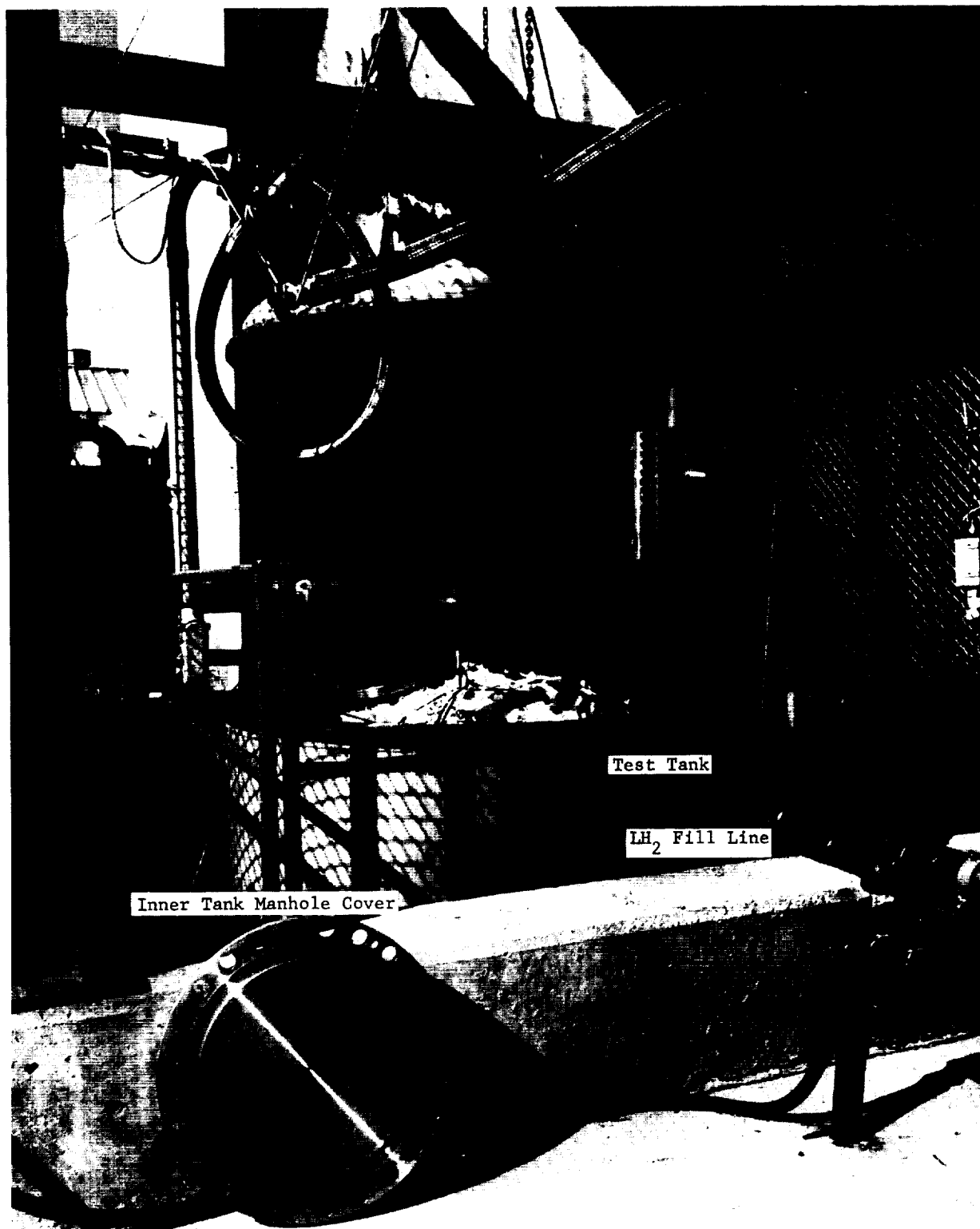


Fig. 5 Test Vessel, Top Dome Removed



Fig. 6 Assembled Test Vessel



Fig. 7 Outer Tank Barrel Section

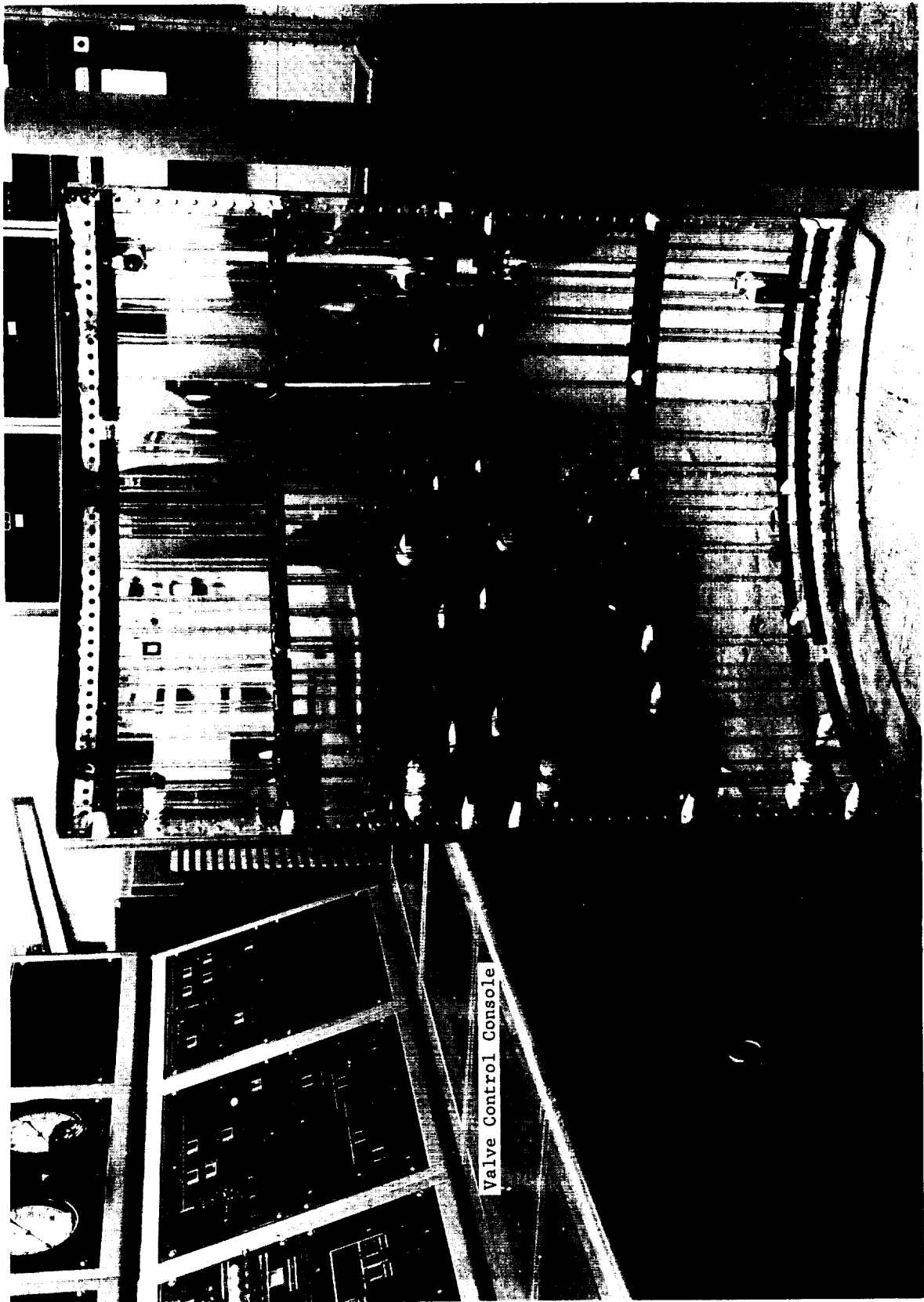


Fig. 8 Heat Chamber Section



Fig. 9 Vent and Flow Section

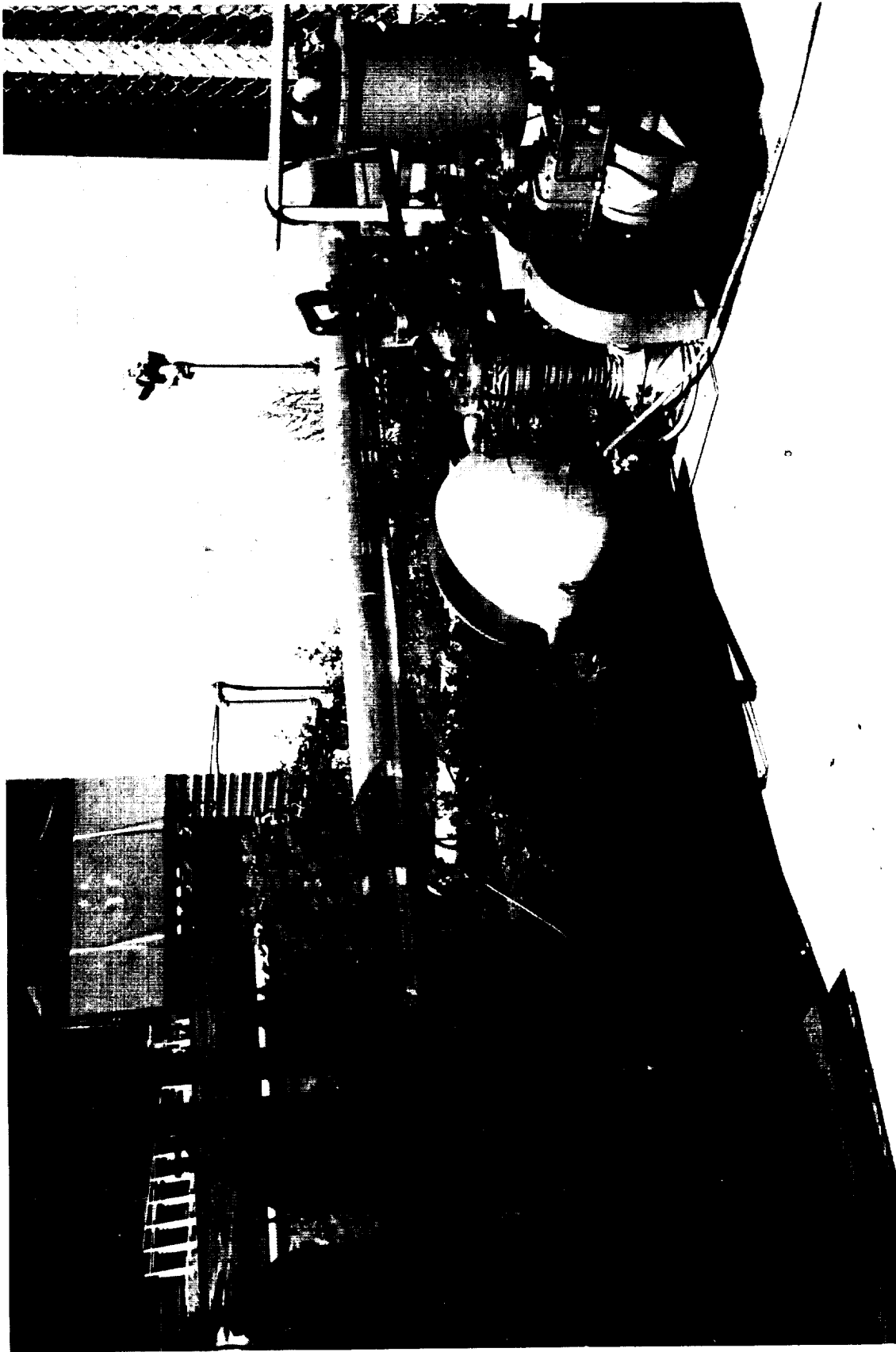


Fig. 10 Vacuum Pump and Pressurization System

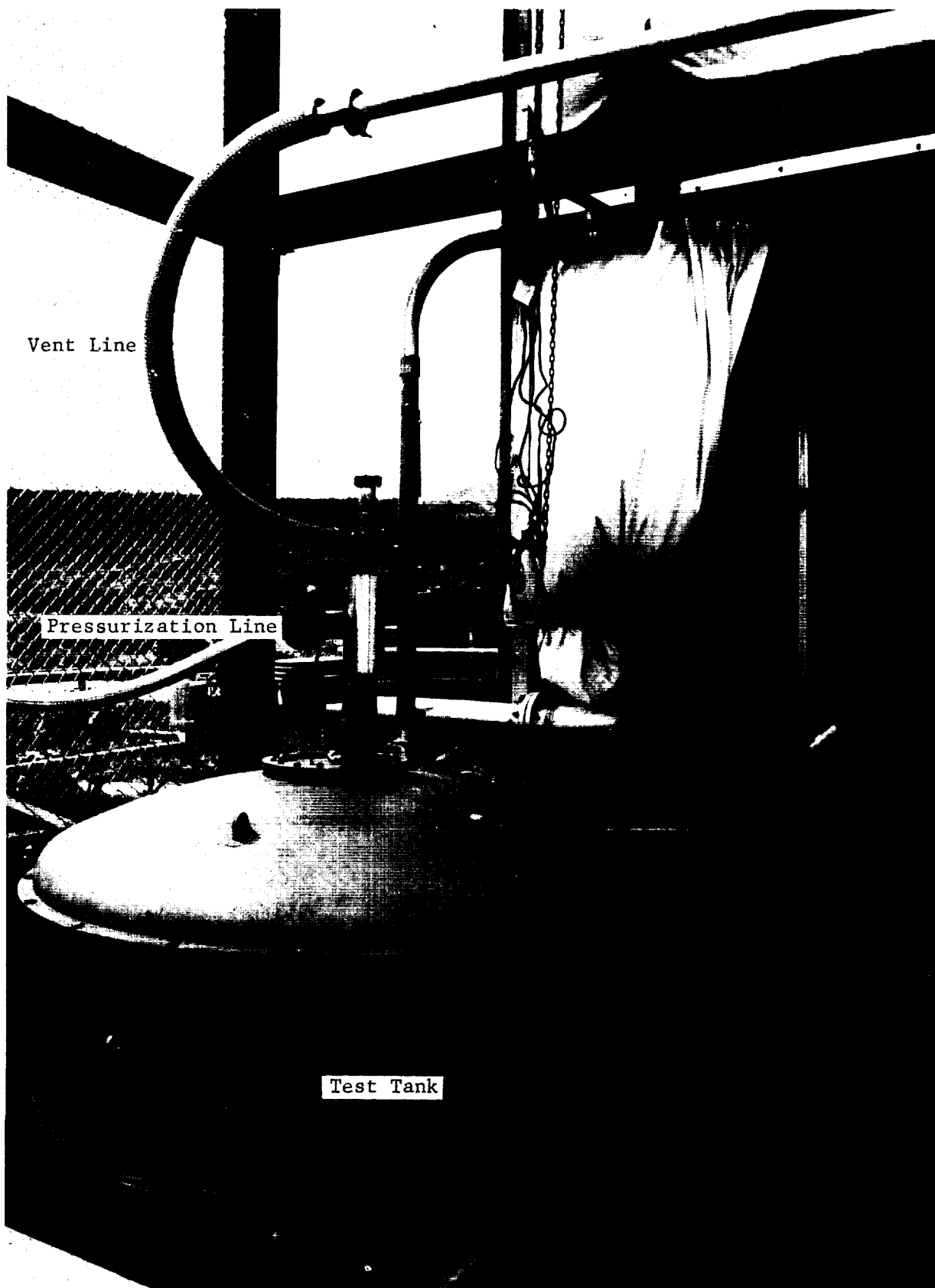


Fig. 11 Pressurization and Vent Lines



Fig. 12 Vent Valve Tree



Fig. 13 LH₂ and LN₂ Dewars during Test

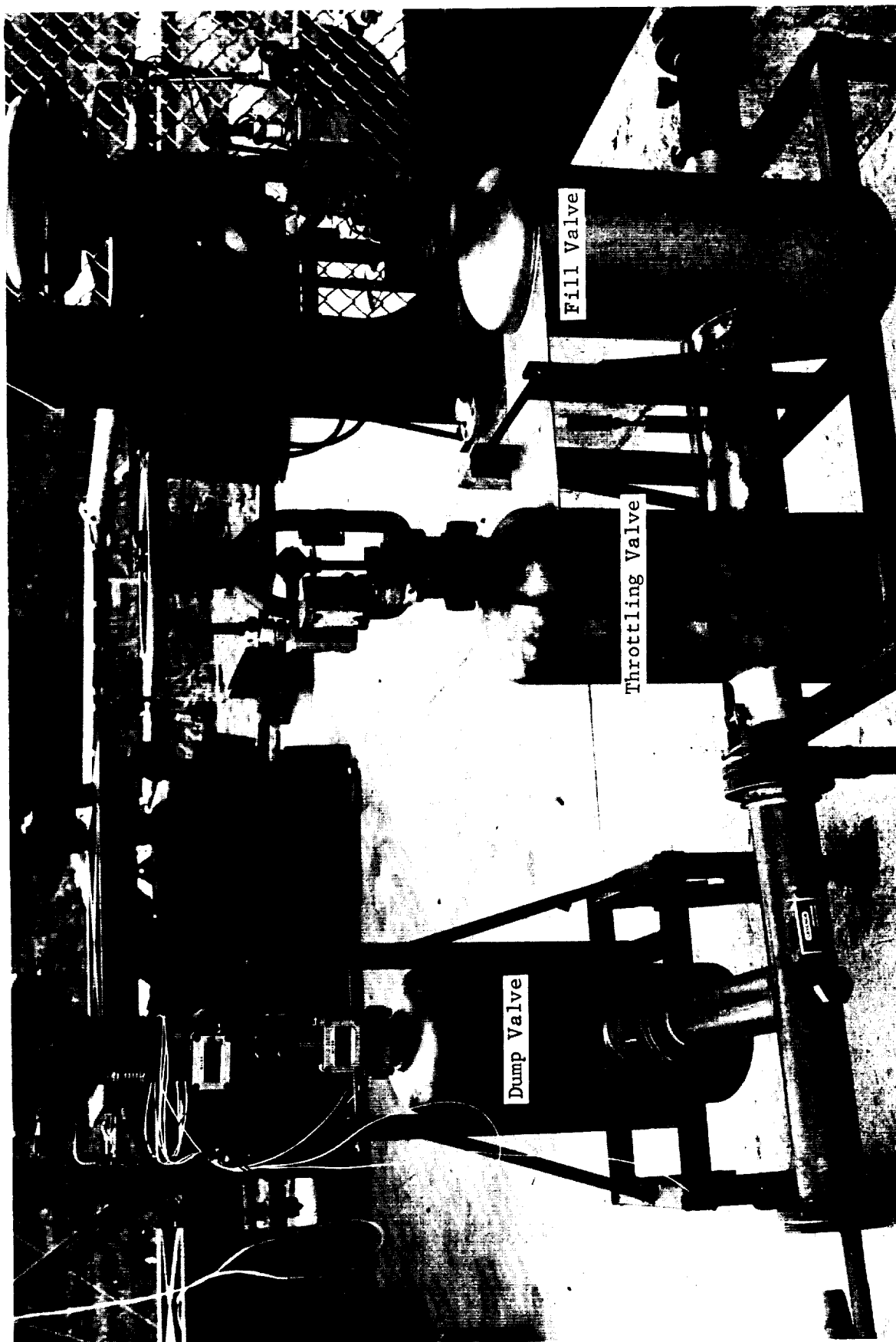


Fig. 14 Fill, Throttling, and Dump System



Fig. 15 Inner Tank, View through Manhole



Fig. 16 Hydraulic Actuator

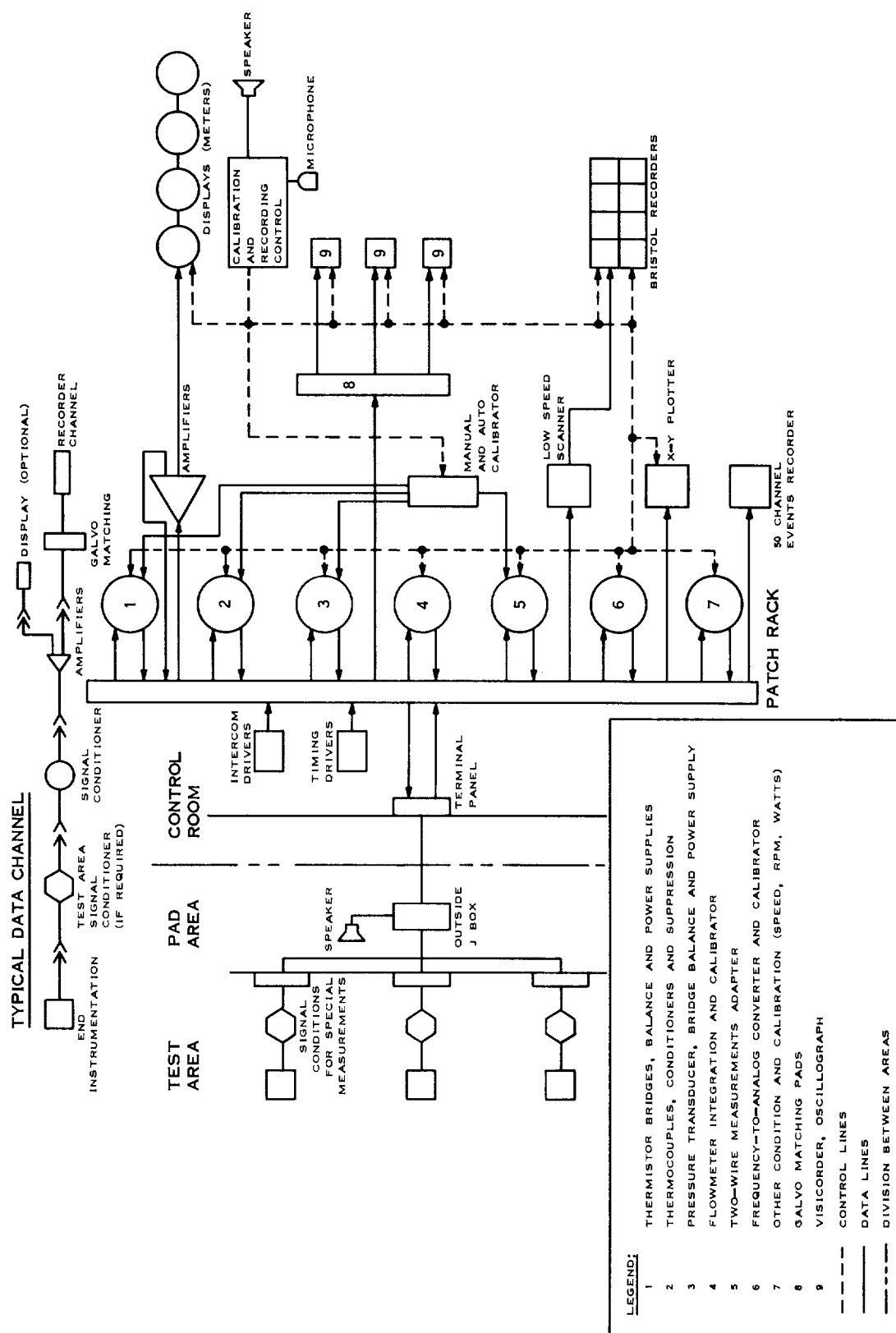
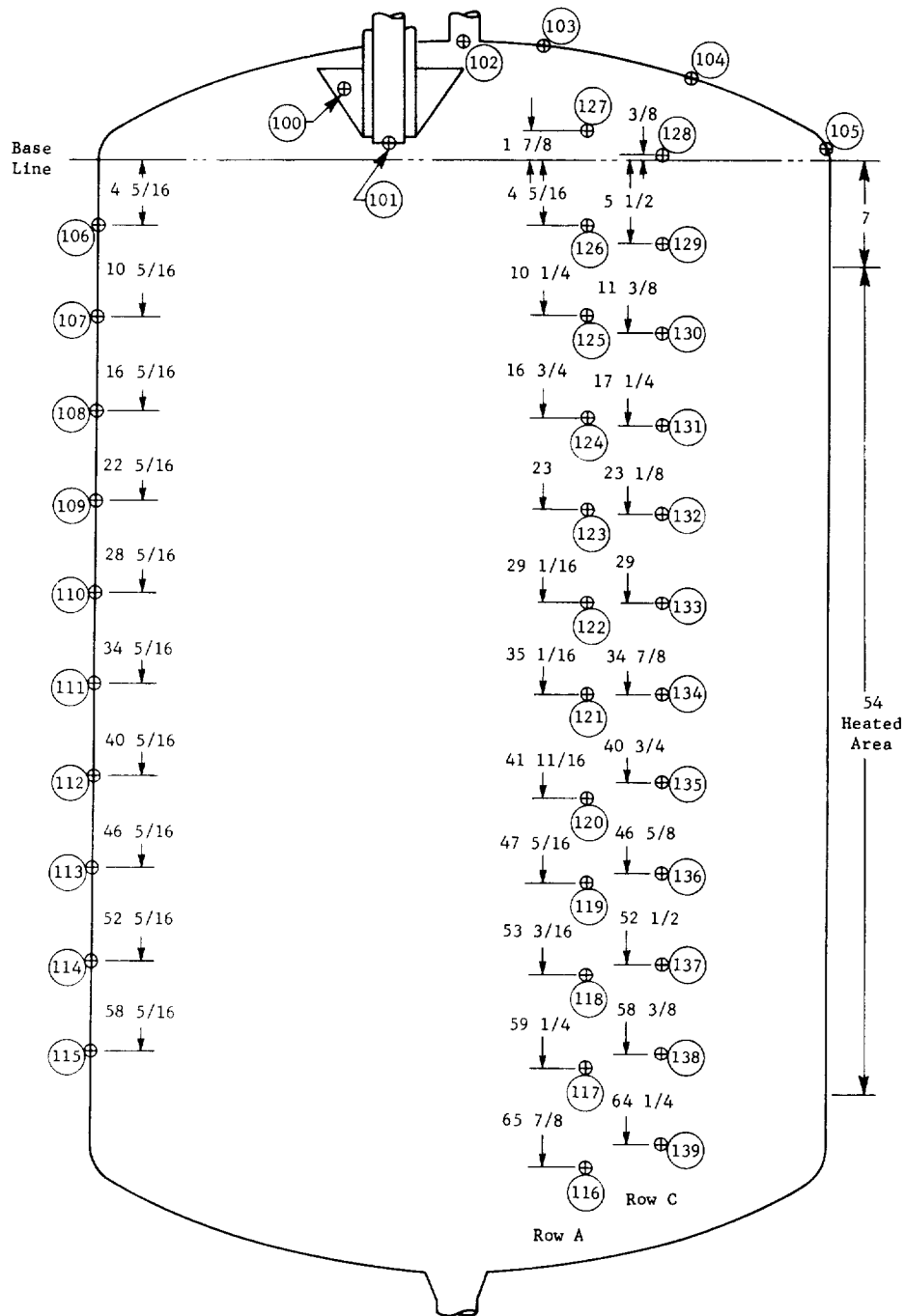


Fig. 17 Liquid Hydrogen Data System Flow Diagram

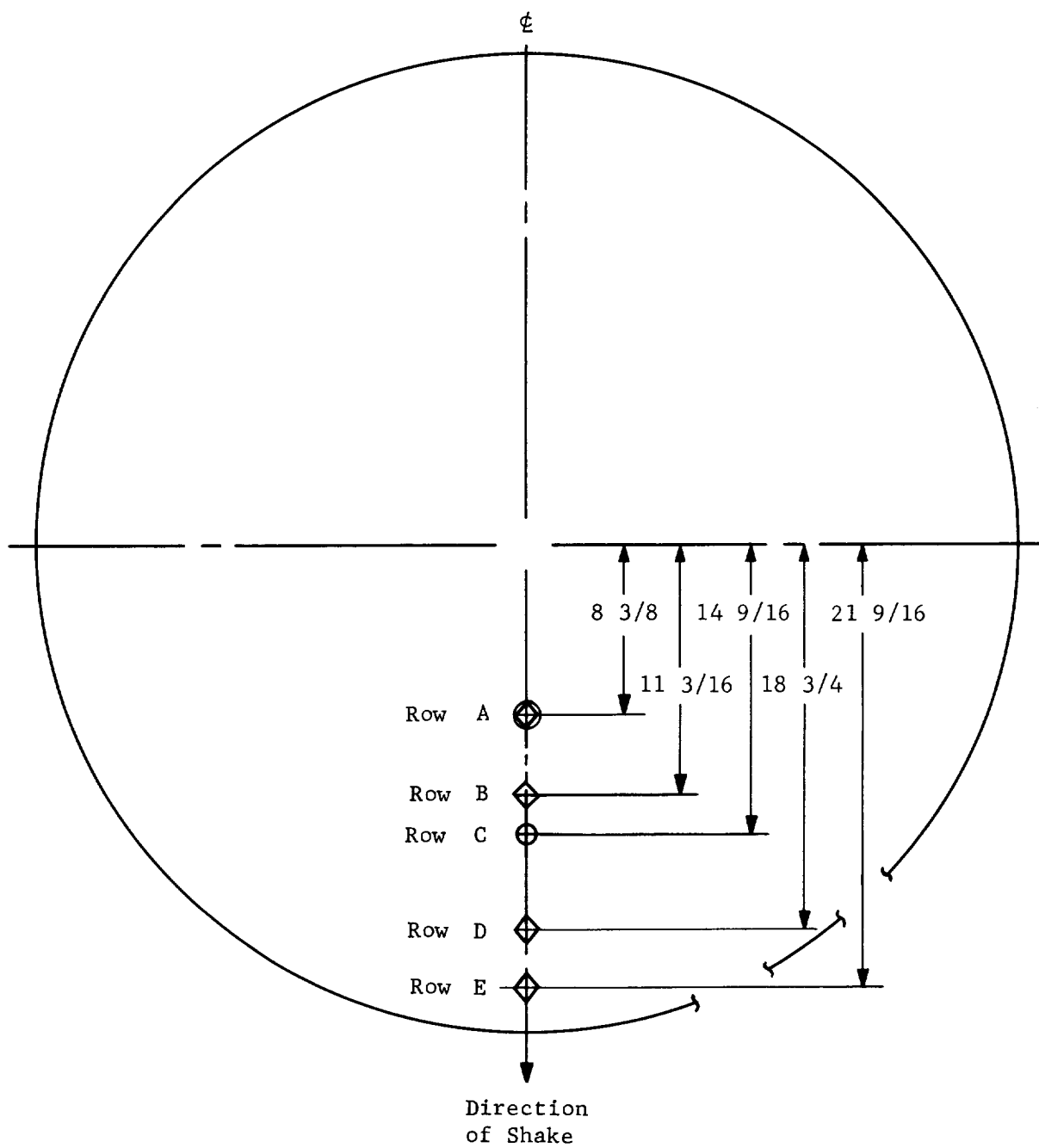


Fig. 18 Control Room During Test



- Note:**
1. Thermocouple locations are shown by ⊕.
 2. Thermocouple designations are given by numbers in circles.
 3. Radial locations are shown on Fig. 20.
 4. All dimensions in inches.

Fig. 19 Thermocouple Locations



Note: All dimensions in inches.

Fig. 20 Radial Locations of Thermistors and Thermocouples

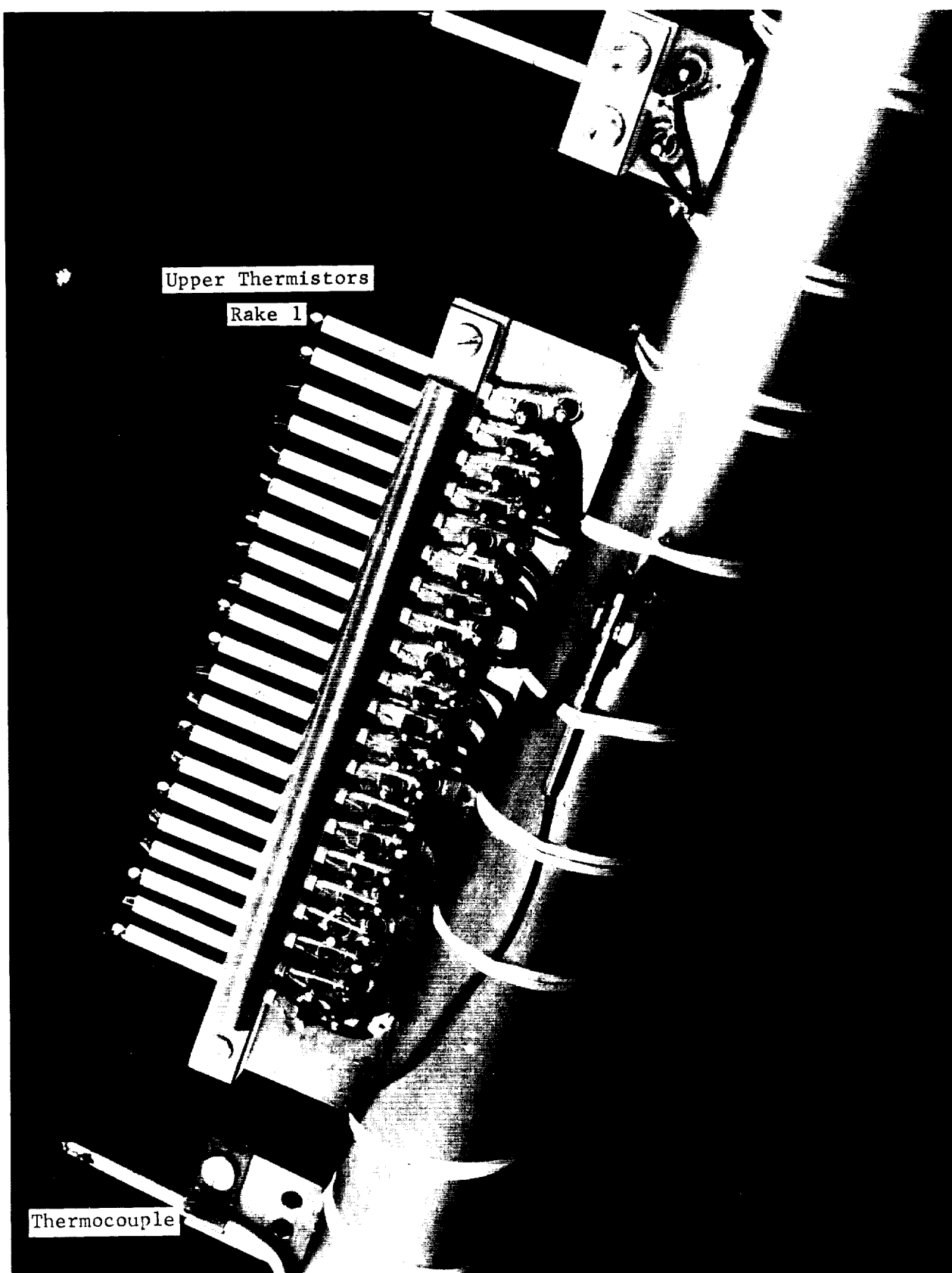


Fig. 21 Thermistors and Thermocouples on Rake No. 1

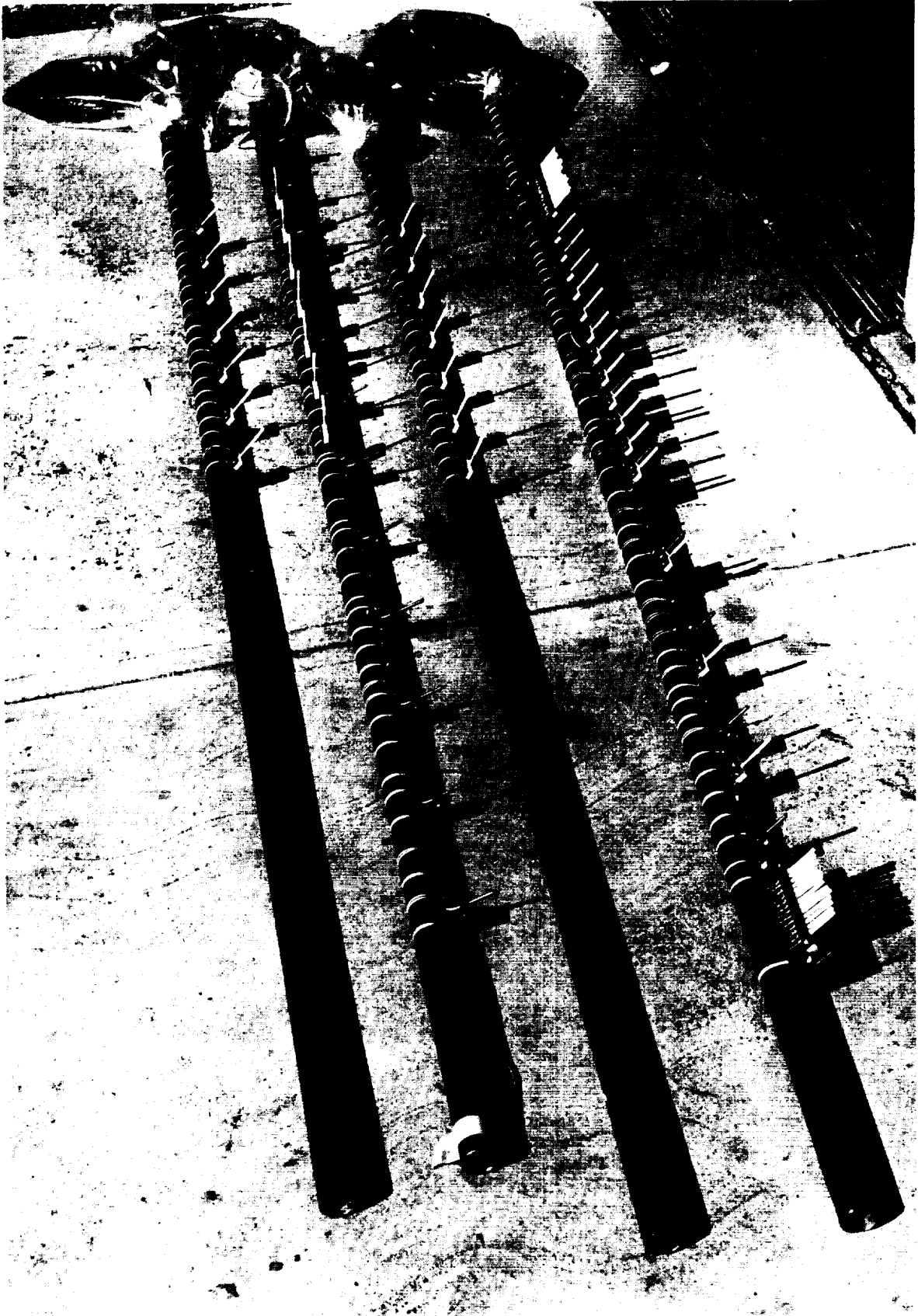


Fig. 22 Instrumentation Rakes Assembly

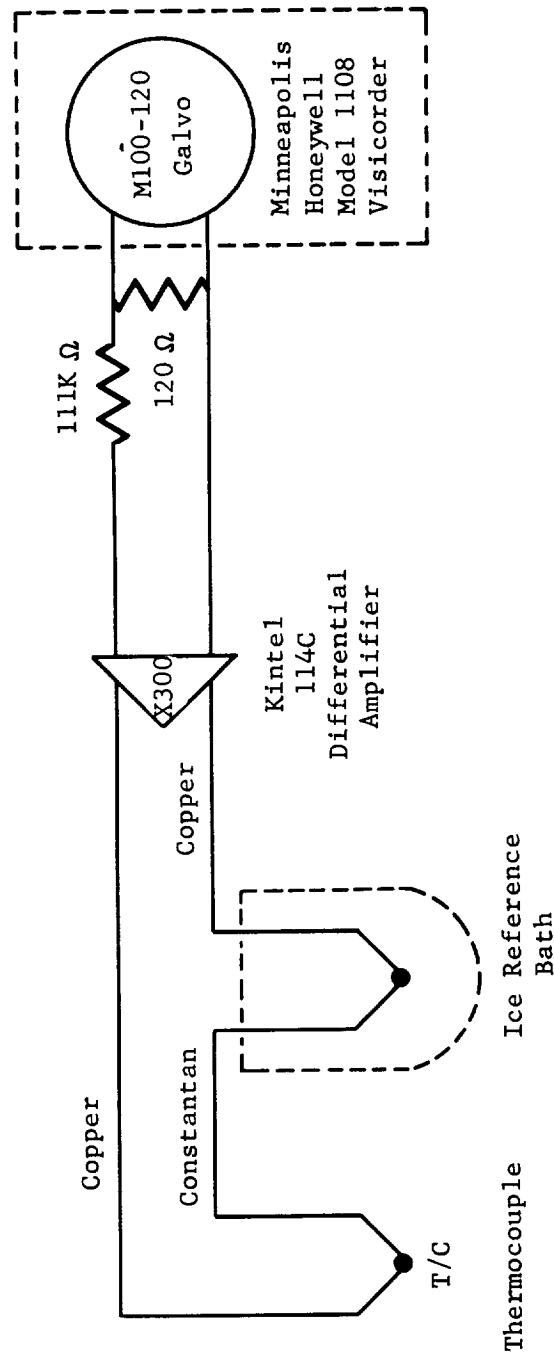


Fig. 23 Gas Temperature Schematic

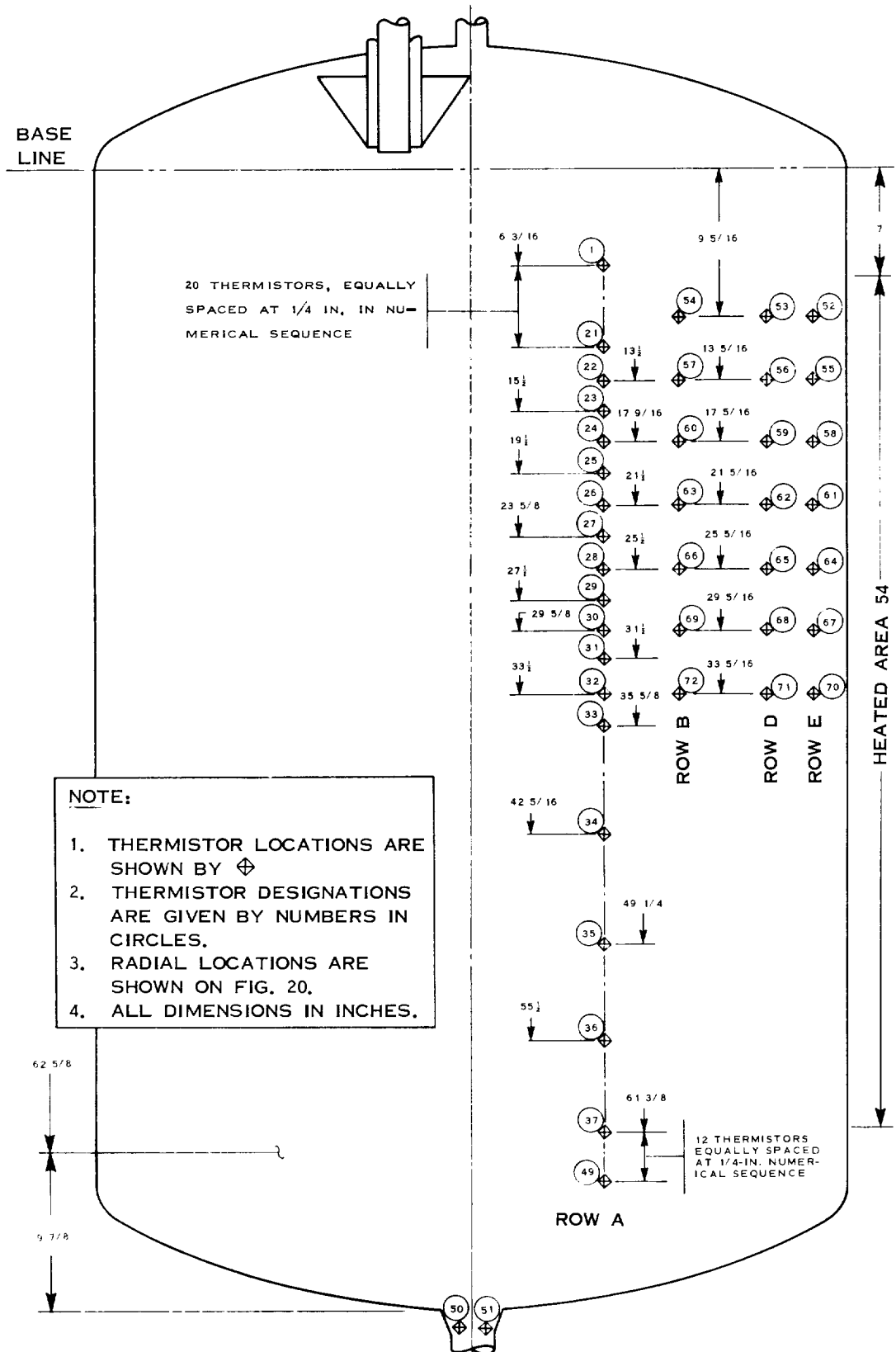


Fig. 24 Thermistor Locations

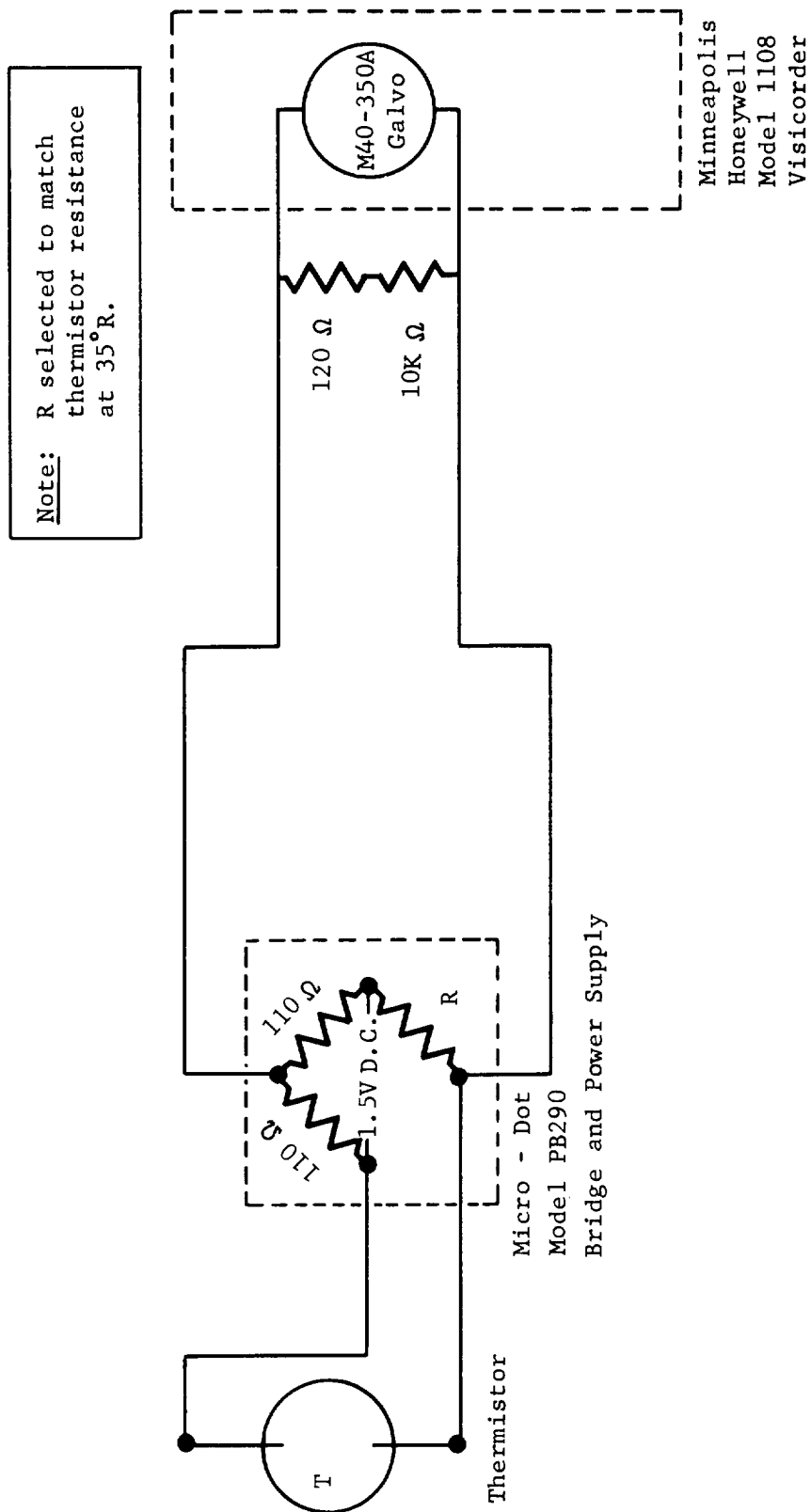


Fig. 25 Thermistor Temperature Schematic

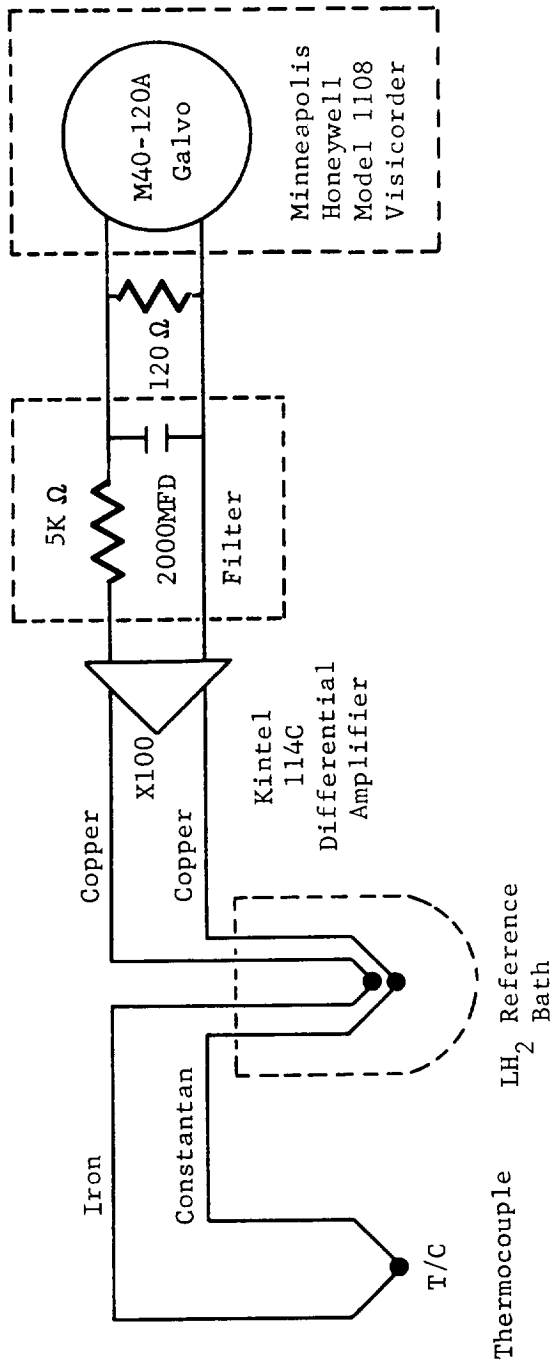


Fig. 26 Tank Wall Temperature Schematic

III. TEST PROGRAM

The liquid hydrogen temperature stratification program was conducted at the Experimental Test Laboratory of the Martin Company, Denver Division, under NASA, MSFC sponsorship (NASA contract number NAS8-5046). Test hardware required for the experimental program was furnished by the Martin Company under a liquid hydrogen research program that had been initiated nearly three years earlier. The stratification test vessel was constructed and hydrostatically tested with liquid hydrogen, and the majority of the supporting test hardware had been designed, fabricated, and partially checked out before the contract date (June 1962). By mid-September 1962 installation of all hardware had been completed, and final systems checkouts were initiated on the overall test installation.

The first systems checkout of the installation was conducted on 27 September 1962. After purging and filling the test vessel, a satisfactory thermistor calibration was made as described in Chapter IV. Following this, several short-duration tests with heating were conducted to obtain some preliminary stratification data, but after approximately 5 min of accumulated heating time, the fuses blew in one of the power phases. No immediate explanation for this malfunction was evident, so the test was terminated to permit a detailed evaluation of the data obtained. The detailed procedures used to fill the vessel, calibrate the instrumentation, and perform the stratification tests are described in Chapter IV.

During the next few days the systems checkout was repeated several times, but each time the fuses blew after about 5 min of accumulated heating. Although there was still no explanation for this malfunction, it was concluded that the planned experimental program could be accomplished satisfactorily because very few of the planned tests involved heating intervals exceeding 3 min.

On 4 October, Tests 1 and 2, as defined in the revised test plan (Table 2), were conducted. Both tests were considered satisfactory, but the fuses blew after 77 sec of heating in Test 2.

On 10 October a series of heating tests were conducted using liquid nitrogen to further check out the heat chamber. In each of these tests the fuses blew so it was decided to disassemble the tank for inspection. The inspection revealed no obvious discrepancies, so the tank was reassembled without making any modifications.

On 17 October, Tests 3, 4, and 5 were conducted. By allowing the chamber to cool off for approximately 1 hr between tests, no major electrical failures occurred. However, the fuses blew in Test 4, after 204 sec of heating (planned duration was 240 sec). This test duration was considered adequate to yield valid data.

Following these tests, the tank was disassembled and the heat chamber was removed for inspection. The cause of the malfunction was discovered as soon as the first section of the heat chamber was removed. Adjacent ends of bus bars of different electrical phase were so close to each other that the thermal expansion of the bus bars, after an extended period of heating, resulted in short circuit. To overcome this difficulty, four lamps were removed from the end of each heat chamber section so that the bus bars could be shortened about 1 in., which provided a minimum gap of $1\frac{1}{2}$ in. The tank was reassembled and no further difficulty was experienced from this source throughout the remainder of the test program.

On 2 November, Tests 7, 8, 10, and 11 were conducted with no difficulty whatsoever. This completed all of the planned tests that did not require shake or outflow.

On 20 November, 12 tests (including 2 reruns) were conducted in accordance with the revised test plan, and all systems performed satisfactorily. These tests were No. 1 (rerun), 6, 9, 25, 24, 10 (rerun), 13, 14, 15, 16, 22, and 23. Test No. 1 was rerun because in the original run the tank was not vented, resulting in a pressure buildup during the test from an initial pressure of 52 psia to a final value of 94 psia. In the rerun, designated as test No. 1A, the tank was vented as required to maintain a constant pressure of 52 psia throughout the test. Test No. 10 was rerun because of wiring error in the heat chamber circuit in the original run resulted in a lack of power to one section of the heat chamber. The rerun is designated as Test No. 10; the original run was voided.

At this time the liquid hydrogen supply was exhausted, and the remaining tests had to be postponed until additional liquid could be obtained. On 11 December, the additional liquid hydrogen was received, and on 13 December, Tests 17, 18, 19, 20, 21 and 23 (rerun) were conducted. Test 23 was rerun because in the original run heating and shaking were inadvertently initiated simultaneously, while the plan was to initiate shake 60 sec after the start of heating. However, the data obtained in the rerun were, for some unknown reason, very inconsistent, and therefore only the data

from the original run are included in this report. The one remaining test, No. 12, was successfully conducted on 3 January 1963, together with several other tests to determine heat chamber efficiency. This completed the experimental program.

Table 2 Revised Test Plan

Test No.	Tank Top Pressure (psig)	Pressurizing Gas	Predicted Heat Flux (Btu/sq ft-sec)	Heat Duration (sec)	Shake Frequency (cps)	Shake Amplitude (in.)	Outflow Duration (sec)	Remarks
1	40	He	0.586	180				
2	10	He	0.586	120				
3	20	He	0.586	180				
4	60	He	0.586	240				
5	40	H ₂	0.586	180				
6	40	He	0.586	180	0.87	1.0		
7			0.586	240				
8	40	He	0.145	480				
9	40	He	0.145	480	1.0	0.5		
10	40	He	0.261	360				
11	40	He	0.348	240				
12	40	He	0.871	120				
13	20	He	0.261	120	0.5	1.0		
14	20	H ₂	0.261	120	1.0	1.0		
15	20	He	0.261	120	0.87	1.0		
16	20	He	0.261	120	1.50	0.5		
17	20	He	0.261	120	15.0	.087		2g peak acceleration
18	20	He-H ₂			0.87	1.0	120	Initial pressurization with He, outflow pressurization with H ₂
19	20	He-H ₂	0.261	120			120	Outflow to follow heat
20	20	He-H ₂	0.261	120			120	Outflow concurrent with heat
21	20	He-H ₂	0.261	120	0.87	1.0	120	Outflow to follow heat Shake during heat and outflow
22			0.261	240	0.87	1.0		Self-pressurized
23	20	He	0.261	120	0.87	1.0		Shake to start at 60 sec after start of heat
24	20	He	0.261	120				
25	20	He	0.145	240				

IV. TEST PROCEDURES

Test operations for the stratification program were controlled from the control center shown in Fig. 18. Many of the test operations were performed by personnel stationed in the test area. Hazardous operations, however, were performed remotely with no personnel in the test area. In general, remote control was necessary whenever the test vessel contained liquid hydrogen, and progress during these operations were monitored on closed-circuit television. This chapter describes the general test procedures that were followed in conducting the stratification program.

A. PRETEST CHECKOUT

Before each test, a checkout procedure was executed that included safety coordination, weather check, gas trailer and K-bottle check, dewar liquid level check, and valve operations check.

B. PURGE AND FILL

After the pretest checkout was satisfactorily completed, the purge and fill operation was initiated. Following a gaseous nitrogen purge through the test vessel, it was partially filled with liquid nitrogen to cool down the system. Helium gas was then used to force the liquid nitrogen out of the tank. Therefore, when the drain operation was completed, the tank contained a helium atmosphere suitable for introduction of liquid hydrogen. A positive helium pressure was maintained in the tank to prevent any air or nitrogen gas from entering. The instrumentation standpipe was then purged with hydrogen gas, and the liquid level manometer lines were purged with helium to remove any contaminating nitrogen gas or air. At this point the transfer line purge and liquid hydrogen fill were initiated.

With the dump valve open and the fill valve closed, the dewar transfer valve was cracked open and the transfer line was purged with hydrogen vapor from the dewar. After several minutes, the dump valve was closed, the fill and vent valves were opened, and the liquid hydrogen filling operation began. The test vessel was

filled until the liquid level manometer indicated approximately $4\frac{1}{2}$ -in. of water, equivalent to a liquid hydrogen level a few inches above the heated zone of the tank. After the filling operation was completed, the fill and transfer valves were closed, and the manual valve in the purge tee at the dewar was opened sufficiently to prevent a large pressure buildup in the transfer line. The transfer line was not vented down to the atmospheric pressure, however. This would result in air being drawn into the line where it would condense and freeze, thus preventing further transfer through the line until it had completely warmed up.

C. INSTRUMENTATION CALIBRATIONS

In general, all instrumentation was calibrated before each series of tests. The following discussion describes the pertinent features of the calibration procedures.

1. Gas Temperature Thermocouples

The gas temperature thermocouple channels were calibrated by voltage substitution. Each thermocouple was disconnected at the program board, and the output from a Leeds and Northrop potentiometer was inserted into the amplifier input in several steps. The Bureau of Standards conversion tables (Ref 3) were used to determine the temperature vs emf relationships.

2. Thermistors and Tank Wall Thermocouples

The tank wall thermocouple channels and the liquid temperature thermistor channels were calibrated by subjecting the sensors to a series of known temperatures, and recording the outputs on the oscillographs.

These known temperatures were produced by saturating the liquid hydrogen in the test vessel at several different pressure levels in the range of 0 to 70 psig in the following manner. The tank vent was closed and the heat was turned on until the tank self-pressurized to about 60 psig. The vent valve was then opened momentarily and the heat reapplied as necessary until the entire body of liquid became saturated at a pressure in excess of 60 psig, as evidenced by the lack of a sudden decrease in pressure during venting. Once this saturated condition was attained, the vent valve was opened and closed several times. This procedure

promoted violent boiling of liquid, and assured that the entire bulk of the liquid was at the saturation temperature corresponding to the vessel pressure. This process was repeated, with the tank pressure decreasing approximately 10 psi at each step, until ambient pressure was reached. The tank pressure and all thermistor and thermocouple outputs were continuously recorded throughout this procedure, thus providing records of galvanometer deflections for each measurement channel for each of the known saturation temperature steps.

3. Pressures

All pressure transducer channels were calibrated by subjecting the transducer to a known pressure and recording the output. For transducers with a range less than 5 psi, the known pressure was provided by a mercury manometer. For the remaining transducers, the known pressure was provided by a dead weight tester.

4. Heat Chamber Voltage

A 0 to 500v ac variable voltage source was connected to the primary of the step down transformer to apply known voltages in several steps. These voltages were measured with a John Fluke Model 803 A.C. voltmeter, accurate to ± 1 volt, and the channel output was recorded for each step.

5. Heat Chamber Current

A 0 to 5 amp ac current source was substituted for the secondary of the current transformer, and a calibration procedure similar to the one used for heat chamber voltage was performed. The current was measured with a Weston Model 904 AC ammeter, accurate to ± 0.025 amp.

D. STRATIFICATION TESTS

After the test vessel had been filled with liquid hydrogen and the instrumentation calibration procedures had been completed, a 1 min countdown was initiated for the stratification test. At T-50 sec, the instrumentation recorders were turned on, and all recorders were checked for proper operation. At T-30 seconds, the tank was pressurized to the desired level and allowed to stabilize. At T-0, the recorders were marked, and the heat lamp

power was turned on by energizing the contactor relay from the control console. After the heat had been applied for the desired time interval, the recorders were again marked and the heat lamp power was turned off. The recorders were allowed to run for an additional 20 sec. During the heating process, the tank top pressure was maintained constant at the desired level by manually controlled addition of pressurant or venting, as required.

E. SHAKE PROCEDURE

In those tests that required shaking of the test vessel, additional operations were performed. As soon as the tank had been filled with liquid, the hydraulic pump and controls were turned on, and pressure was applied to the actuator. The frequency selector on the function generator was set at the desired value. Then, at the required time, the amplitude control on the function generator was gradually turned up until the tank oscillation was at the desired amplitude. The amplitude was monitored on the TV screen with the aid of a fixed pointer and a calibrated scale attached to the test vessel. Amplitude control was initiated at T-10 sec so that the tank would be oscillating at the required frequency and amplitude at T-0 when the heat was turned on. At the end of the planned test duration, the heater and shaker were turned off simultaneously.

F. OUTFLOW PROCEDURE

In those tests that required outflow, additional operations were performed. Before the start of pressurization, the pressurant selector valve was switched to the helium source. Pressurization was initiated by opening the main shutoff valve. In test No. 19, in which the heating period preceded outflow, the shutoff valve was closed when the desired operating pressure was reached, and the heating period was initiated. At the end of the heating period, the pressurant selector valve was switched to the hydrogen source, and the pressurant shutoff valve and liquid outflow valve were opened simultaneously. For the remaining outflow tests, as soon as the desired pressure level was reached with the helium pressurant, the pressurant selector valve was switched to the hydrogen source, and the liquid outflow valve was simultaneously opened. For tests No. 20 and 21, the heater power was turned on at the start of outflow. For tests No. 18 and 21, shaking was also initiated at the start of outflow.

G. HEAT LEAK CALIBRATION

After receiving the test vessel from the vendor, a long-term boiloff test was conducted to determine the magnitude of the ambient heat leak into the test vessel. For this test the vessel was filled with liquid hydrogen and the change in liquid level over a period of 12 hr was monitored. The data obtained were used to determine the magnitude of the error that may be introduced in the heat flux calculations as a result of the ambient heat leak. The measured ambient heat leak was 0.2 Btu/sec, which is negligible compared to the heat rates used in the tests.

H. HEAT CHAMBER CALIBRATION

Proper interpretation of the test data requires that the heat flux to the liquid be accurately known for each test. The power input to the heat chamber is readily determined from the voltage and current measurements, using an assumed unity power factor. Determining the heat input to the liquid was a more difficult problem, however, and required calibration tests at several different rates of heat input.

To calibrate the heat chamber, it was operated for liquid temperature rise and the boiloff rate were measured. The boiloff rate was determined with an orifice flow section installed in the vent line near the top of the tank, with both the inlet temperature and the differential pressure of the orifice being measured. The sensible enthalpy gain of the liquid in the test vessel was minimized by keeping the vent line pressure loss, including that of the orifice, as small as possible, thus limiting the saturation temperature increase to about 0.2°R. The sensible enthalpy gain corresponding to this temperature increase was included in the computation of the net heat input. The results of the calibration tests are presented in Chapter V (Fig. 75).

V. TEST RESULTS

A. DATA REDUCTION METHODS

The data reduction methods used to reduce the recorded data to a presentable form were essentially the same for all the measurements. The liquid temperature measurements required the greatest attention because they were the primary measurements of the test program.

From the liquid temperature calibration tests previously described, oscillograph traces were obtained corresponding to a series of known temperatures applied to each of the thermistors. The calibration was conducted so that the liquid was always saturated, and the known temperatures were determined from accurate measurements of the tank pressure, together with the saturation pressure vs temperature curve shown in Fig. 27.

As an example, portions of one oscillograph record obtained from one of the calibrations are presented in Fig. 28. The measurement numbers are identified on the record, and the measured pressure and corresponding saturation temperature for each calibration step are also shown. From such oscillograph traces, calibration curves similar to those in Fig. 29 were prepared showing galvanometer deflection vs liquid temperature.

To reduce the data from a stratification test, it was then only necessary to measure the deflections of the traces at the desired point in time on the oscillograph record, and read the corresponding temperatures from the appropriate calibration curves. A portion of an oscillograph record for a typical test (No. 10) is shown in Fig. 30 with the measurement numbers identified.

A more difficult type of record to reduce is shown in Fig. 31. This record was obtained during test No. 18 which included both shake and outflow. The drastic effect of the oscillation of the fluid on the liquid temperature measurements near the liquid surface is shown. The period during which several of the thermistors are being sloshed in and out of the liquid as the liquid level gradually decreases is clearly evident. For tests of this type (No. 18 and 21), no attempt was made to reduce the thermistor data, except to determine the time at which each thermistor became uncovered.

In principle, the data reduction procedure for the other types of measurements was the same as that for the thermistors.

B. INTERPRETATION OF DATA

The scale effects in predicting the stratification behavior of a prototype from experimental model test data should be discussed before examining the test results. Since the dominant mode of heat transfer at the heat flux values used in these tests is nucleate boiling, which is independent of size effects, it is sufficient, for obtaining similarity in heat transfer mechanism, to maintain equality of heat fluxes between model and prototype. The temperature rise of the liquid is a function of the total heat input (Q) divided by the volume (V). The total heat input is in turn equal to the product of the heat flux (q/A), the heated area (A), and the time (t). Thus, equal temperature rise in model and prototype requires that

$$\left(\frac{(q/A) A t}{V} \right)_{\text{model}} = \left(\frac{(q/A) A t}{V} \right)_{\text{prototype}},$$

which, since the heat fluxes are equal, leads to the requirement

$$\frac{t_{\text{model}}}{t_{\text{prototype}}} = \frac{\left(\frac{V}{A} \right)_{\text{model}}}{\left(\frac{V}{A} \right)_{\text{prototype}}}.$$

Assuming geometrical similarity,

$$\frac{V}{A} \propto L,$$

where L is some characteristic dimension, hence

$$\frac{t_{\text{model}}}{t_{\text{prototype}}} = \frac{L_{\text{model}}}{L_{\text{prototype}}}.$$

If the comparison is based on net heat input per unit wall area (Q/A), then, since

$$\frac{Q}{A} = (q/A)t,$$

the following scale factor should be used:

$$\frac{\left(\frac{Q}{A}\right)_{\text{model}}}{\left(\frac{Q}{A}\right)_{\text{prototype}}} = \frac{L_{\text{model}}}{L_{\text{prototype}}}.$$

Since, for most of the tests in this program, the duration of heating, and hence the net heat input per unit wall area, was much greater than would be required for simulation of actual flight conditions of large vehicles, data are presented for several intermediate times after the start of heating for each run. Note, however, that the purpose of this test program was not to simulate any particular vehicles, but rather was to investigate stratification in a general way and to provide comparison with the previously developed analytical model.

The major portion of data from this test program is presented in Fig. 32 thru 57 as graphs of liquid temperature vs volume at several selected times during each run. The volume used for the abscissa of a particular measurement point is the total volume of the tank below a horizontal plane passing through the point of which that measurement was made. The choice of these volumes as abscissa, rather than simply height, was made to simplify the comparison of test data with the analytical model described in Chapter VI. In the upper half of the tank there were, in most cases, four thermistors at (nominally) the same height but at different horizontal distances from the tank centerline. The horizontal distances were based on equal-area annular rings to give each measurement point equal weight in computing the enthalpy gain of the liquid. In almost all cases very little difference was found between the measurements in a given set of the same level. Therefore, to simplify the presentation of data, only the average of each horizontal group of four measurements is plotted. The maximum and minimum measurement for each group are also shown, as short horizontal bars, to indicate the temperature range. In the lower half of the tank only a single measurement at each level was made. One assumption that was made, both in choosing the locations of the measurement points and in presenting the data, is that of circular symmetry; all measurement points are located in a single vertical plane. The smallness in the ranges of temperatures within a given set of measurements at the same level tends to confirm this assumption of symmetry, although in cases where oscillation was included this assumption may be somewhat dubious.

On each of the stratification data graphs, the corresponding saturation temperature is shown as a short arrow on the temperature axis. Since most tests were maintained at a nearly constant pressure, this saturation temperature corresponds to the average pressure during the test. For the few tests in which the pressure varied appreciably, several such saturation temperatures are shown, with the corresponding times indicated.

Also shown on these graphs are the temperature profiles predicted by the analytical model. These are discussed in detail in Chapter VI.

For the four tests (No. 18 thru 21) in which the liquid was drained, the temperature stratification is indicated by measurements of the liquid temperature at the tank outlet during draining. These measurements are plotted as functions of time in Fig. 58 thru 61. In the case of test No. 19, in which the heating period preceded draining, the stratification pattern just before the start of draining is shown in the conventional temperature vs volume graph in Fig 57.

The general trend shown by the data from all the tests is, of course, a definite stratification, with the upper layers showing an appreciable temperature increase and the lower layers showing little or none. In some tests (No. 2, 3, 7, and 12) a two-layer pattern is apparent, while in most of the other tests a multilayer pattern, or even a continuous temperature gradient, seems to more closely fit the data.

In any case, the stratification pattern that is formed seems to be quite stable against disturbances such as liquid oscillation or sloshing, or draining. For example, tests No. 5 and 6, which were run at nominally identical conditions (except for a 1 cps, 1-in. amplitude oscillation of the test vessel in test No. 6), show similar temperature profiles except for the measurements at 18.6 and 25.8 cu ft. Since these two measurements involved only a single thermistor at each level, these differences may not be very significant. Similarly, comparisons between temperature profiles of tests No. 8 and 9, and of tests No. 13, 14, 15, 16, 17, 23, and 24, show no significant effects of oscillation over a wide range of frequencies, including the sloshing frequency of 0.87 cps.

The effect of a time lapse after the termination of heating on the temperature profile is shown for test No. E in Fig. 55 (this test was not included in the test plan). The temperature profiles for $t = 304$ sec, at which time the heater power was turned off, and $t = 370$ sec are quite similar except for a small uniform increase at 370 sec. This increase can be explained by the gradual decay in heat input to the tank after the power is turned off, as shown in Fig. 75, rather than an abrupt cessation.

The effect of liquid outflow on the temperature profile is shown in Fig. 59, which compares, for test No. 19, the temperature profile measured in the tank just after the termination of heating, and prior to the start of outflow, with the temperature measured at the outlet during outflow. As may be seen, no significant disturbance of the temperature gradient resulted during outflow.

Although the purpose of this test program was not to obtain pressurization data, some pressurization data were obtained in the outflow tests. For these tests the pressurant was supplied at an essentially constant rate through a critical flow nozzle, with the nozzle upstream pressure controlled by a pressure regulator, with a 5 cu ft accumulator to smooth out any fluctuations. The initial pressurant was helium; as soon as the desired tank pressure was reached the gas supply was switched from helium to hydrogen, with no interruption of flow, and simultaneously the liquid outflow was initiated. There was thus no attempt to control the tank pressure except for the starting point. The resulting tank pressure is shown for test No. 18 thru 21 in Fig 62 thru 65, respectively ($t = 0$ corresponds to the time at which the pressurant supply was switched from helium to hydrogen. In test No. 18, a slight delay in the opening of the liquid outflow valve resulted in the pressure peak shown. The hydrogen gas flow rate in these tests was 0.0123, 0.0121, 0.0126, and 0.0125 lb_m/sec for tests No. 18, 19, 20 and 21, respectively, with inlet temperatures of 518, 517, 509, and 509°R, respectively.

The gas temperature profiles measured in the tank during these outflow runs are shown at 20 sec intervals in Fig. 66 thru 69. These profiles show, in general, a rather uniform temperature distribution, except for the region near the liquid surface. This indicates a high degree of mixing, or, in other words, an ineffective inlet gas distributor. Because of the time lag of the thermocouples, it is doubtful that the measurements obtained within about 10 cu ft from the liquid level are very accurate.

An attempt was made to measure the liquid level vs time, and thus to obtain the liquid flow rate, for the outflow tests by using the thermistors as point level sensors. The results of this attempt, shown in Fig. 70 thru 73, were quite satisfactory for tests No. 19 and 20, which had no sloshing. For tests No. 18 and 21, in which the tank was oscillated at its first sloshing frequency, the results were, as might be expected, not satisfactory for determining the liquid level. These data can, however, be used to estimate the wave height. As the liquid surface passes by the region of a thermistor, the up-and-down motion of the liquid surface alternately covers and uncovers the thermistor. An examination of the thermistor output under these conditions (a typical record is shown in Fig. 31), shows that the thermistor temperature rises quickly after uncovering to the saturation temperature and remains there for some time, either until the thermistor is again covered or until the thermistor heat dissipation is sufficient to evaporate the film of liquid adhering to it. Since the time required to evaporate this film is apparently greater than the period of oscillation, the thermistor temperature does not exceed the saturation temperature until some interval, approximately 1.5 sec, after the last time it is uncovered by liquid, at which time the galvanometer trace abruptly goes off scale. This time is plotted in Fig. 70 thru 73. Using these data, together with the distances of the thermistors from the tank centerline, the wave height is estimated to be about 18 in. from maximum to minimum.

There is evidence that sloshing during the outflow runs results in the condensation of a considerable amount of the hydrogen pressurizing gas. In test No. 18, for example, the outlet temperature vs time graph, Fig. 58, shows a large enthalpy gain in the final portion of liquid drained, even though no wall heating was applied during this test. The liquid temperature in the tank just before the start of outflow is shown in Fig. 56, and shows that this enthalpy gain occurred during outflow. A similar conclusion can be inferred by comparing the outlet temperatures (Fig. 60 and 61) for tests No. 20 and 21. These tests were nominally identical except for sloshing in test No. 21, and, as can be seen, the enthalpy gain in test No. 21 is significantly greater than that in test No. 20.

Considerable additional information regarding pressurization behavior could be derived from a more intensive analysis of the data obtained in the outflow tests; however, this is beyond the scope of this report.

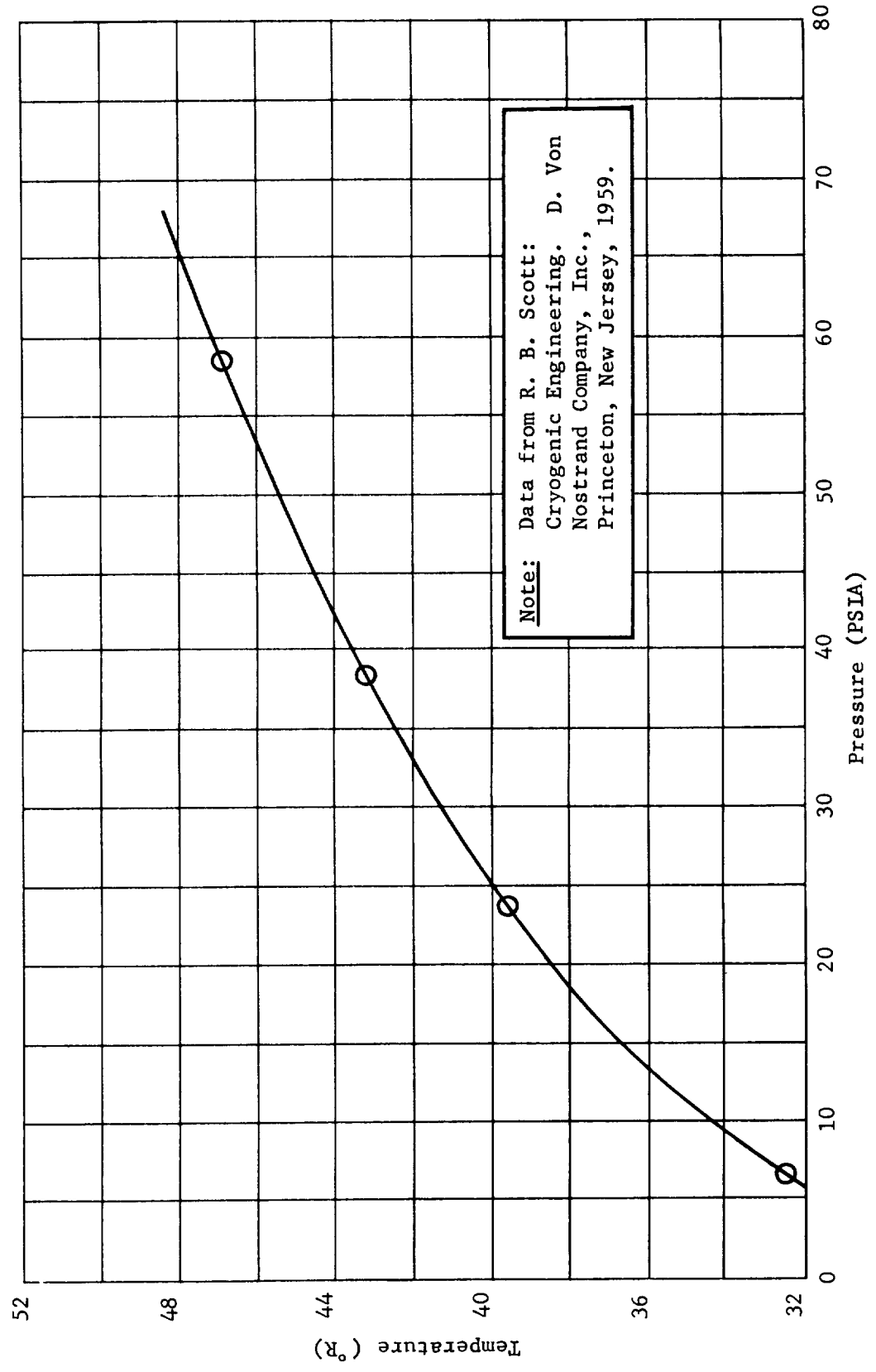


Fig. 27 Vapor Pressure Curve for Parahydrogen

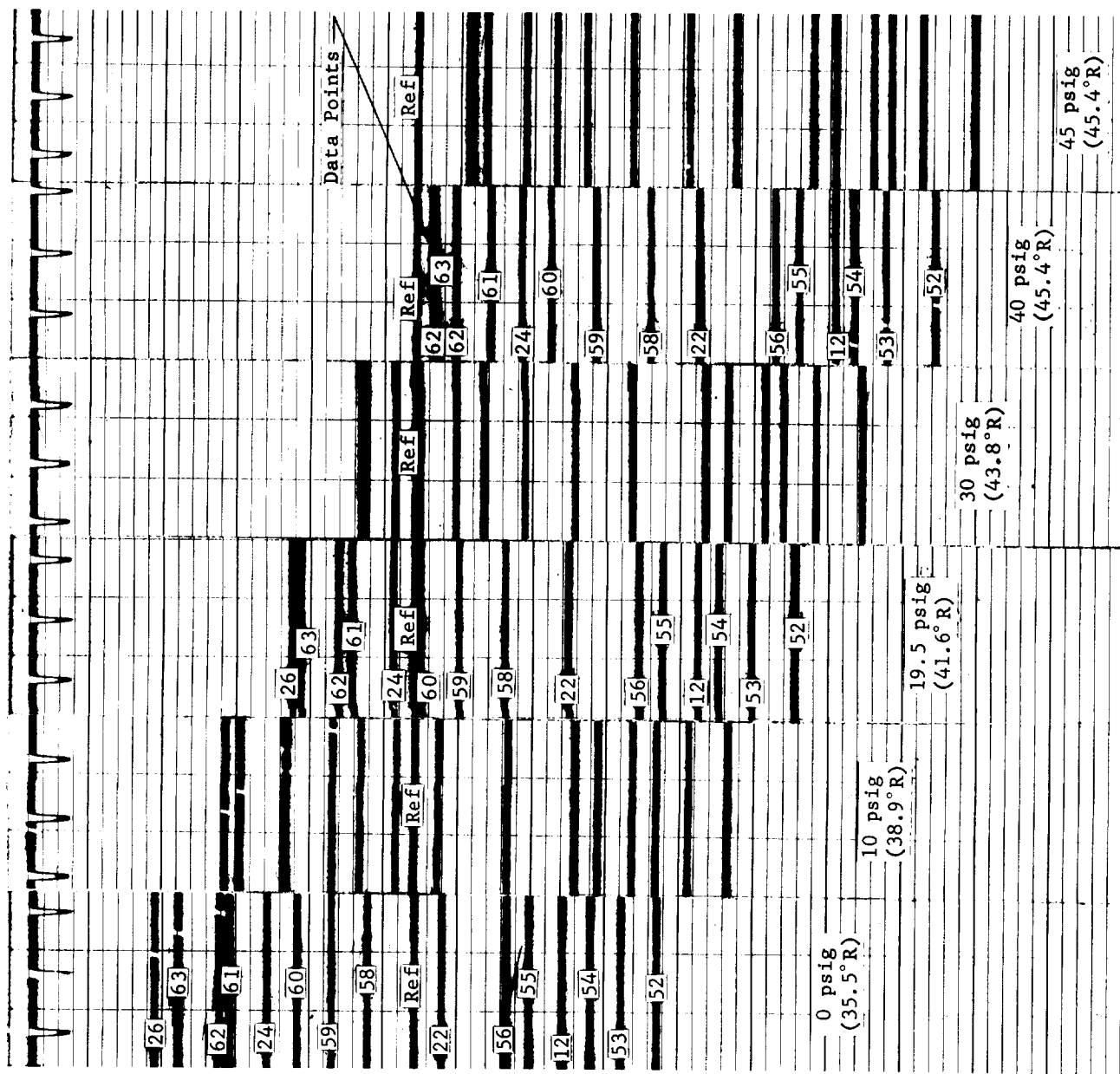


Fig. 28 Typical Thermistor Calibration Records

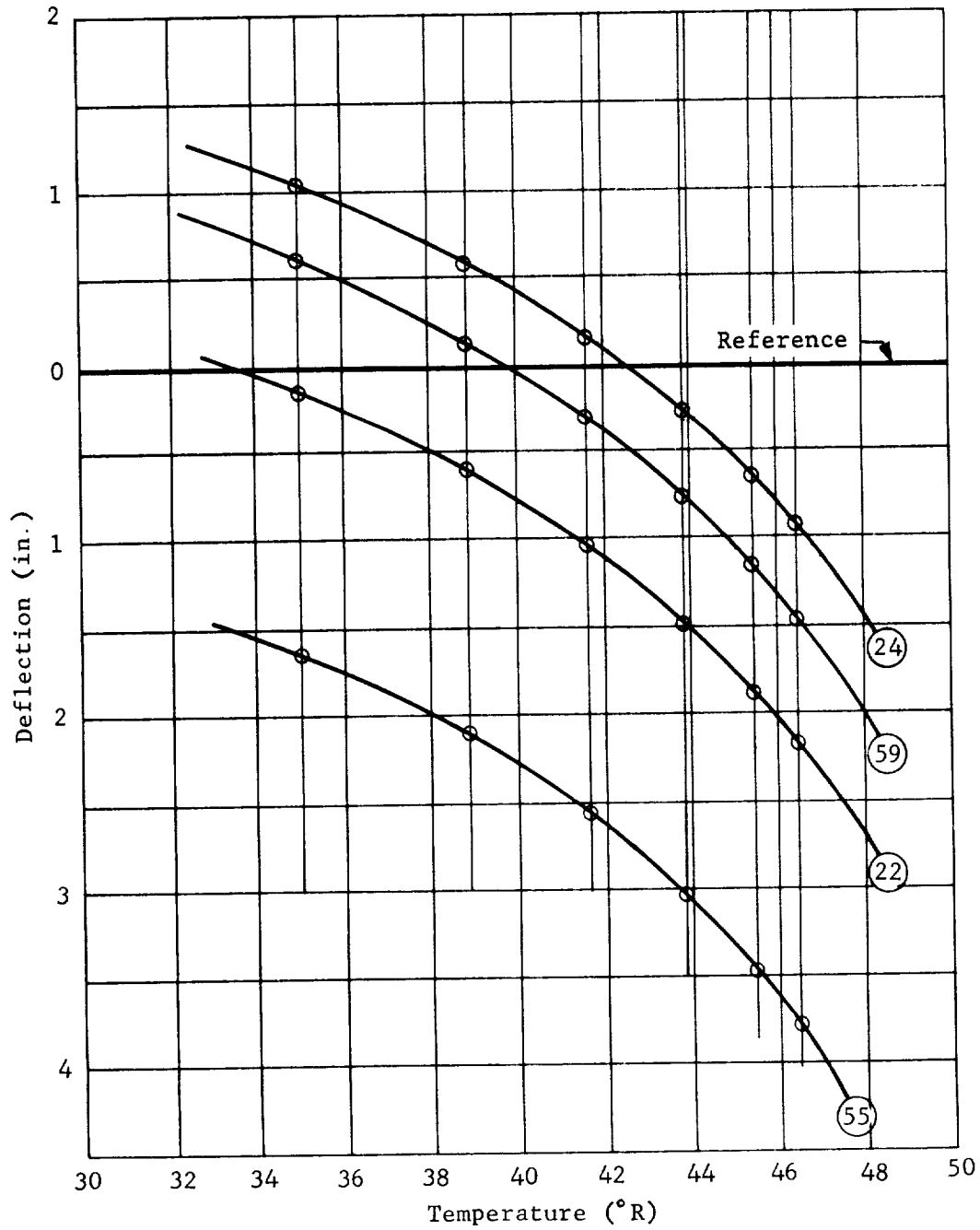


Fig. 29 Typical Thermistor Calibration Curves

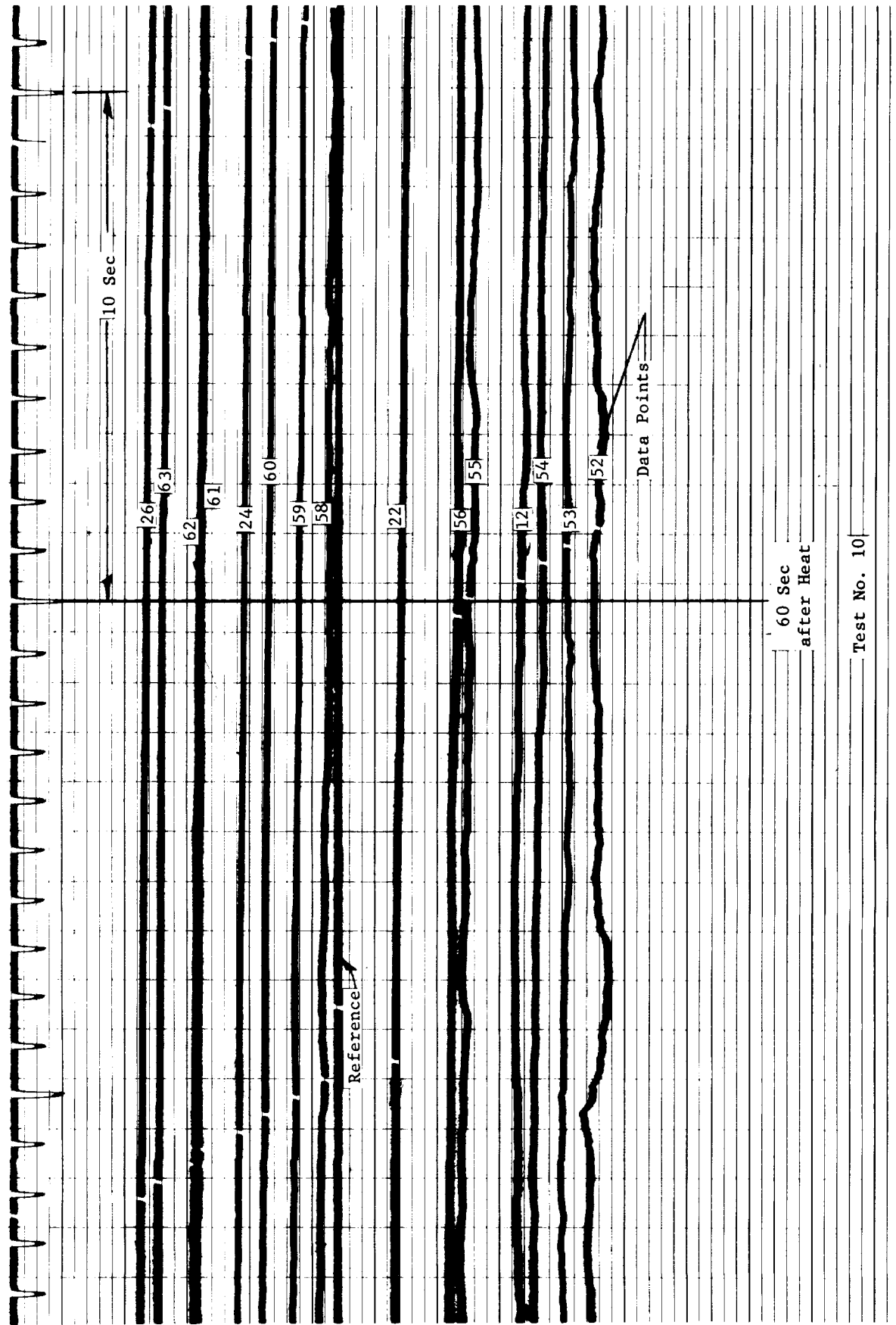


Fig. 30 Typical Thermistor Oscillograph Record

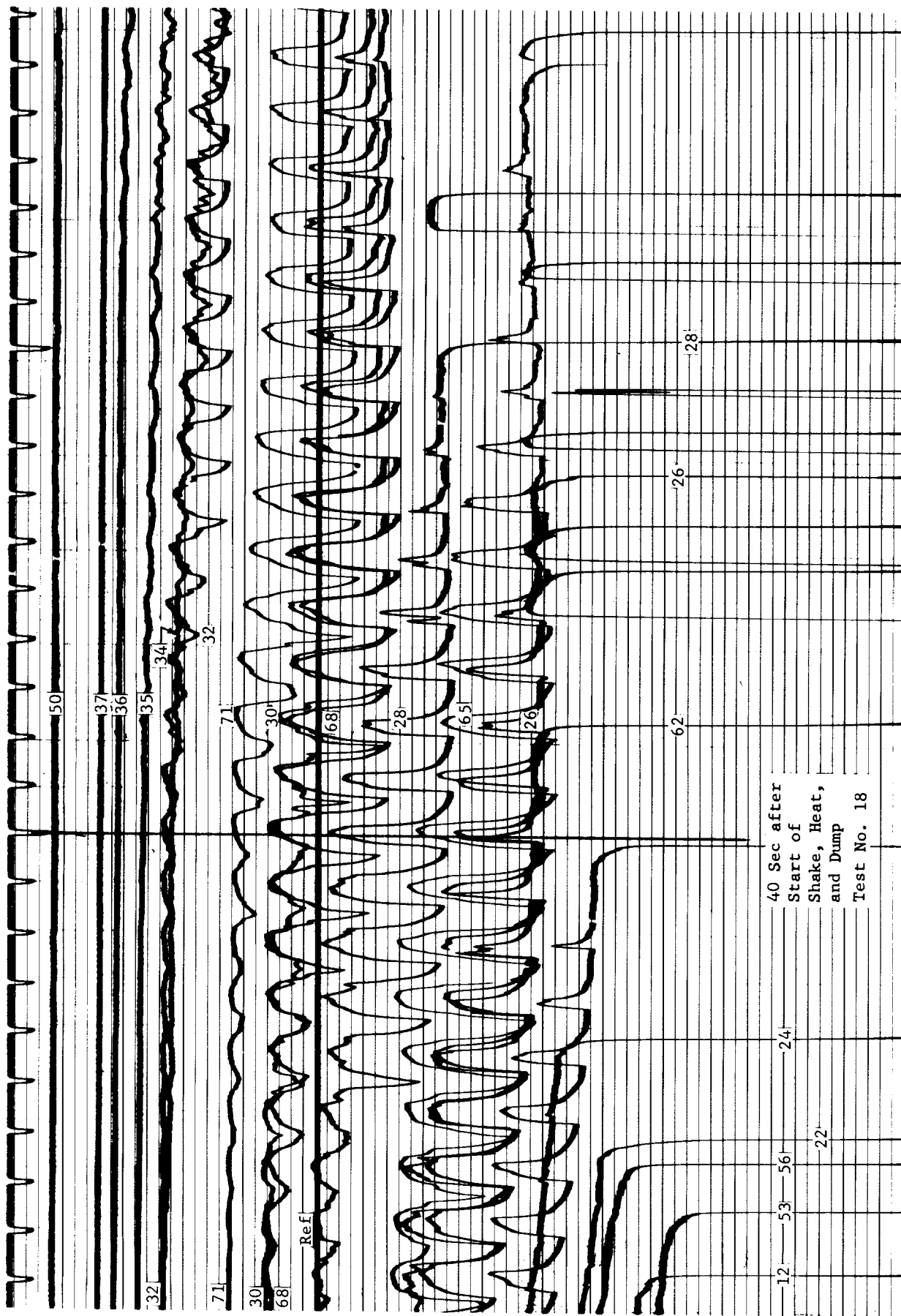


Fig. 31 Typical Thermistor Recordings During Shake and Outflow

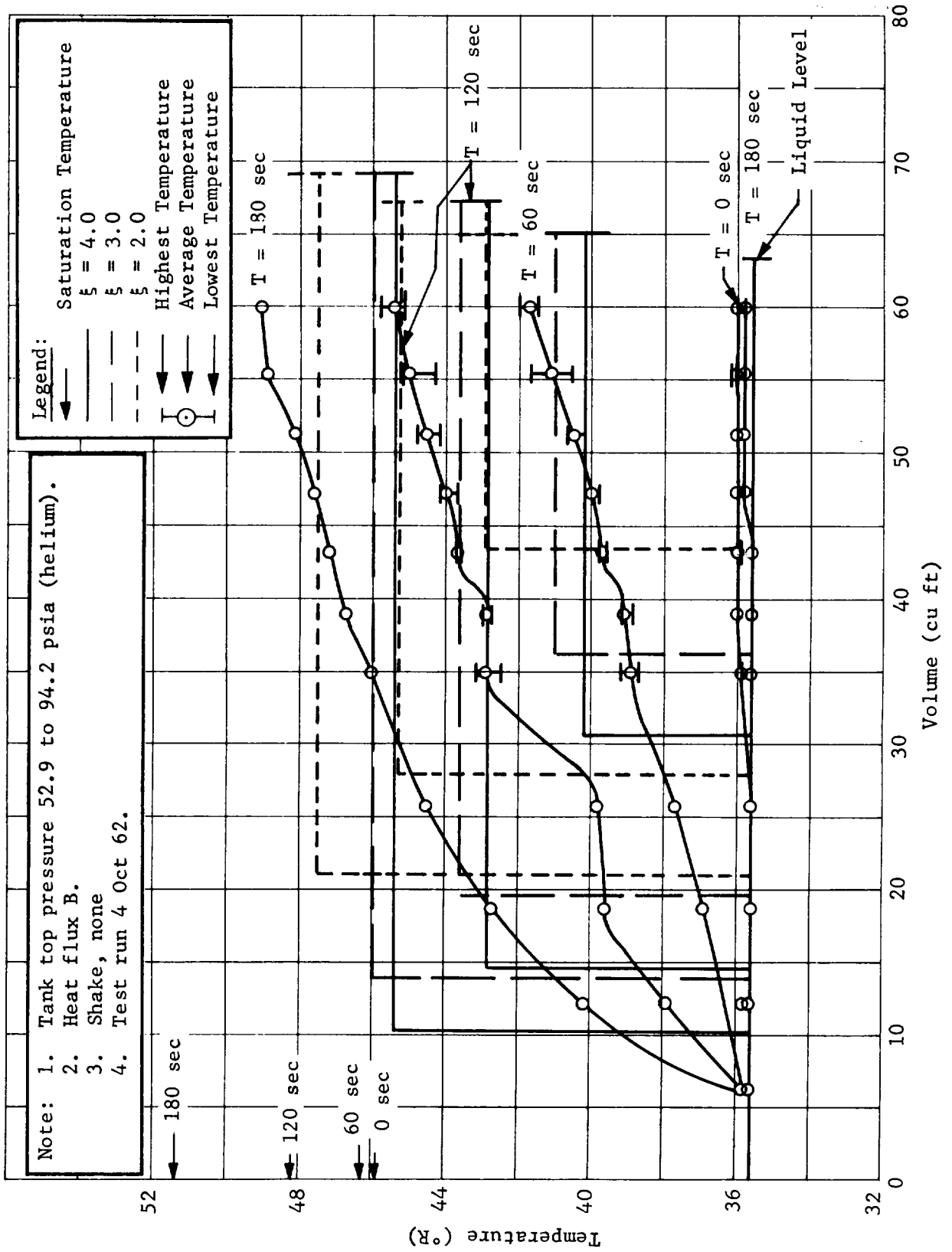


Fig. 32 Stratification Temperature Profile, Test No. 1

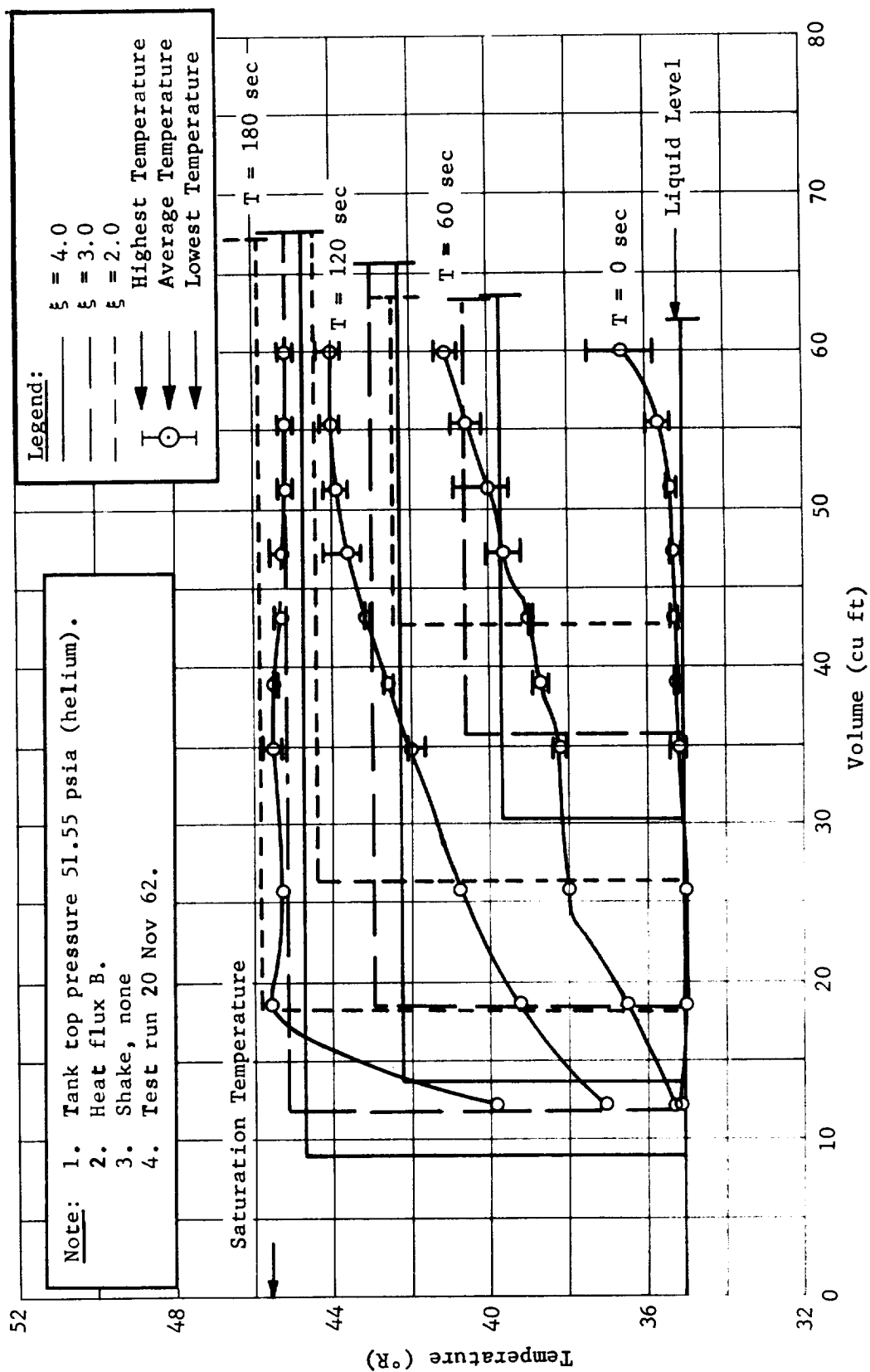


Fig. 33 Stratification Temperature Profile, Test No. 1A

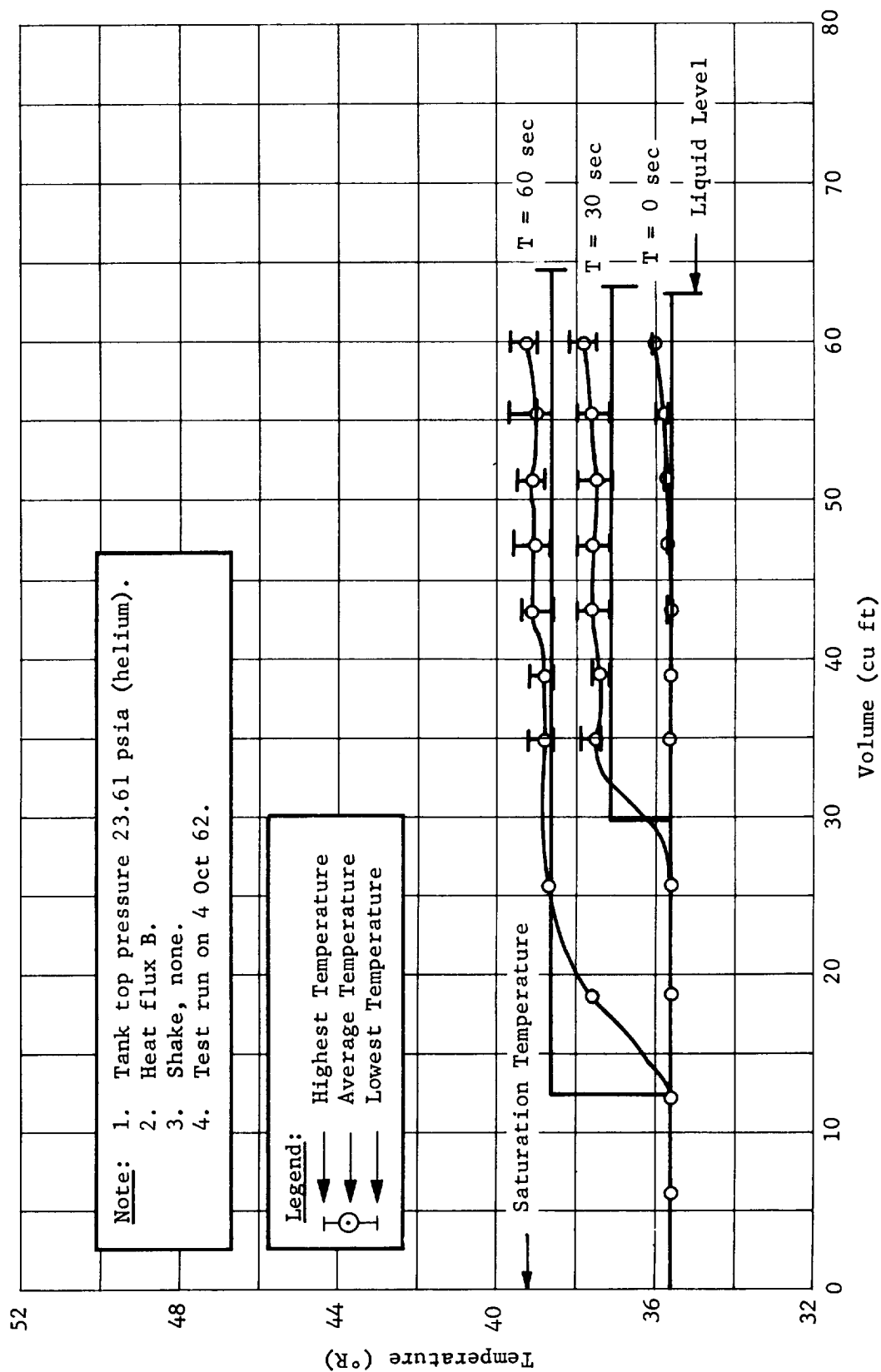


Fig. 34 Stratification Temperature Profile, Test No. 2

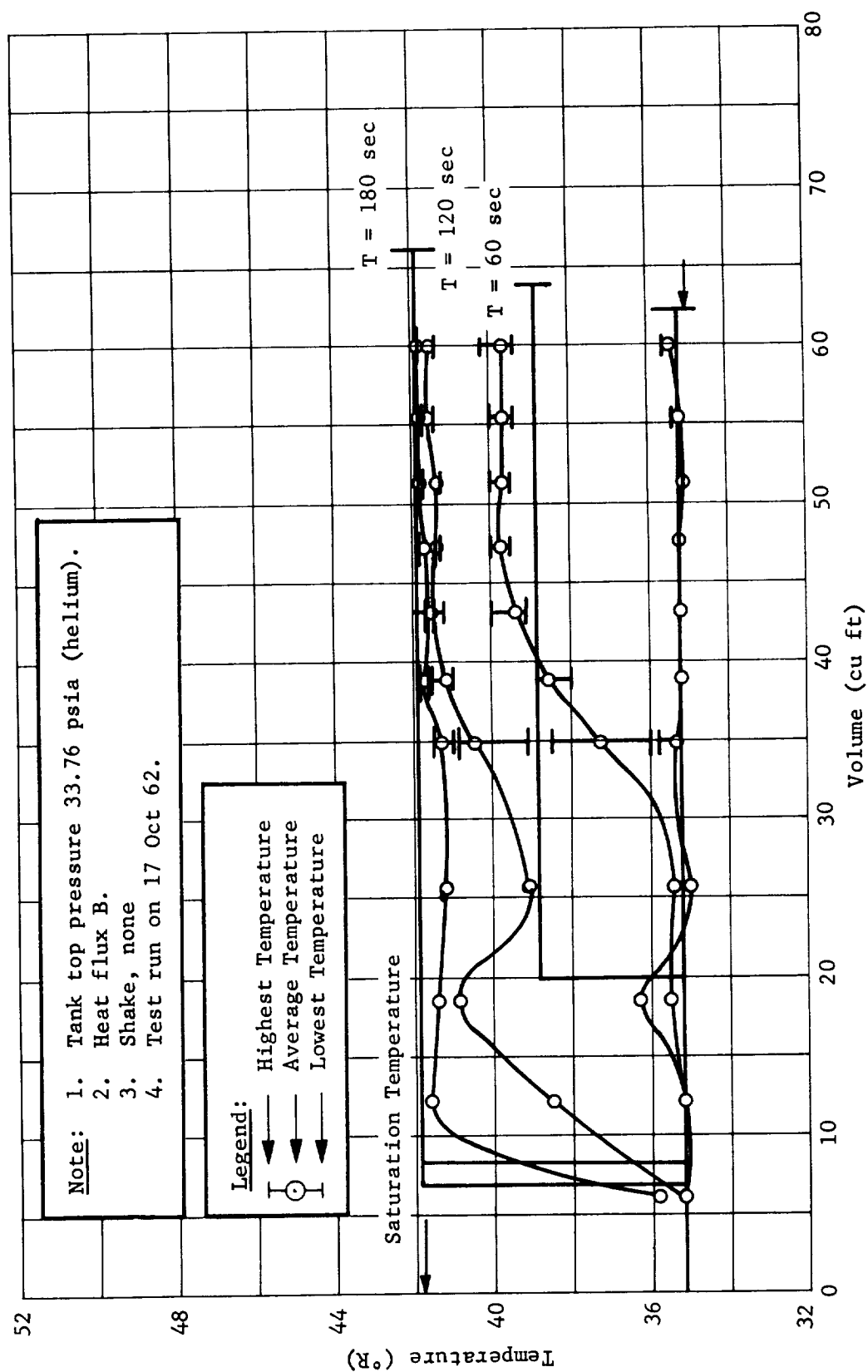


Fig. 35 Stratification Temperature Profile, Test No. 3

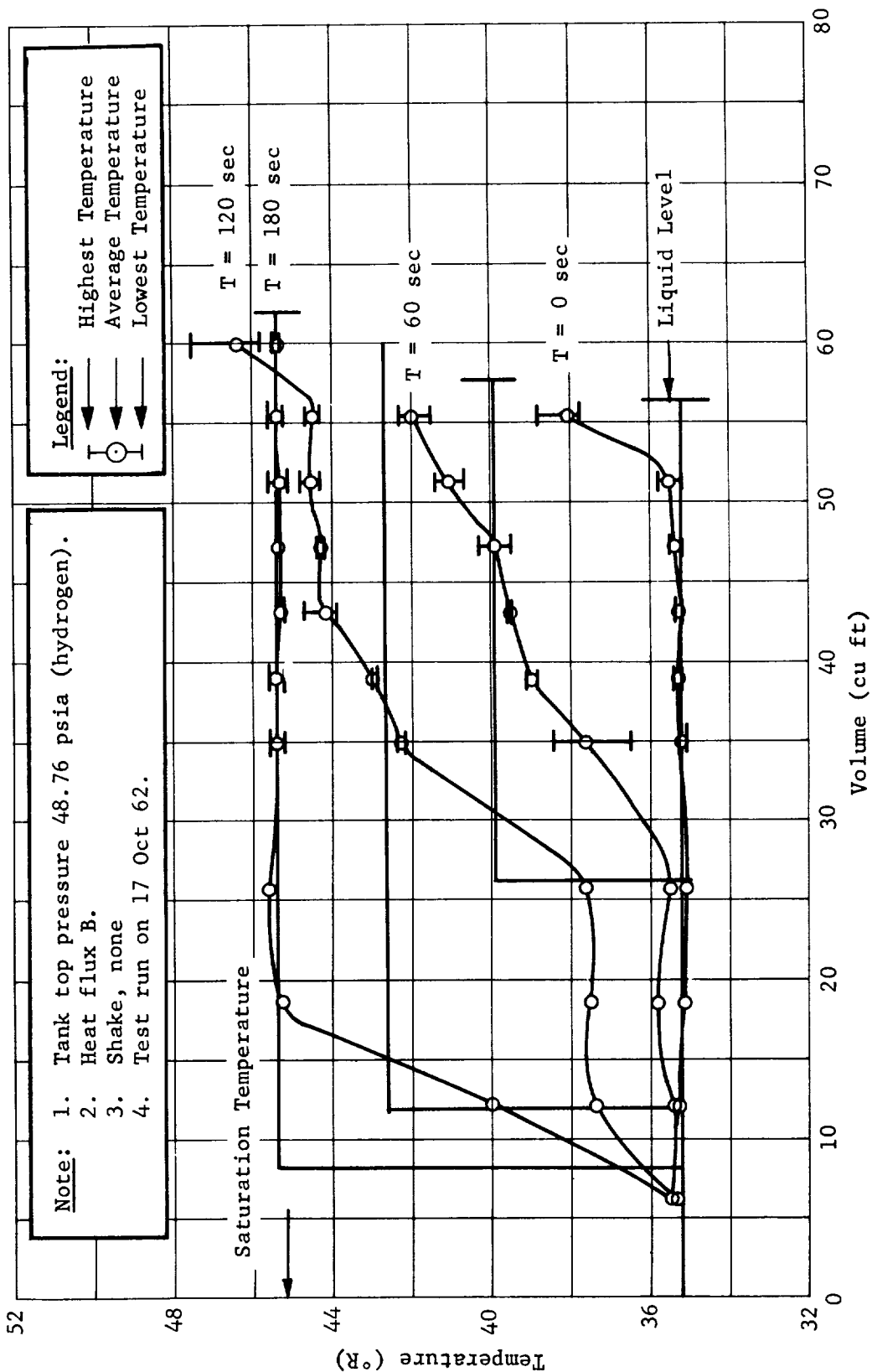


Fig. 37 Stratification Temperature Profile, Test No. 5

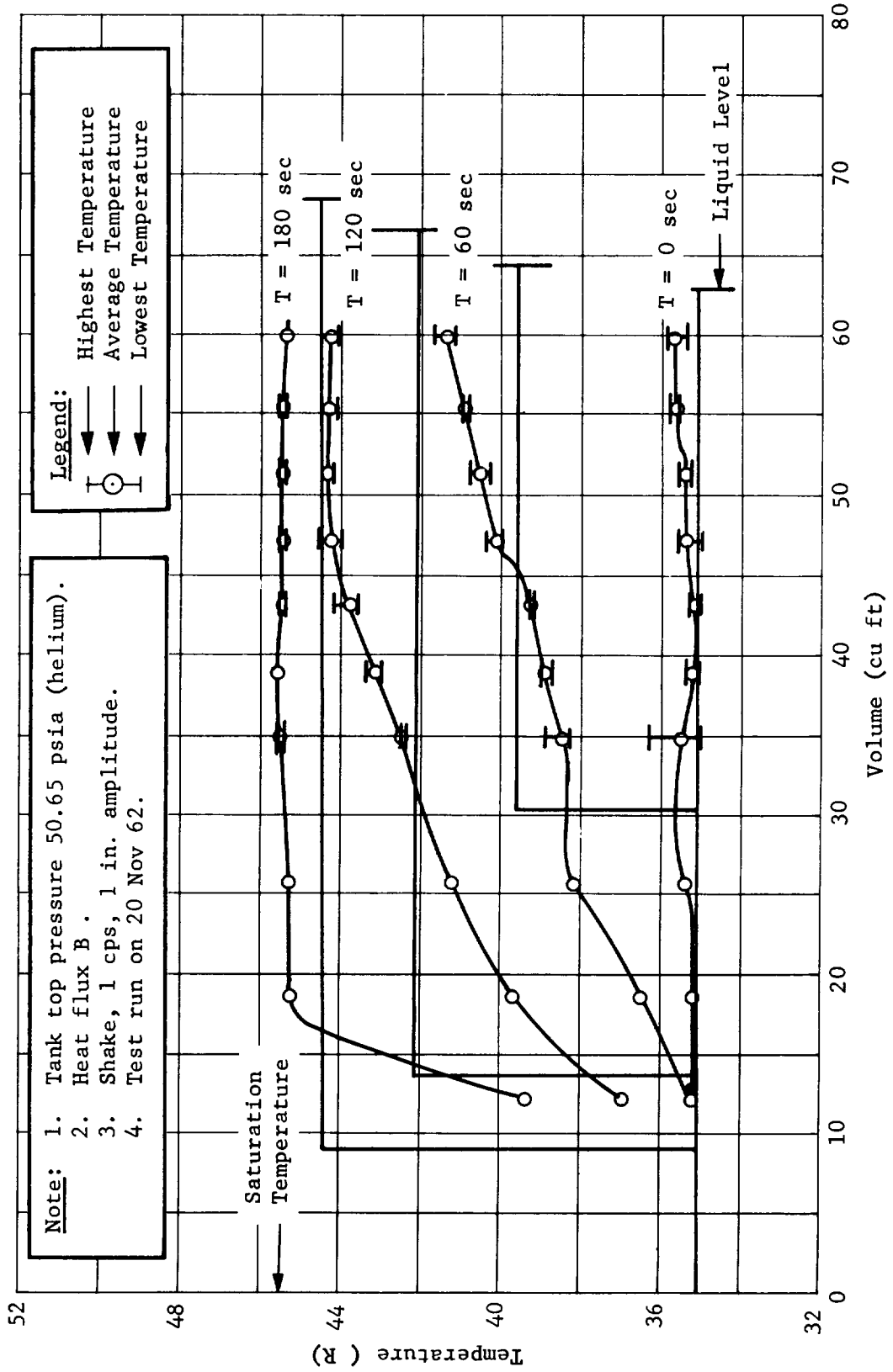


Fig. 38 Stratification Temperature Profile, Test No. 6

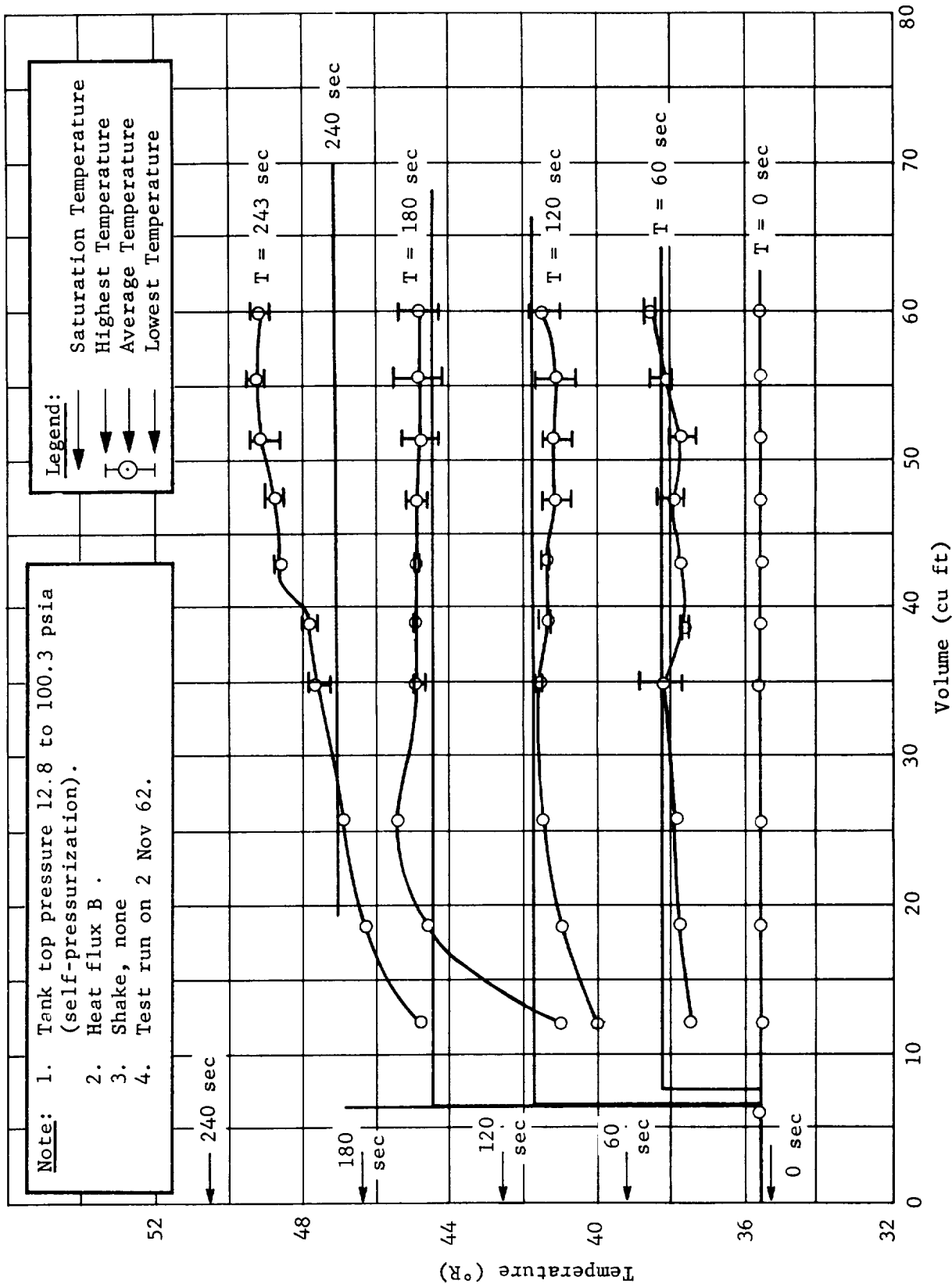


Fig. 39 Stratification Temperature Profile, Test No. 7

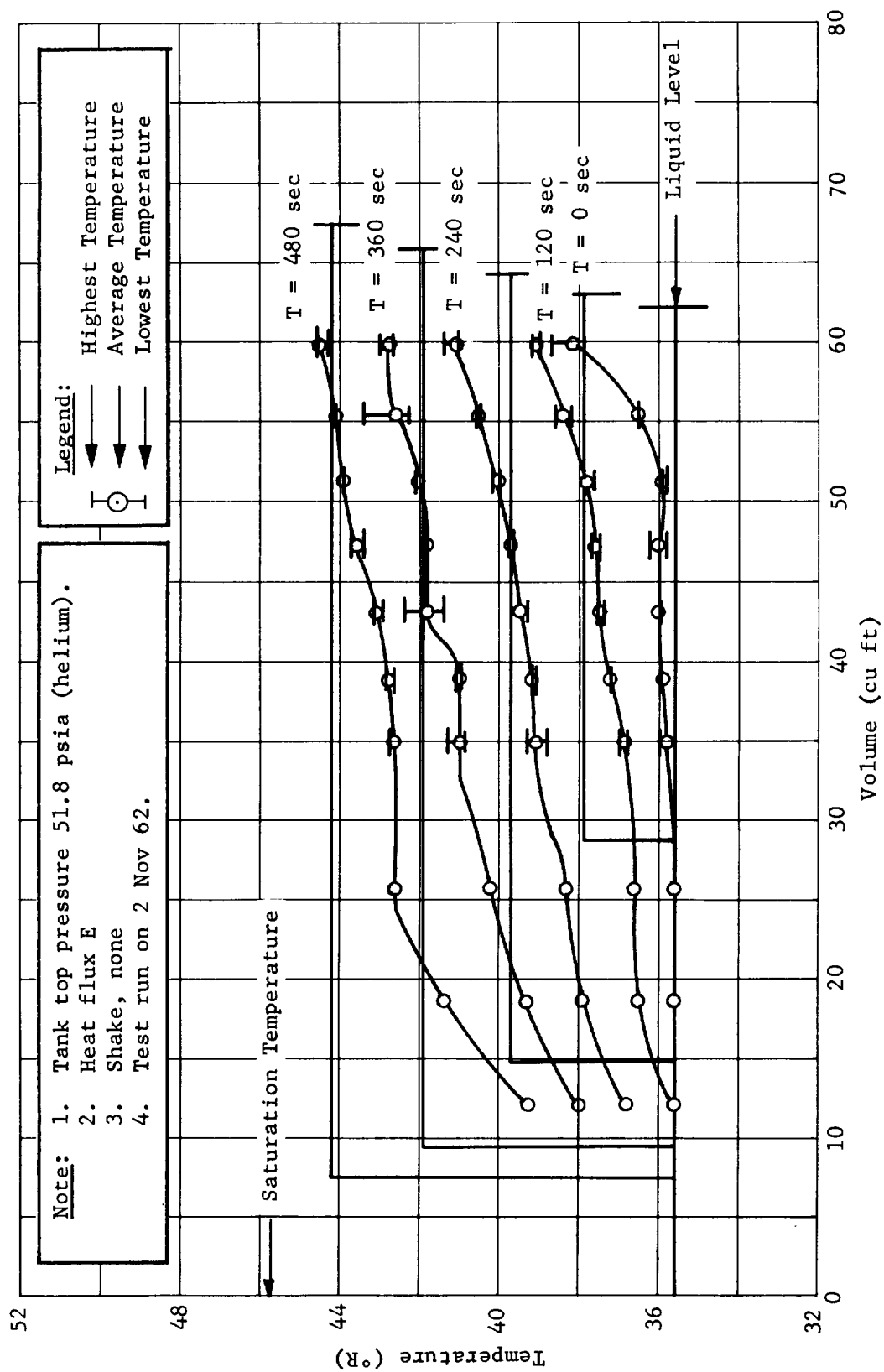


Fig. 40 Stratification Temperature Profile, Test No. 8

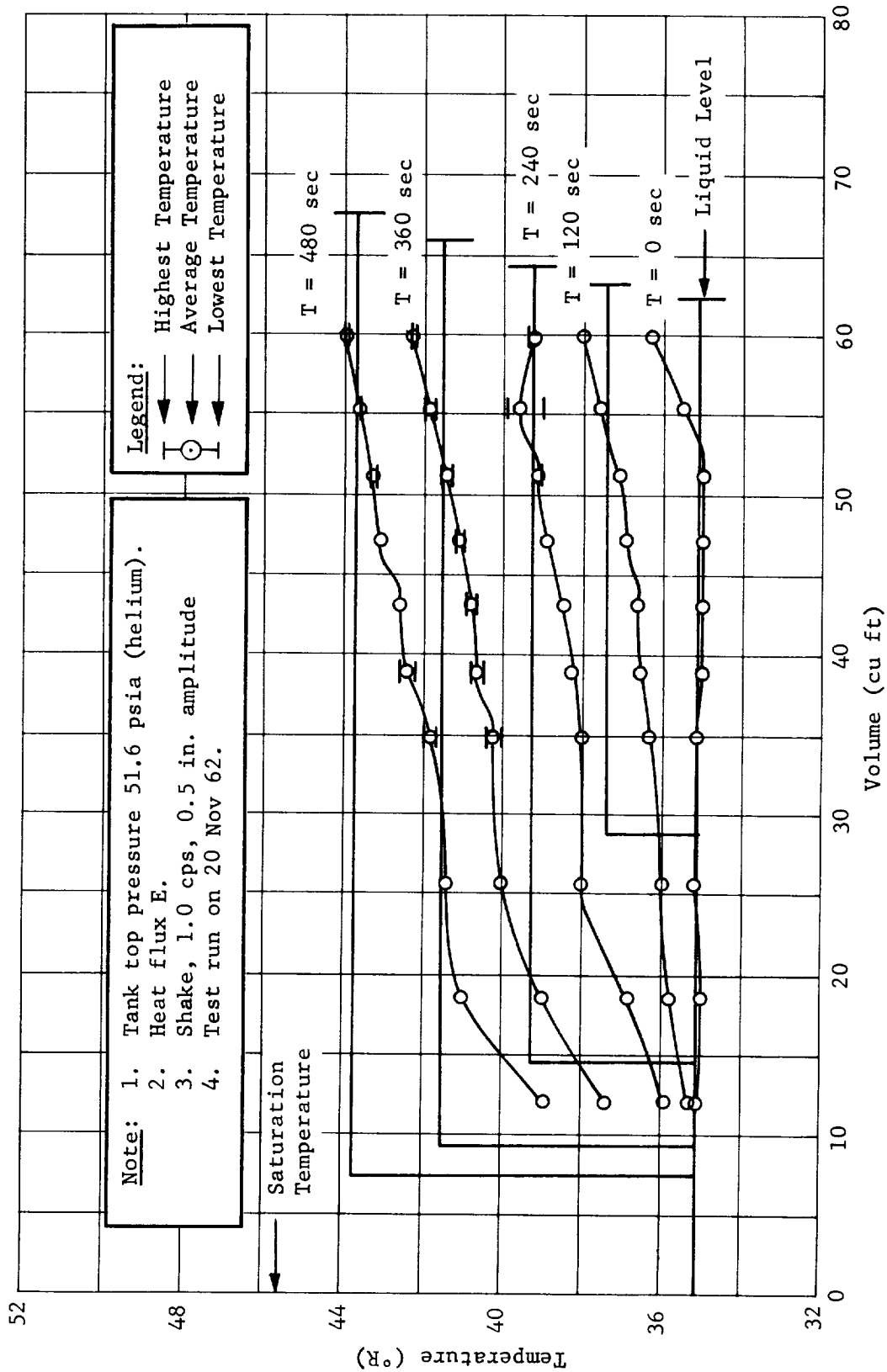


Fig. 41 Stratification Temperature Profile, Test No. 9

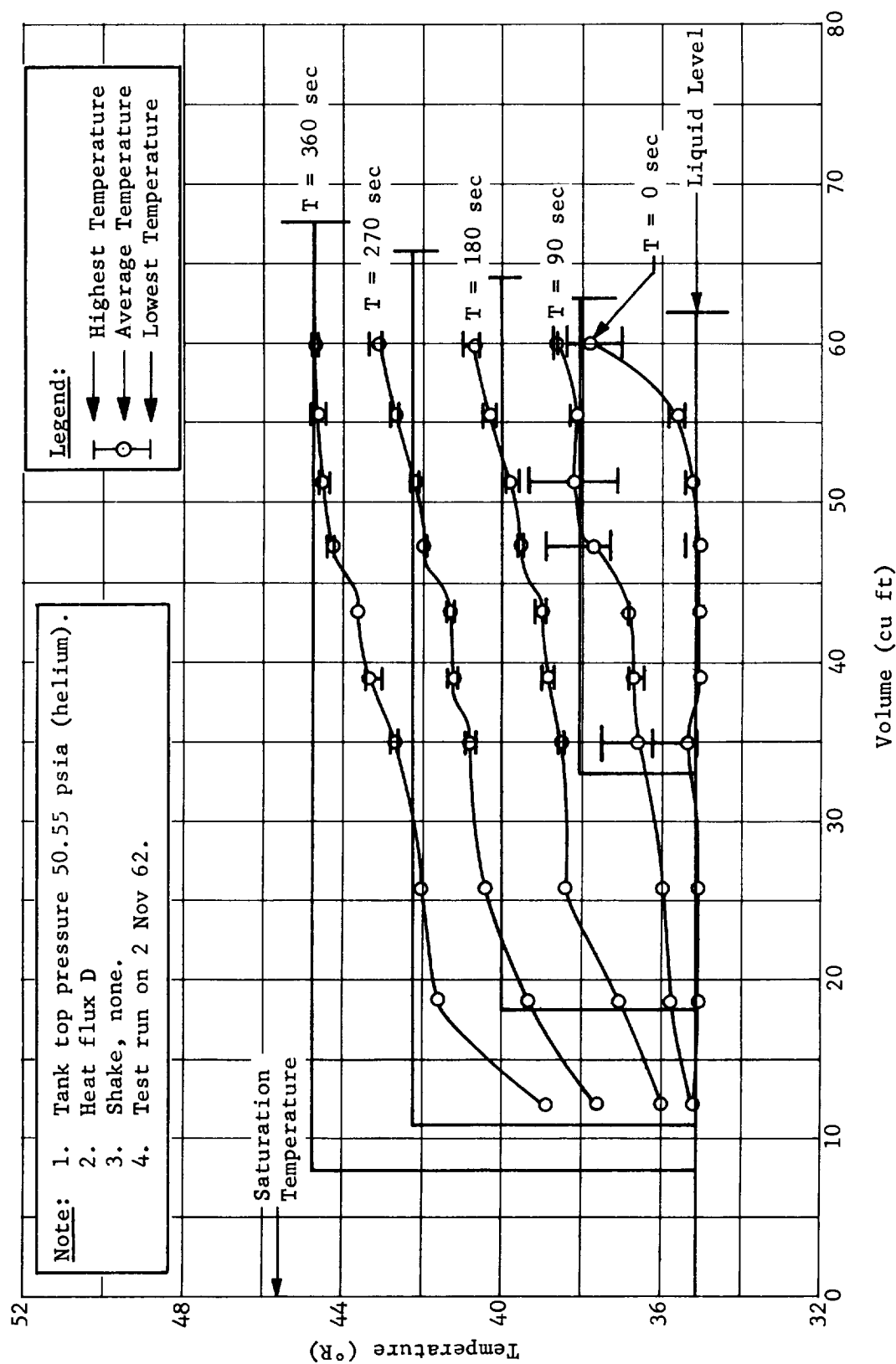


Fig. 42 Stratification Temperature Profile, Test No. 10

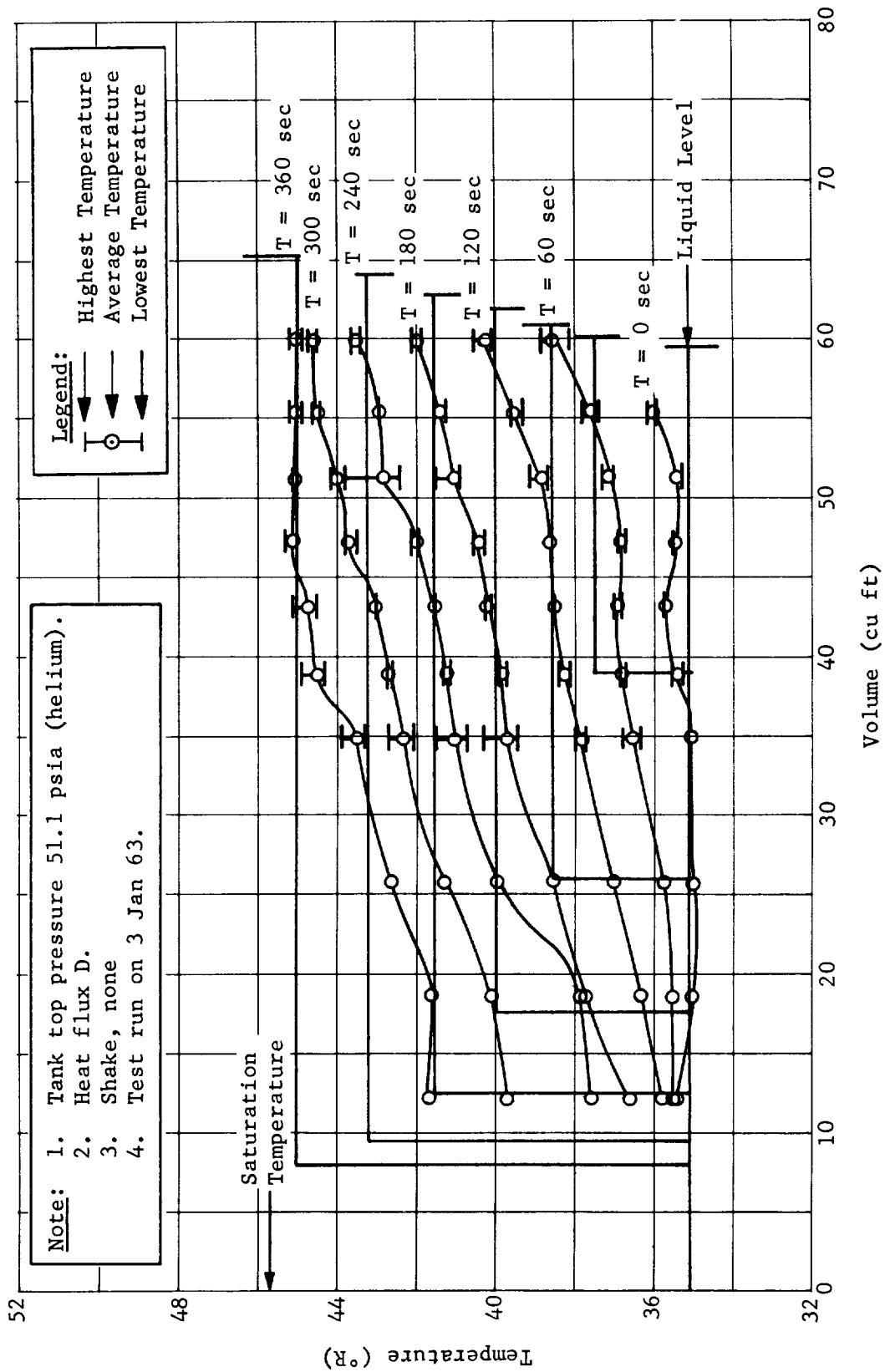


Fig. 43 Stratification Temperature Profile, Test No. 10A

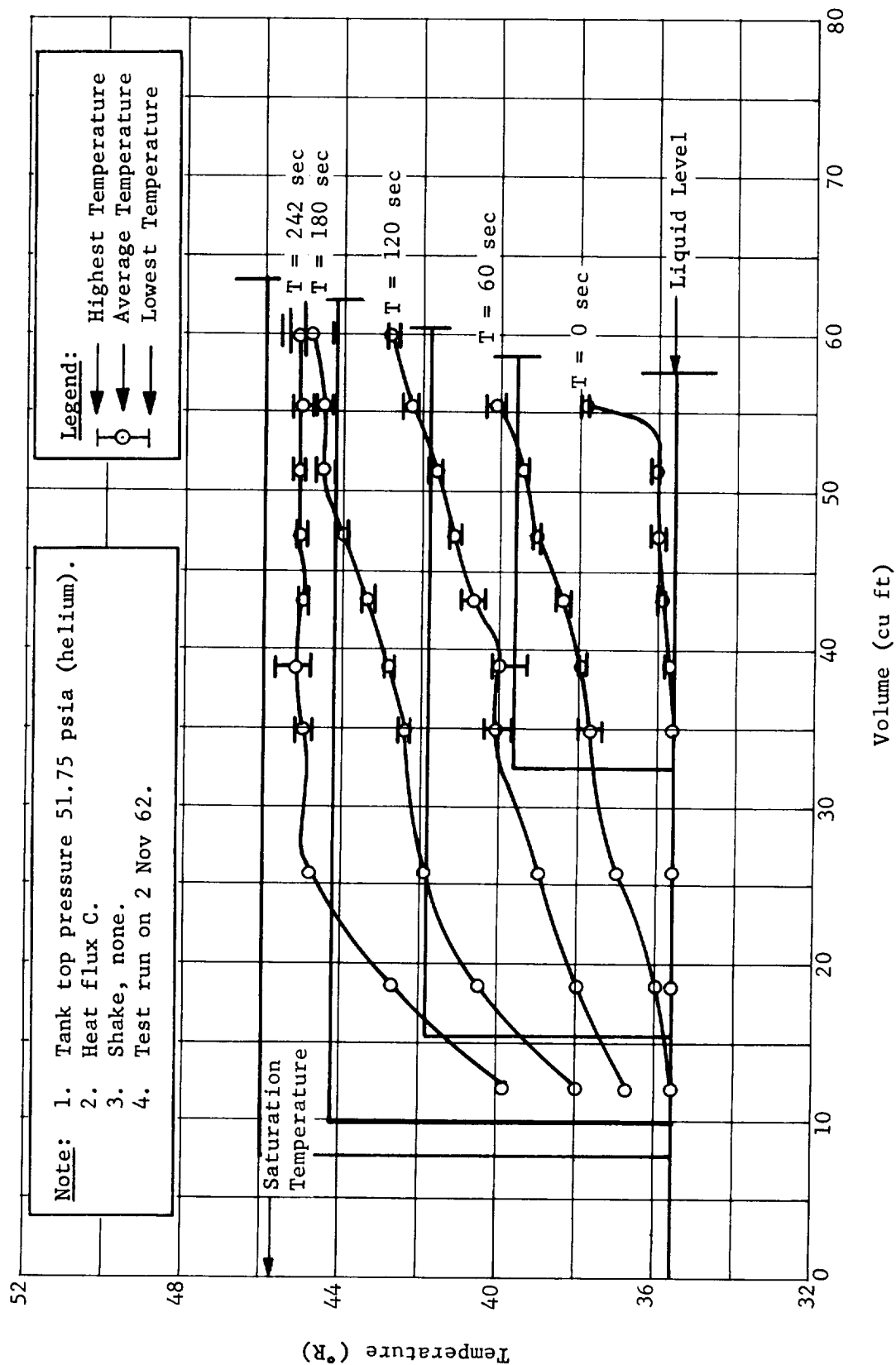


Fig. 44 Stratification Temperature Profile, Test No. 11

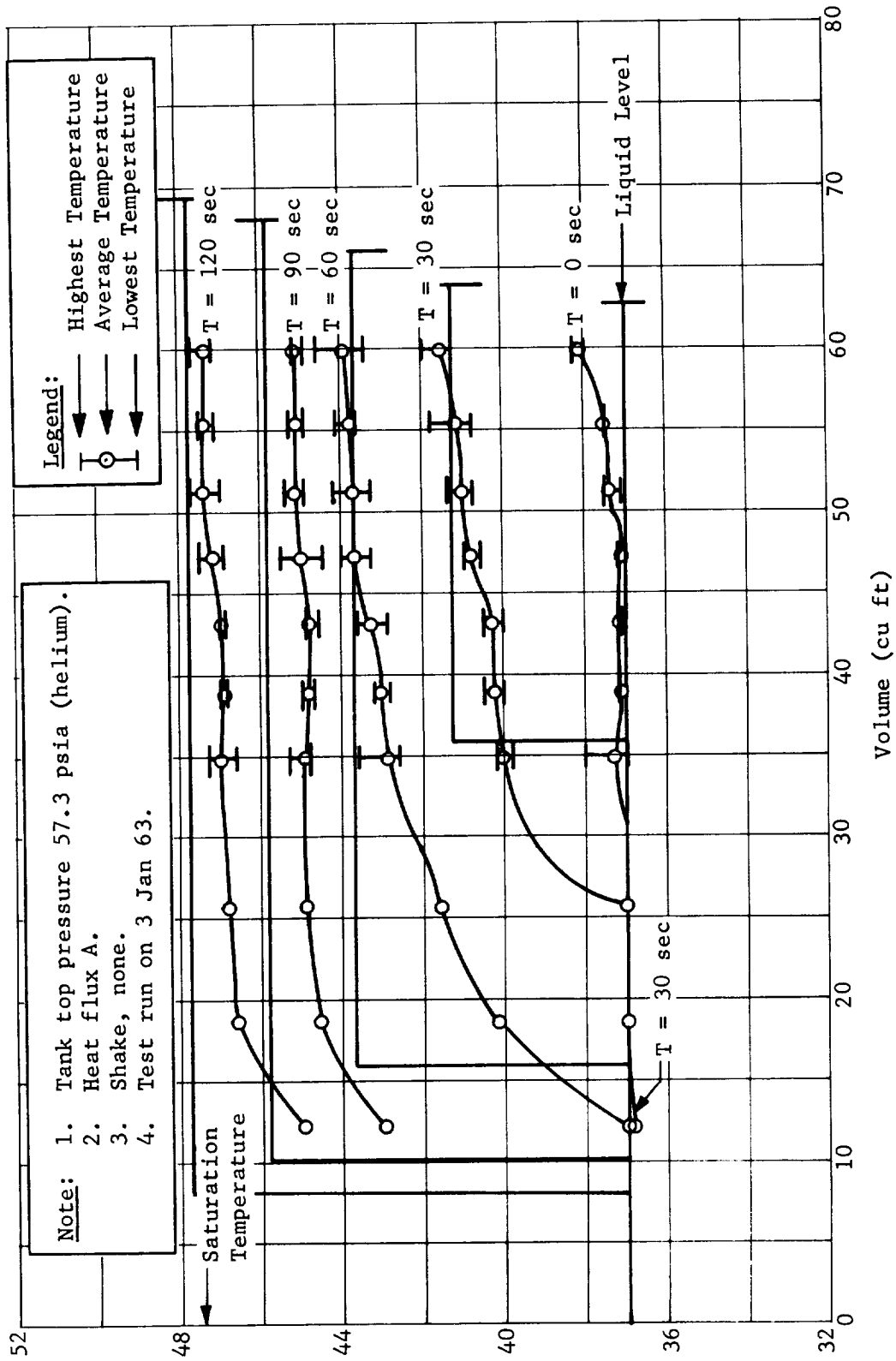


Fig. 45 Stratification Temperature Profile, Test No. 12

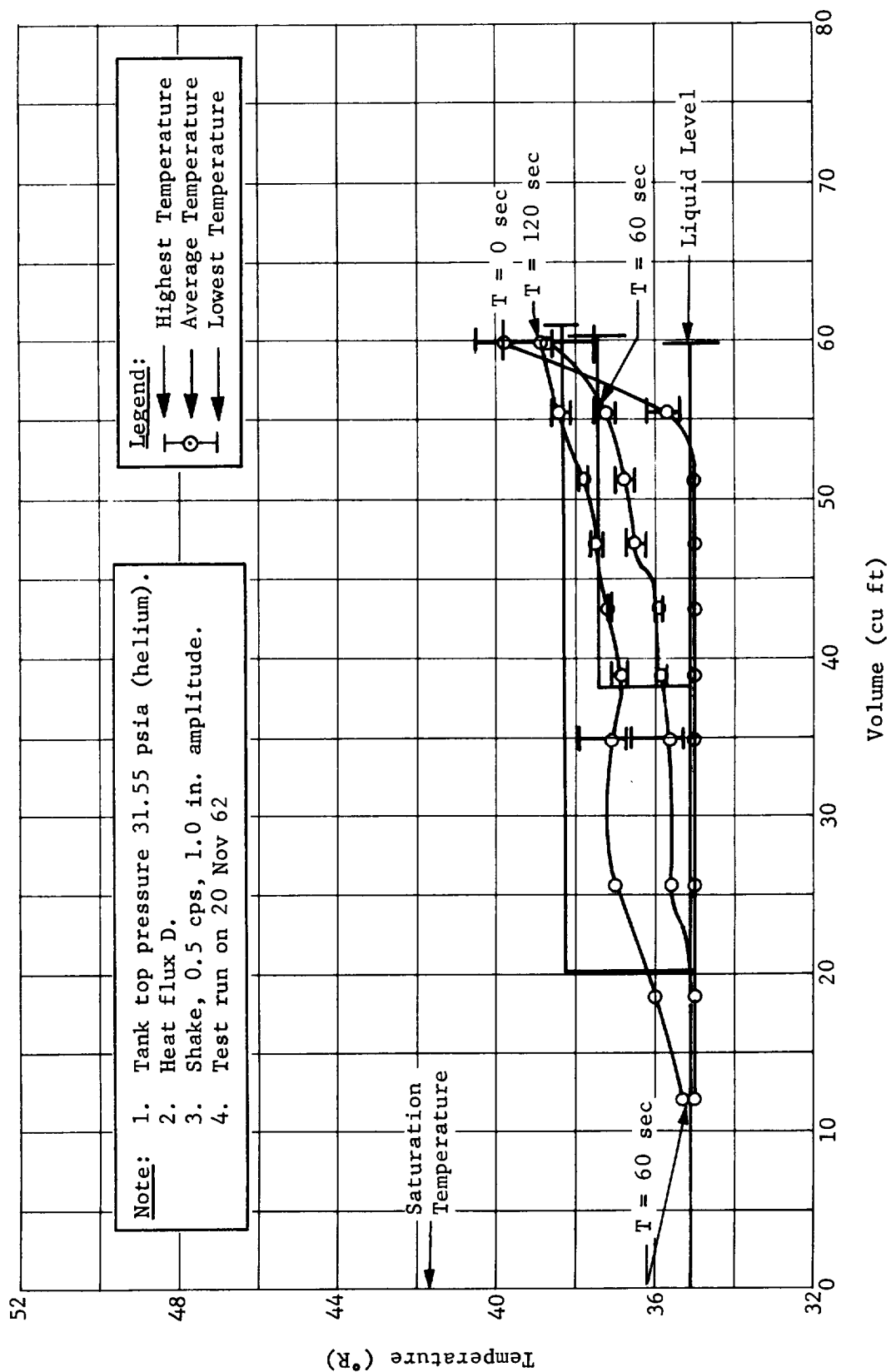


Fig. 46 Stratification Temperature Profile, Test No. 13

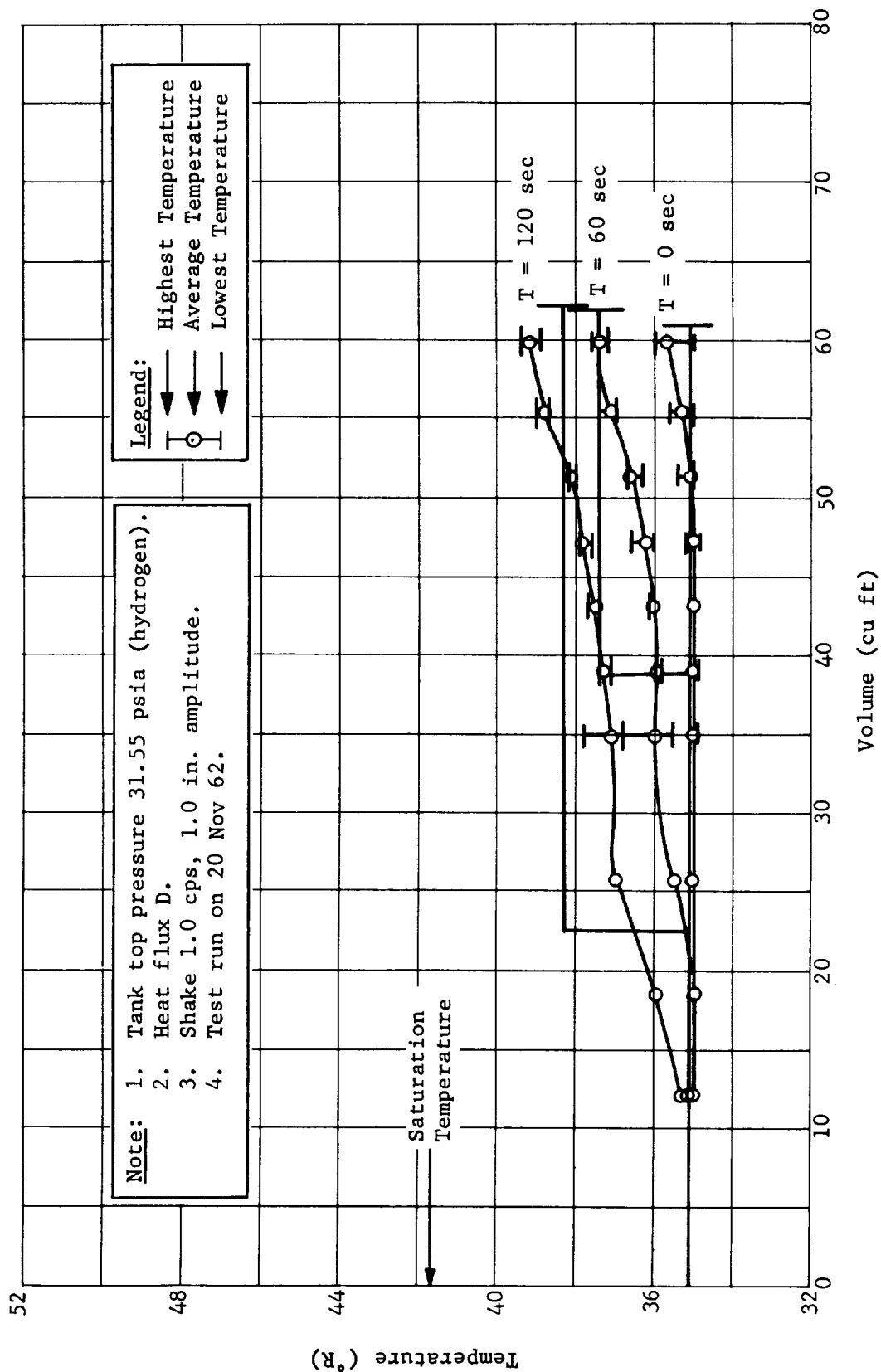


Fig. 47 Stratification Temperature Profile, Test No. 14

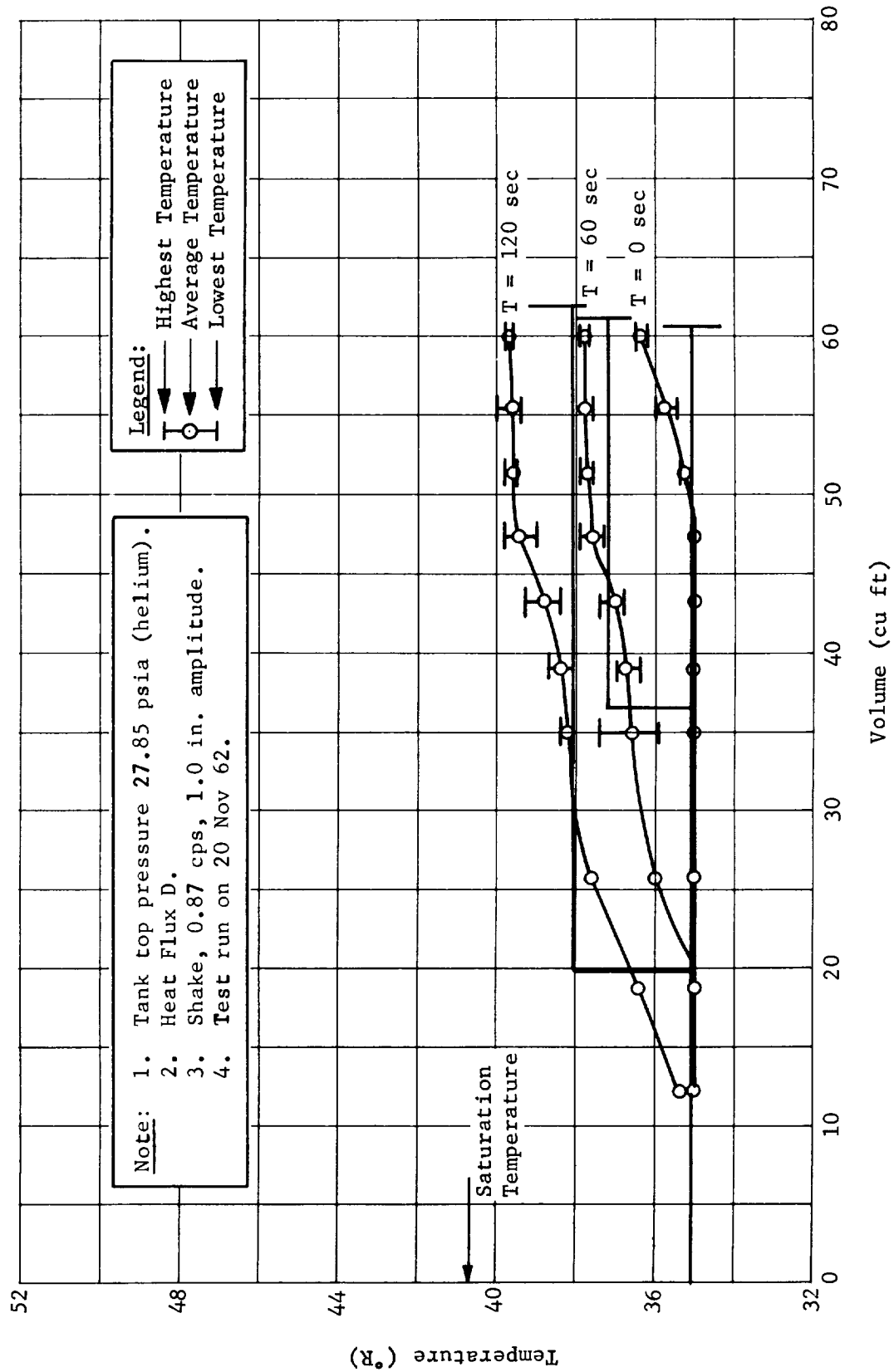


Fig. 48 Stratification Temperature Profile, Test No. 15

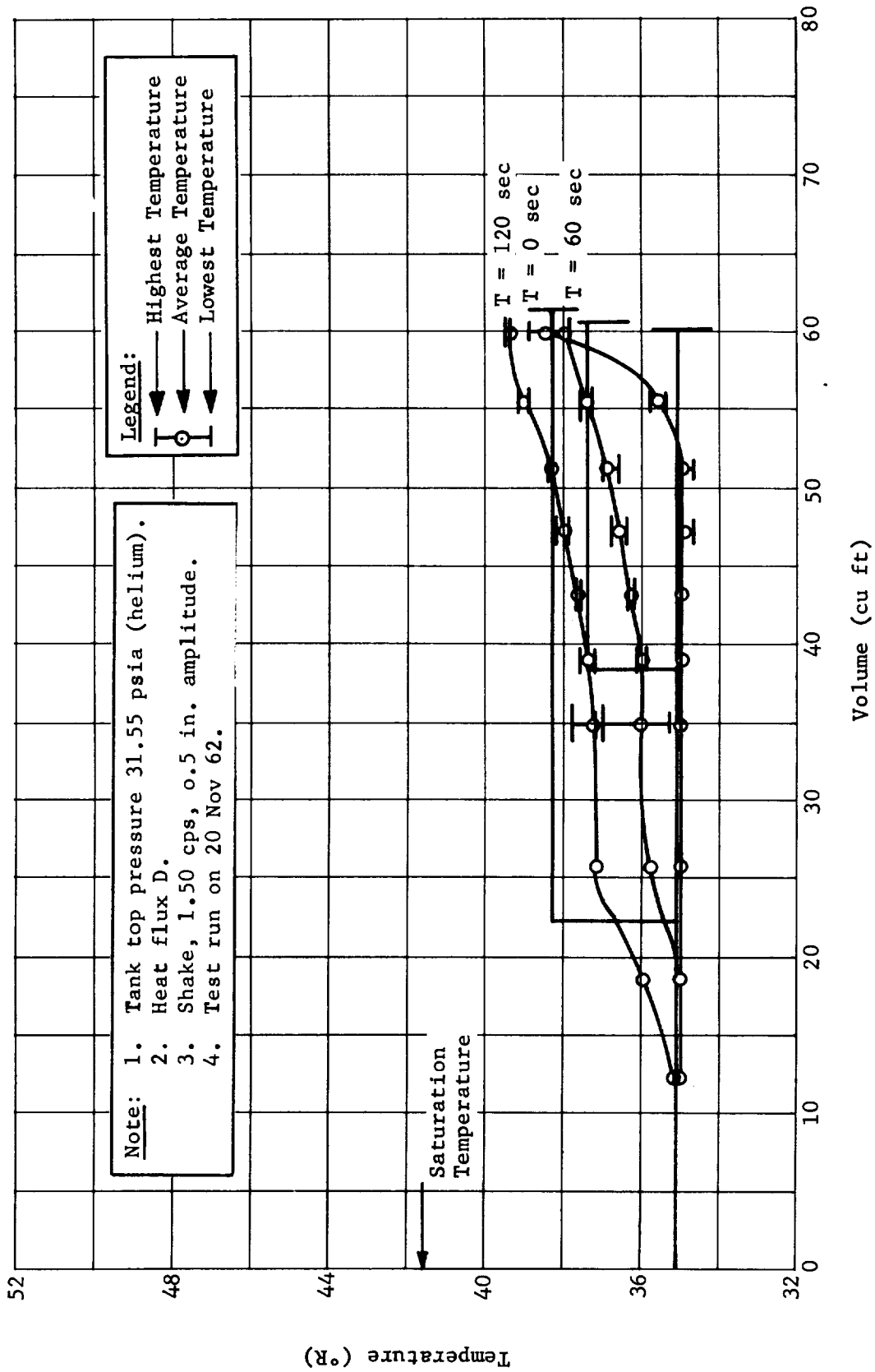


Fig. 49 Stratification Temperature Profile, Test No. 16

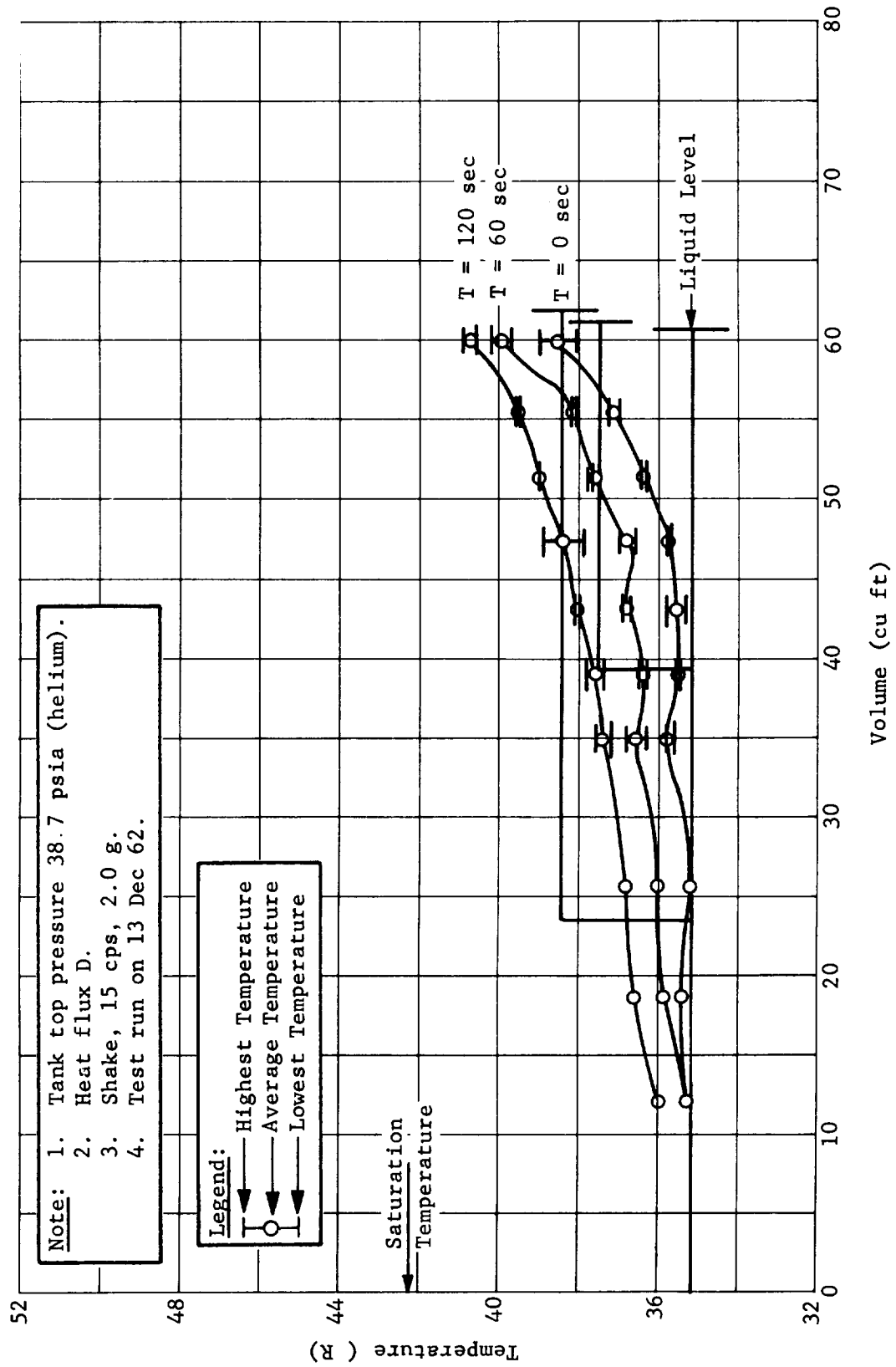


Fig. 50 Stratification Temperature Profile, Test No. 17

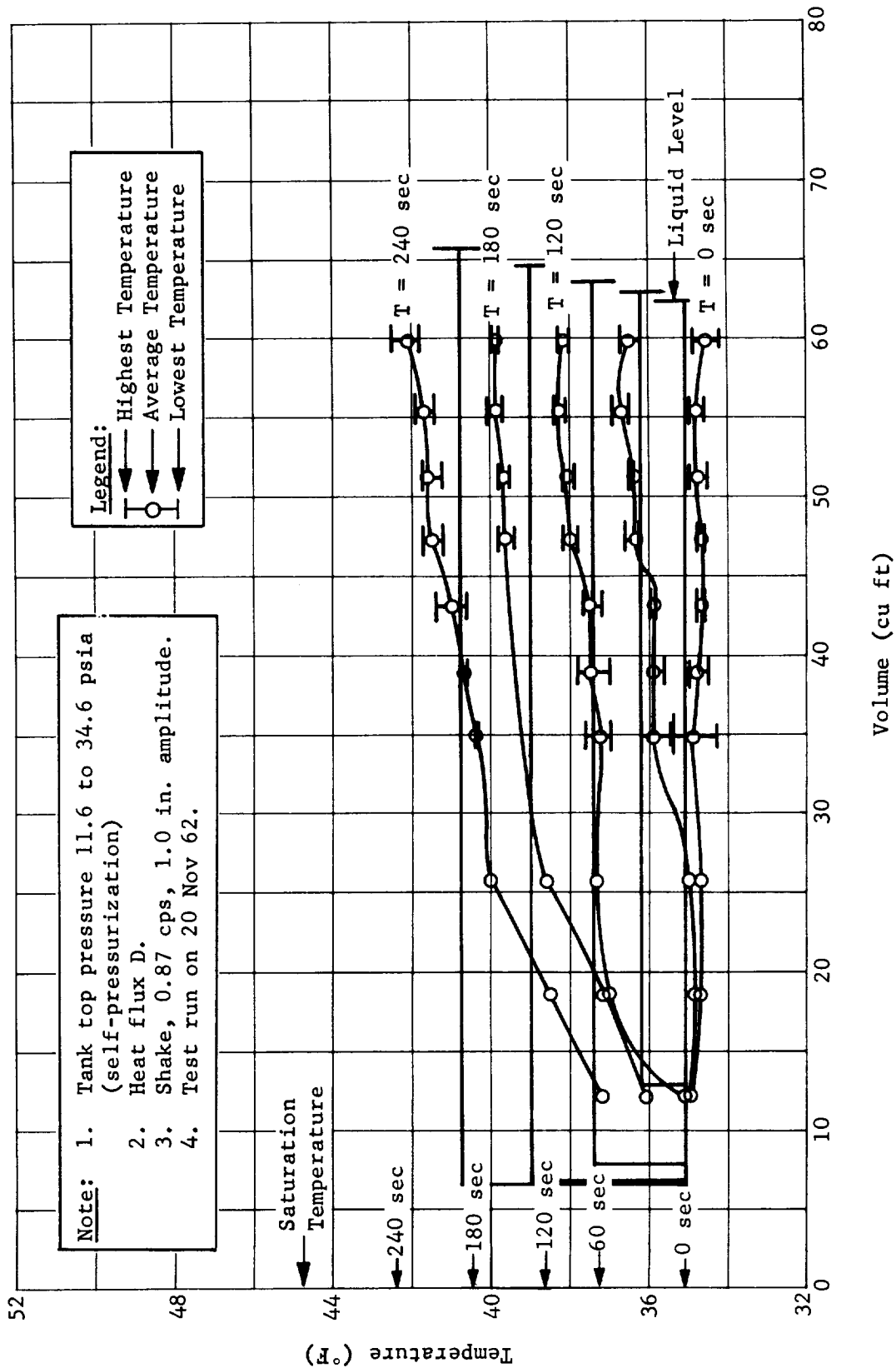


Fig. 51 Stratification Temperature Profile, Test No. 22

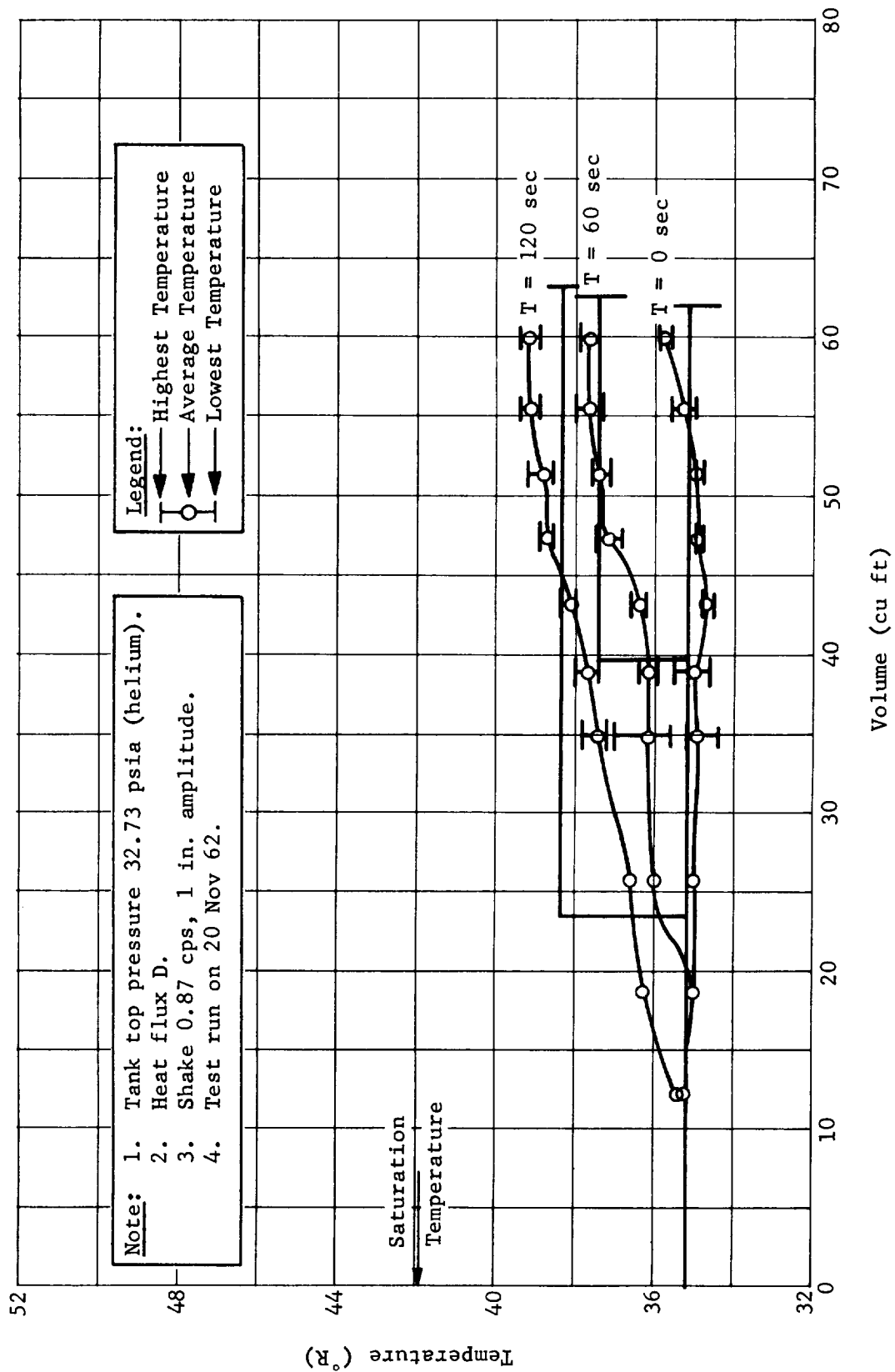


Fig. 52 Stratification Temperature Profile, Test No. 23

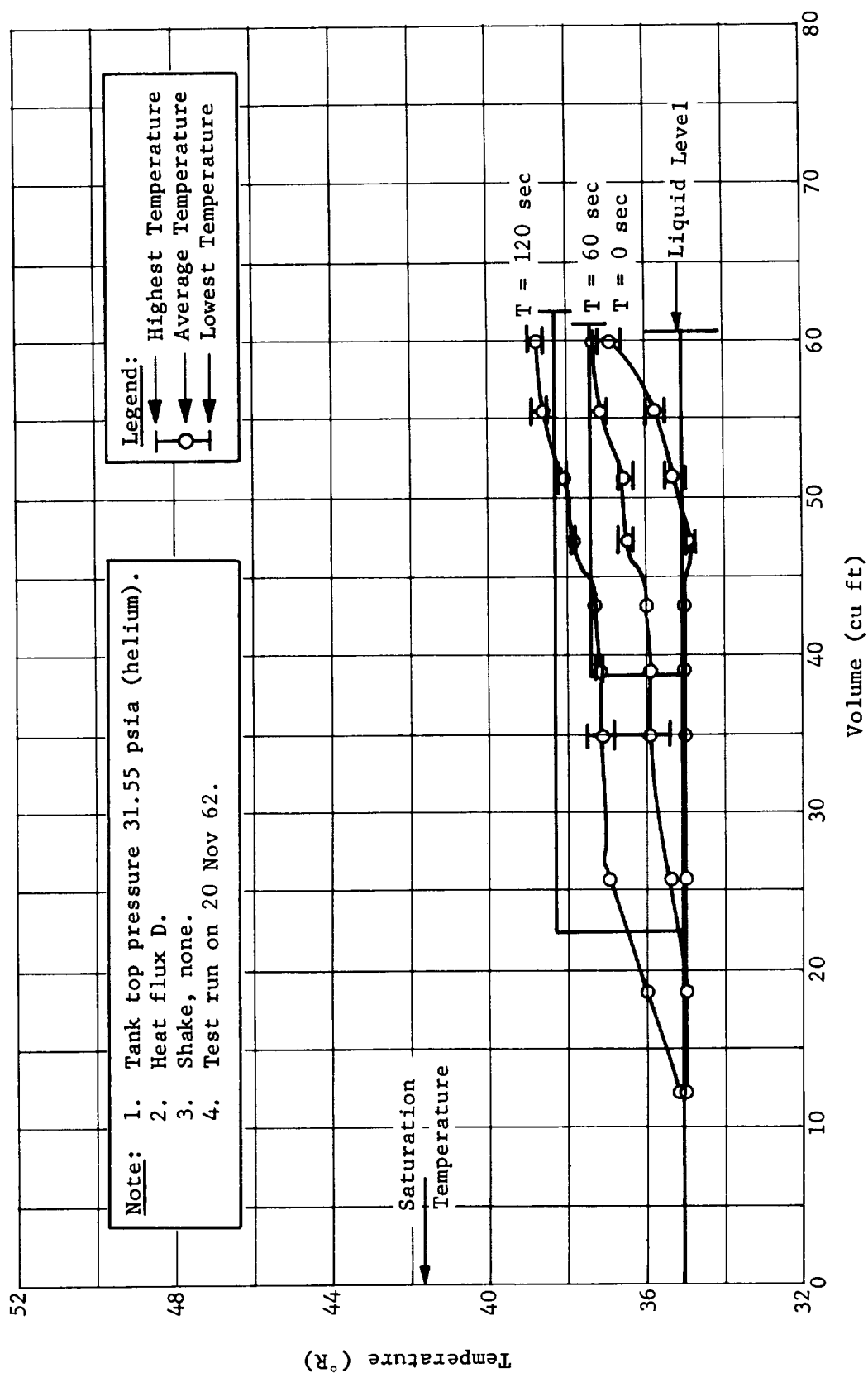


Fig. 53 Stratification Temperature Profile, Test No. 24

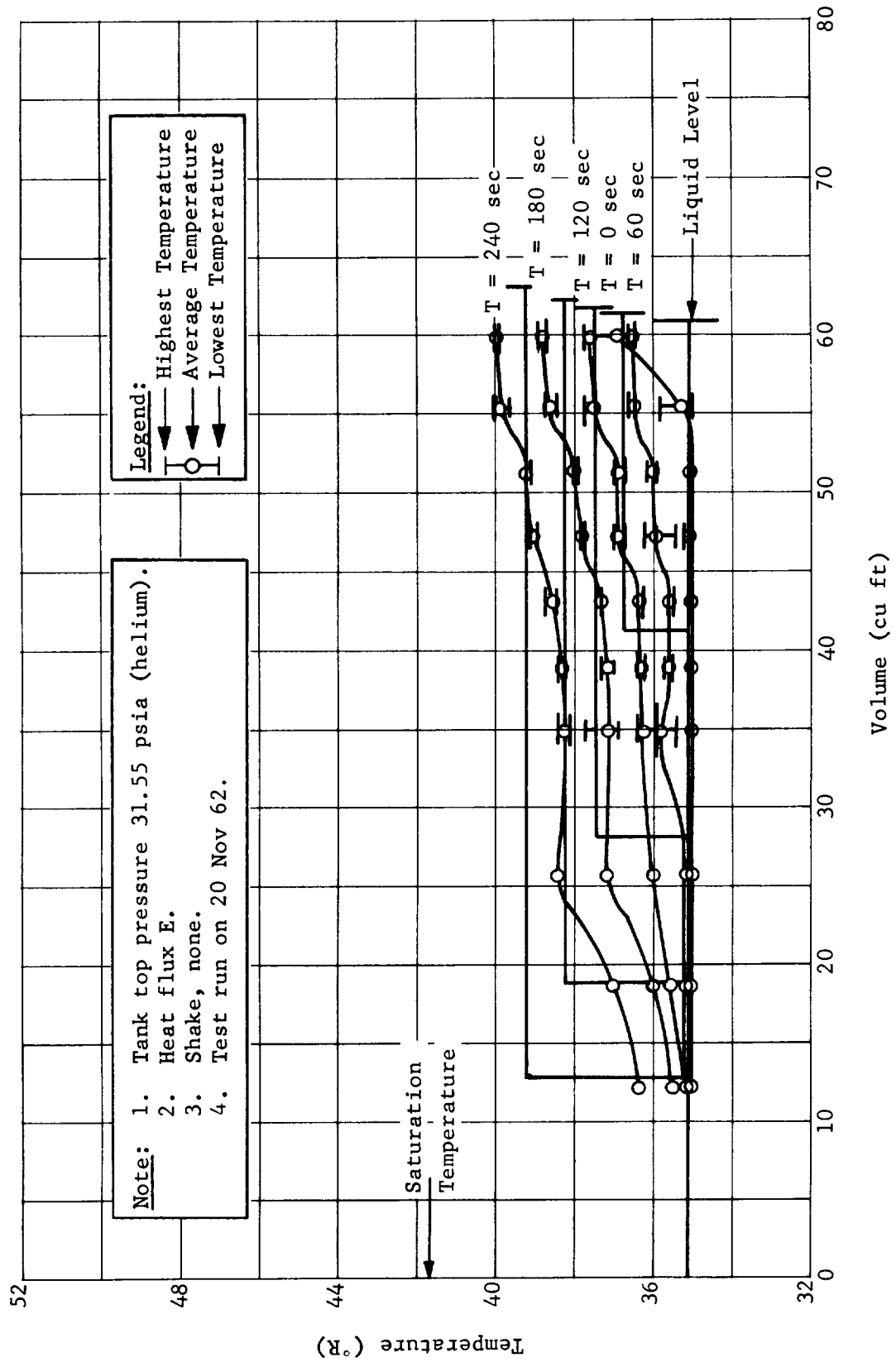


Fig. 54 Stratification Temperature Profile, Test No. 25

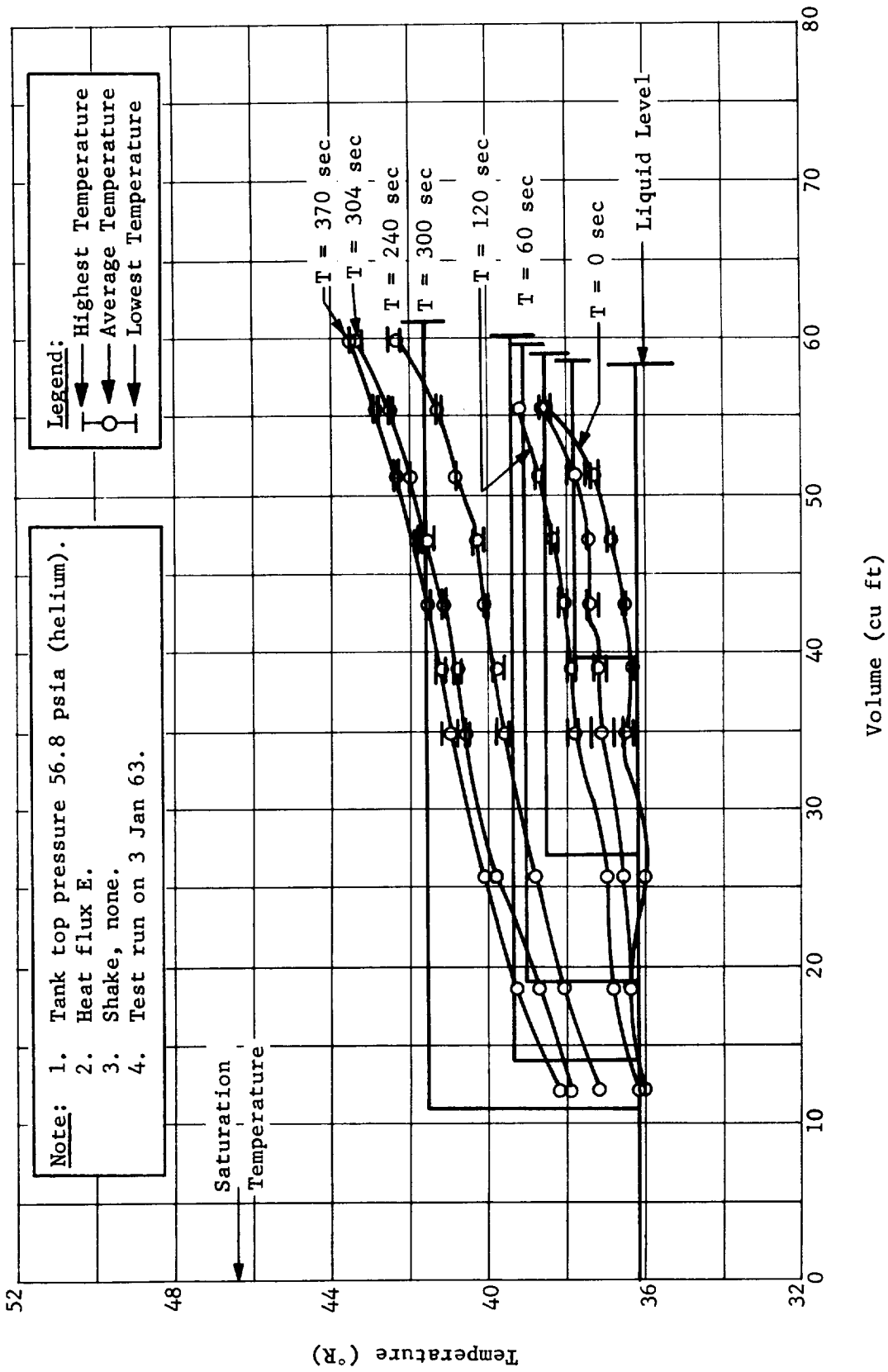


Fig. 55 Stratification Temperature Profile, Test No. E

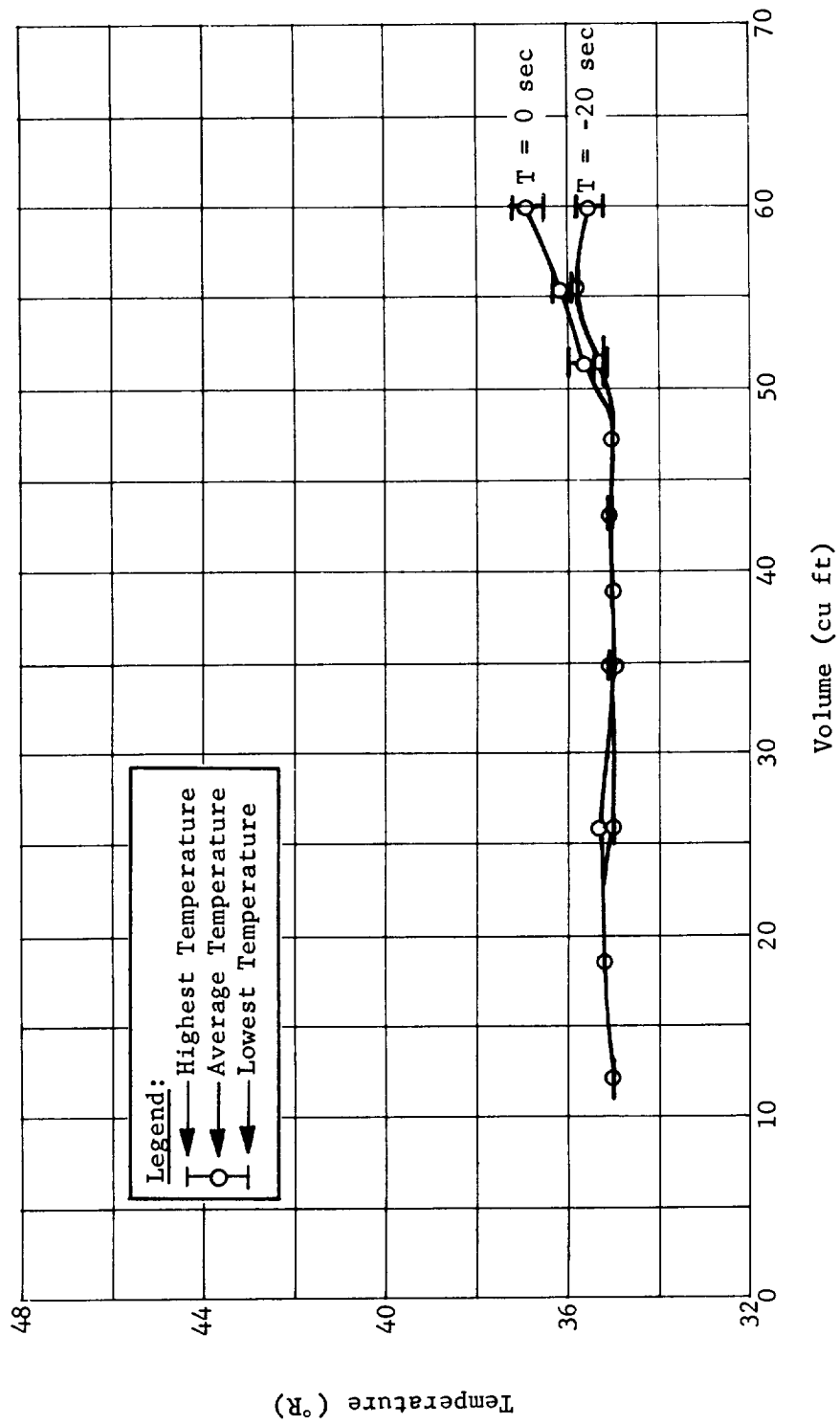


Fig. 56 Stratification Temperature Profile, Test No. 18, Outflow

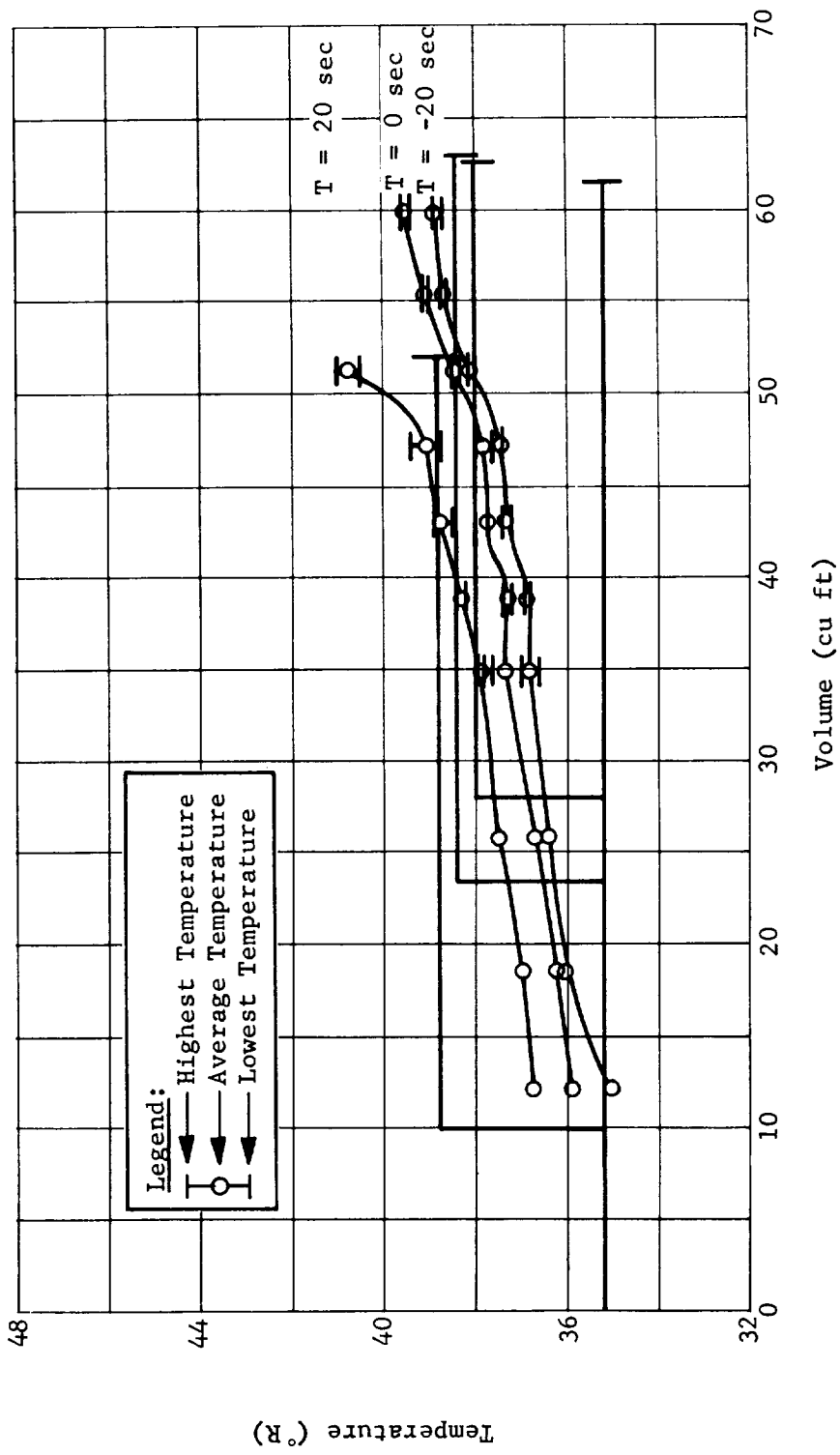


Fig. 57 Stratification Temperature Profile, Test No. 19, Outflow

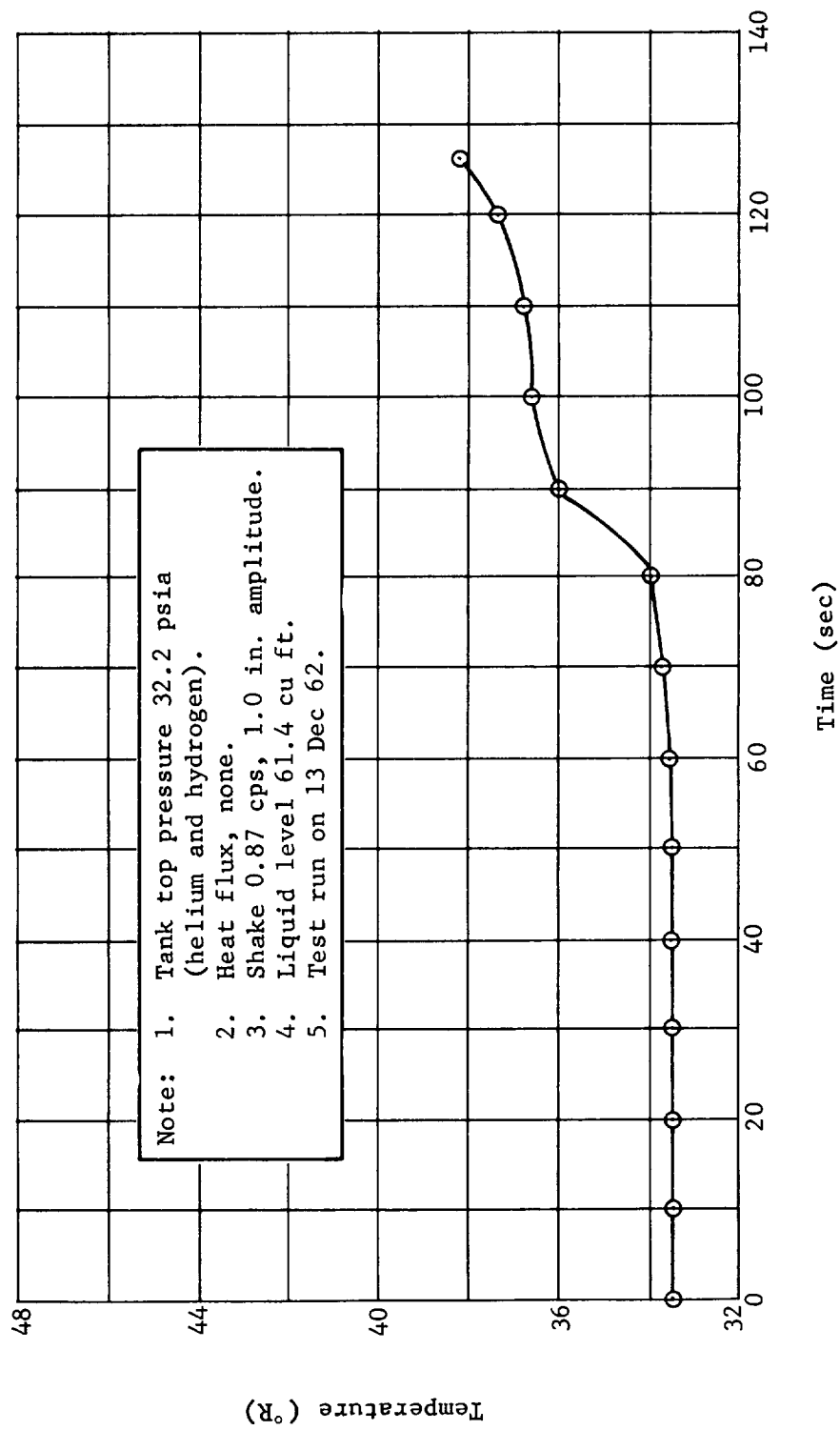


Fig. 58 Outflow Thermistor Temperatures, Test No. 18

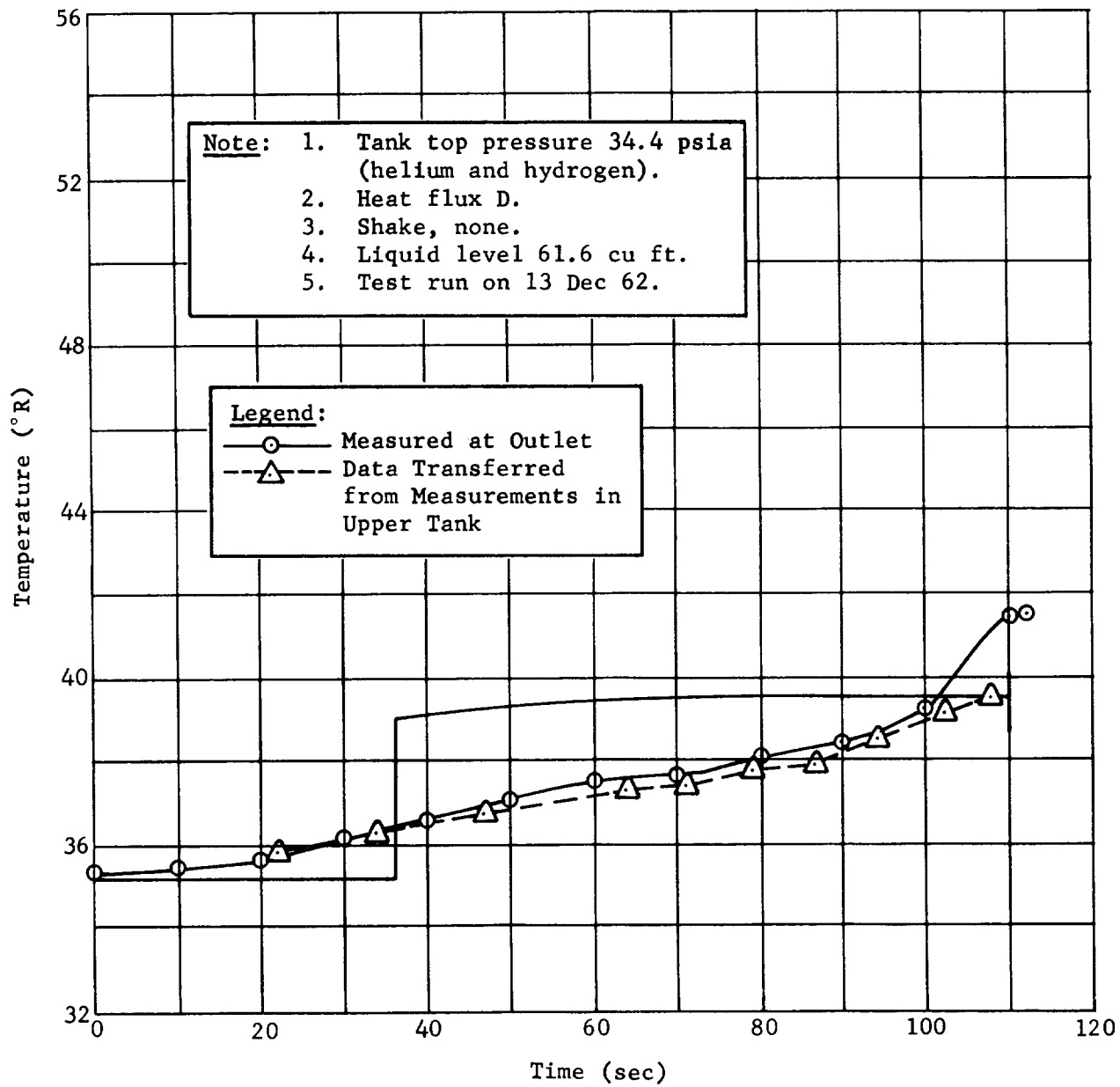


Fig. 59 Outflow Thermistor Temperatures, Test No. 19

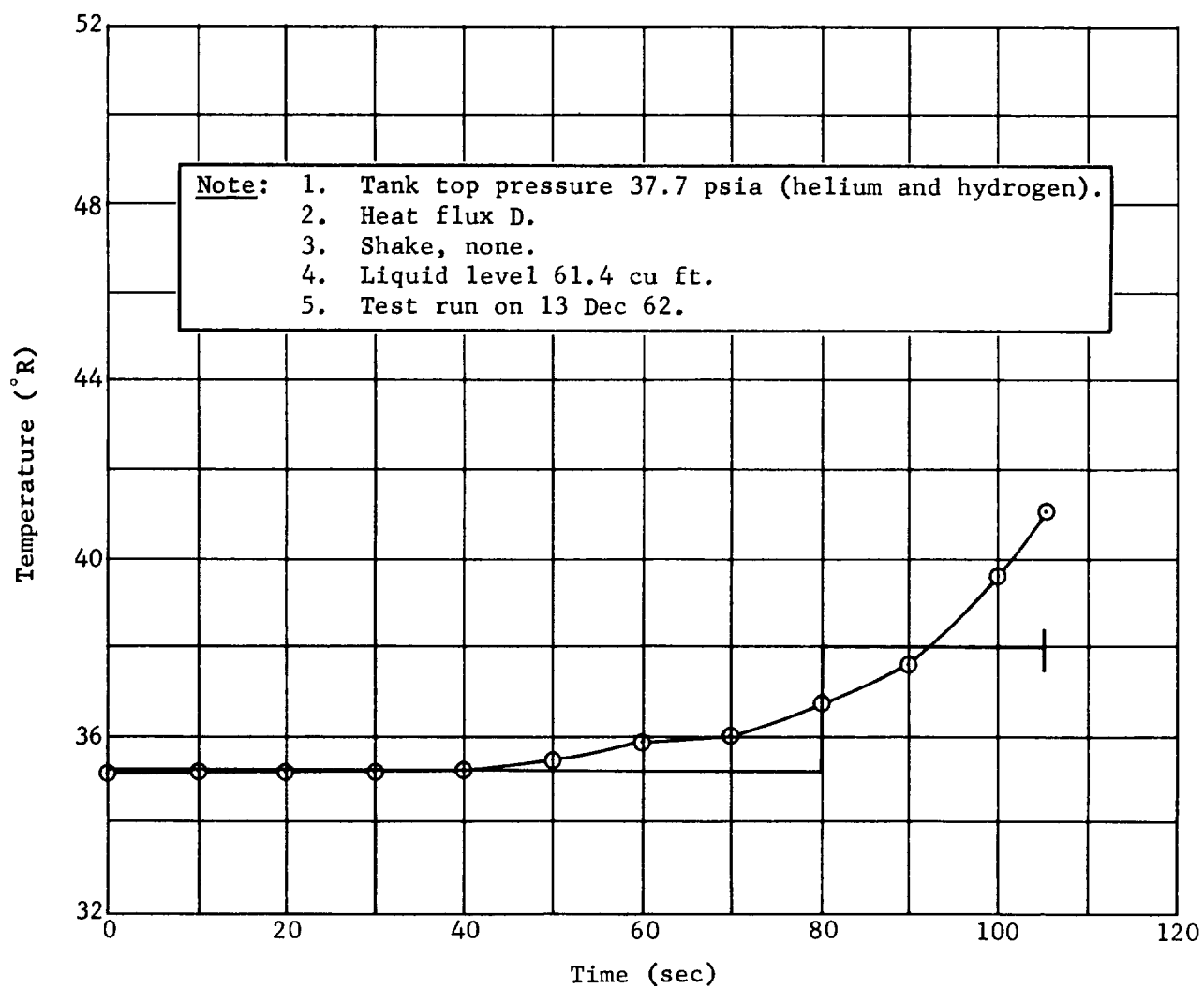


Fig. 60 Outflow Thermistor Temperatures, Test No. 20

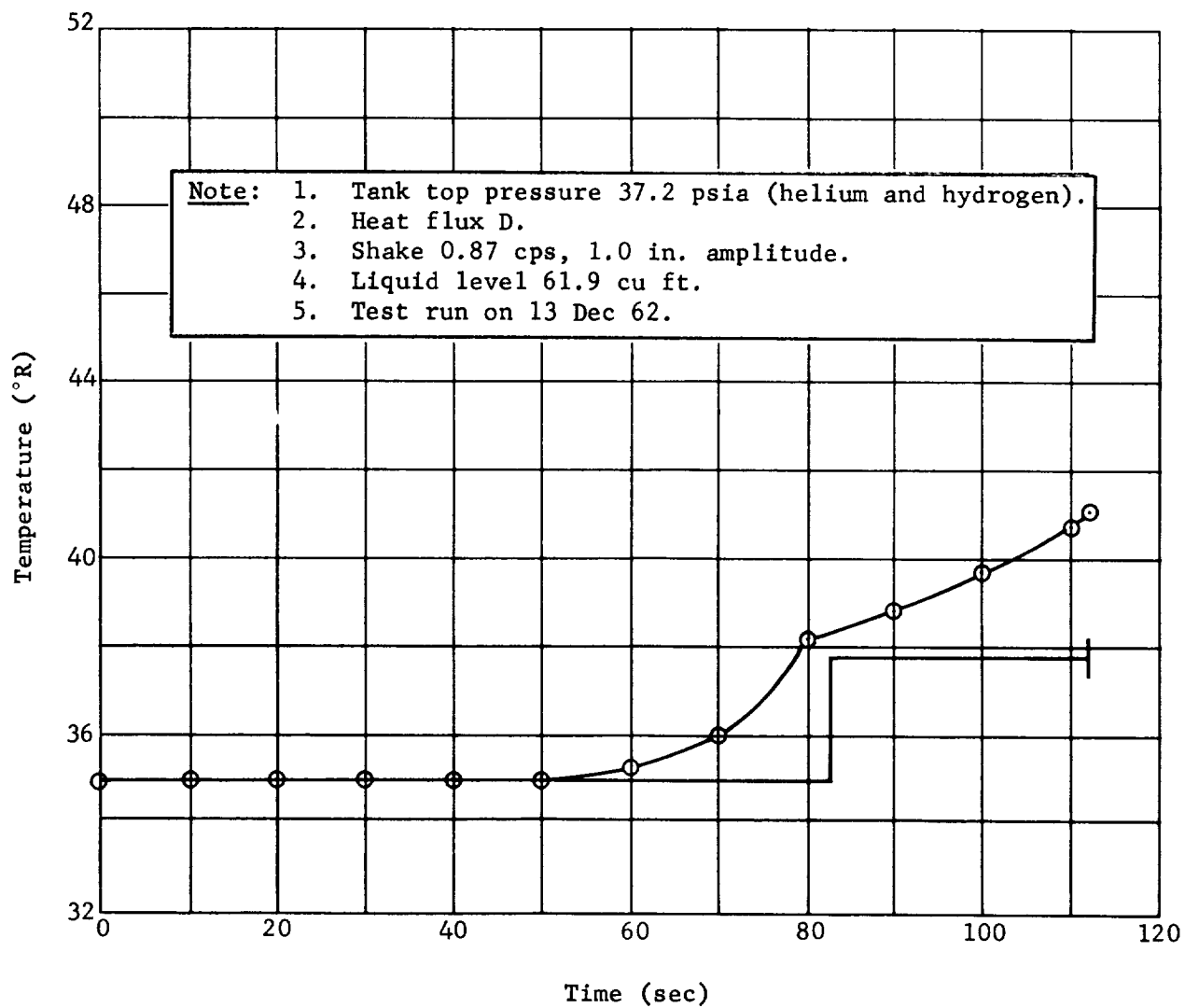


Fig. 61 Outflow Thermistor Temperatures, Test No. 21

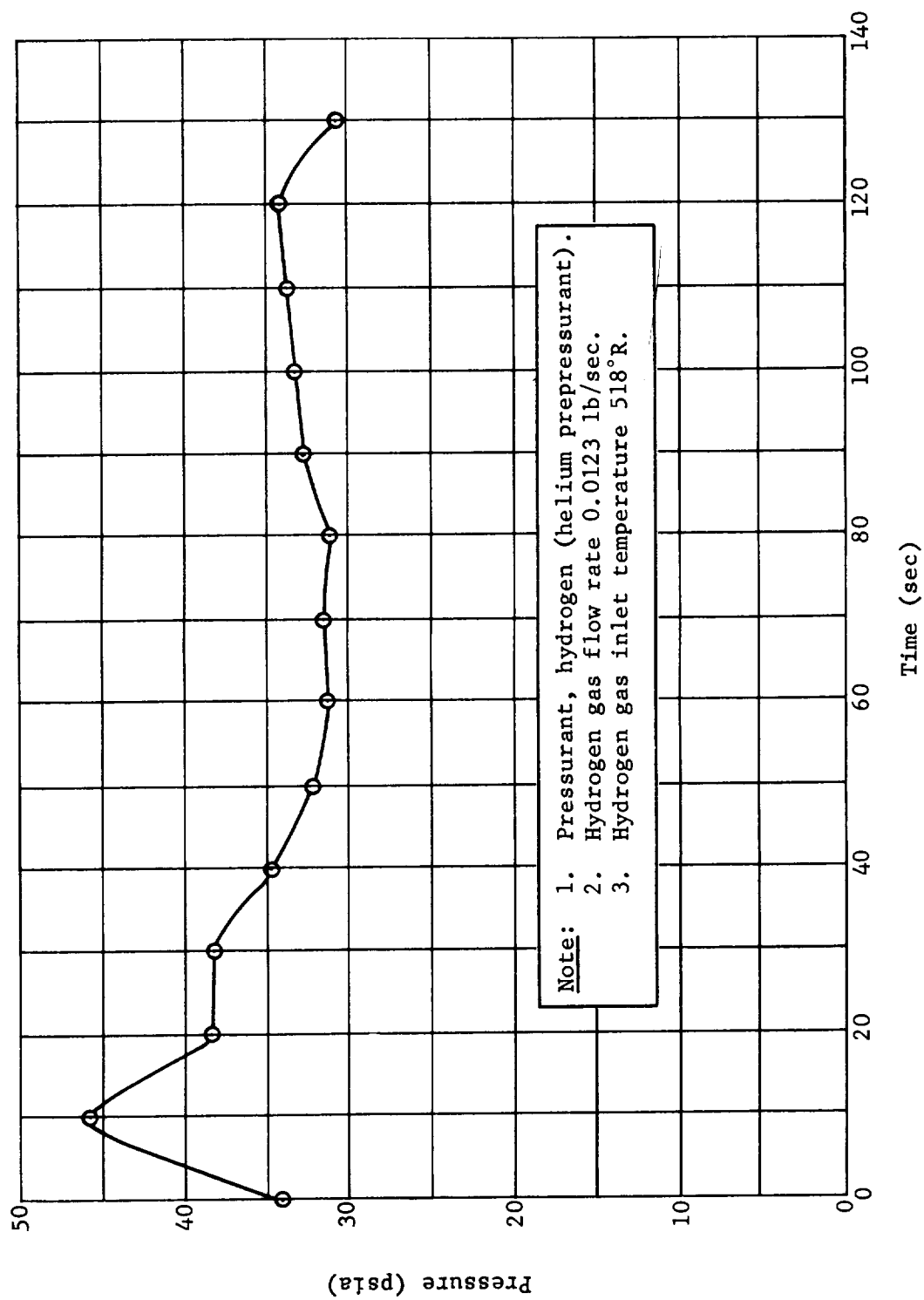


Fig. 62 Tank Top Pressure, Test No. 18

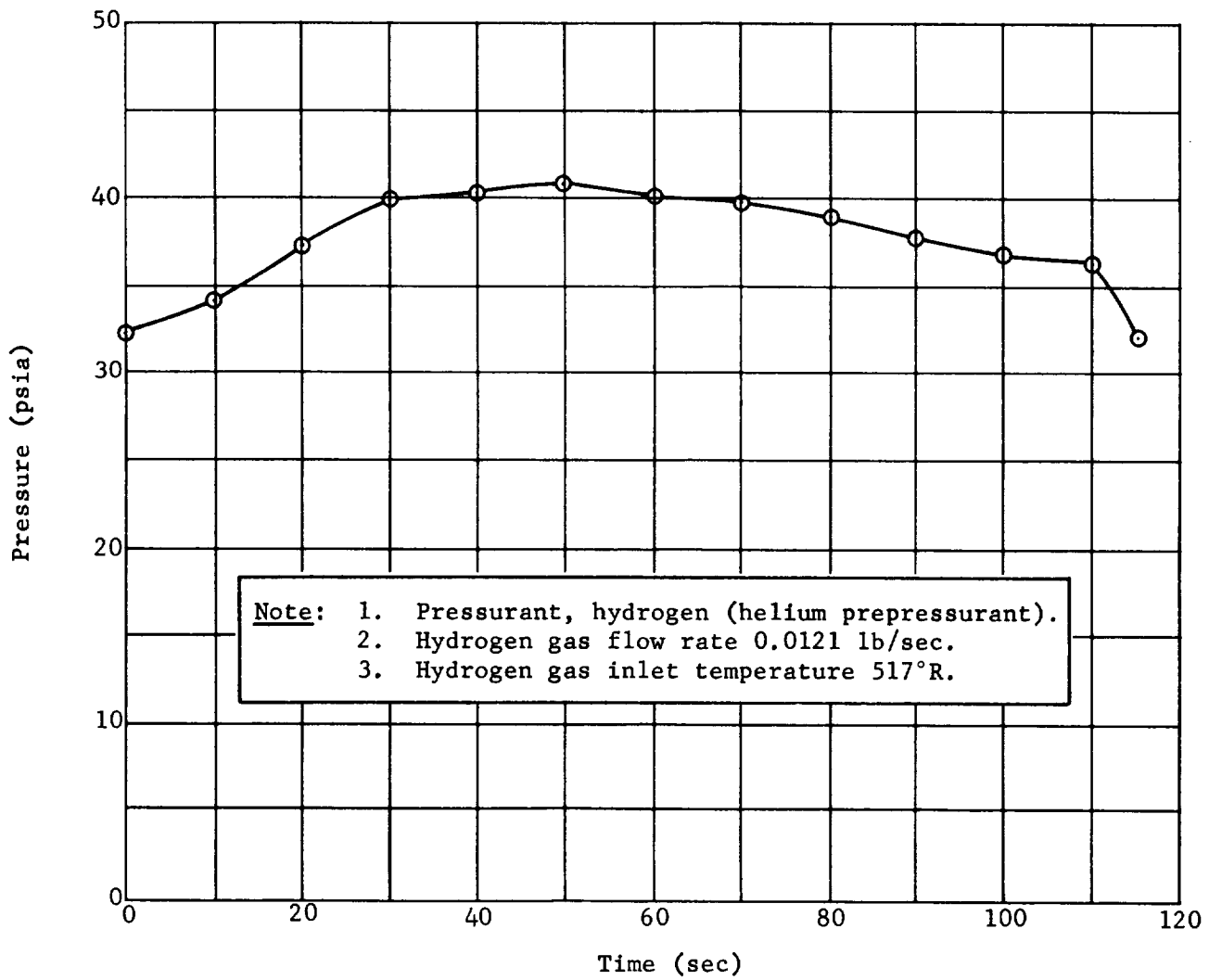


Fig. 63 Tank Top Pressure, Test No. 19

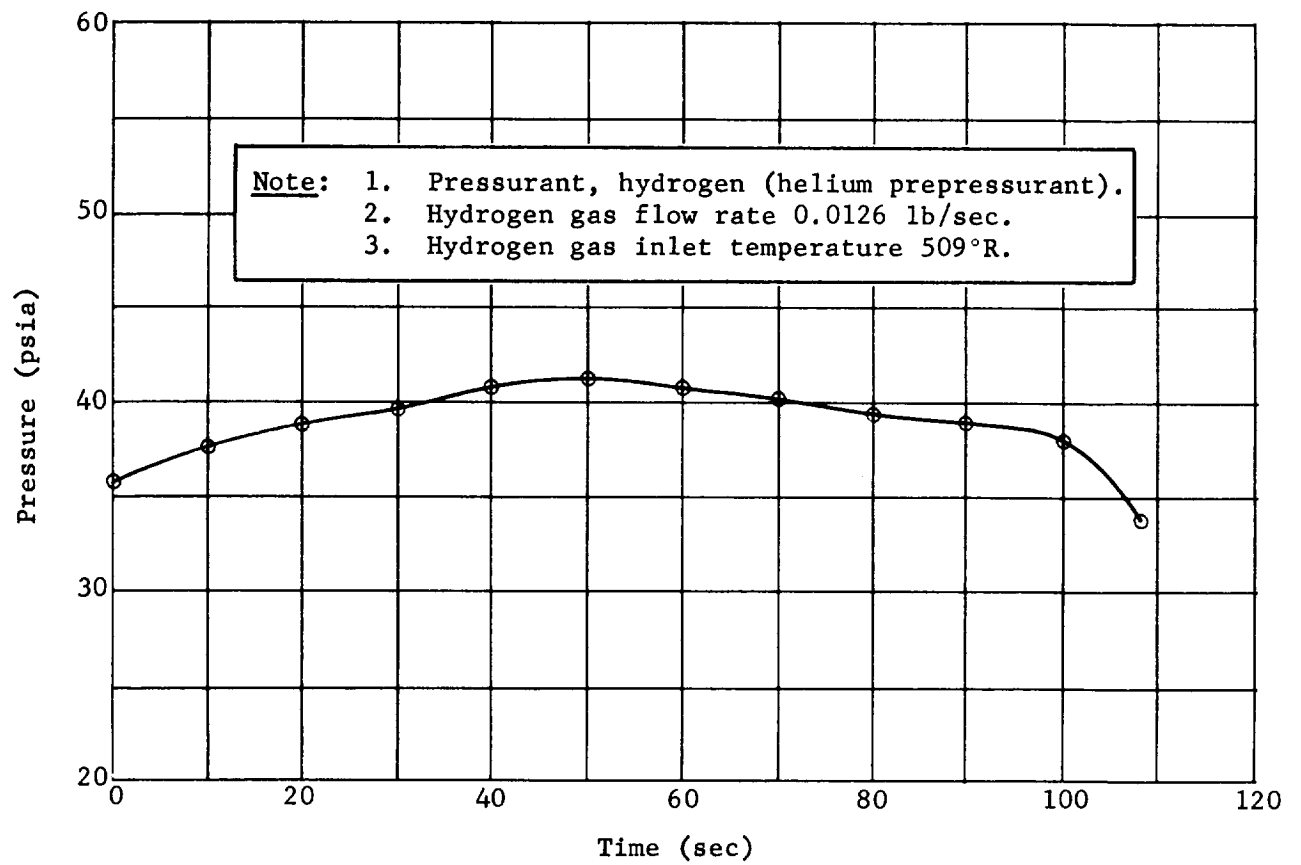


Fig. 64 Tank Top Pressure, Test No. 20

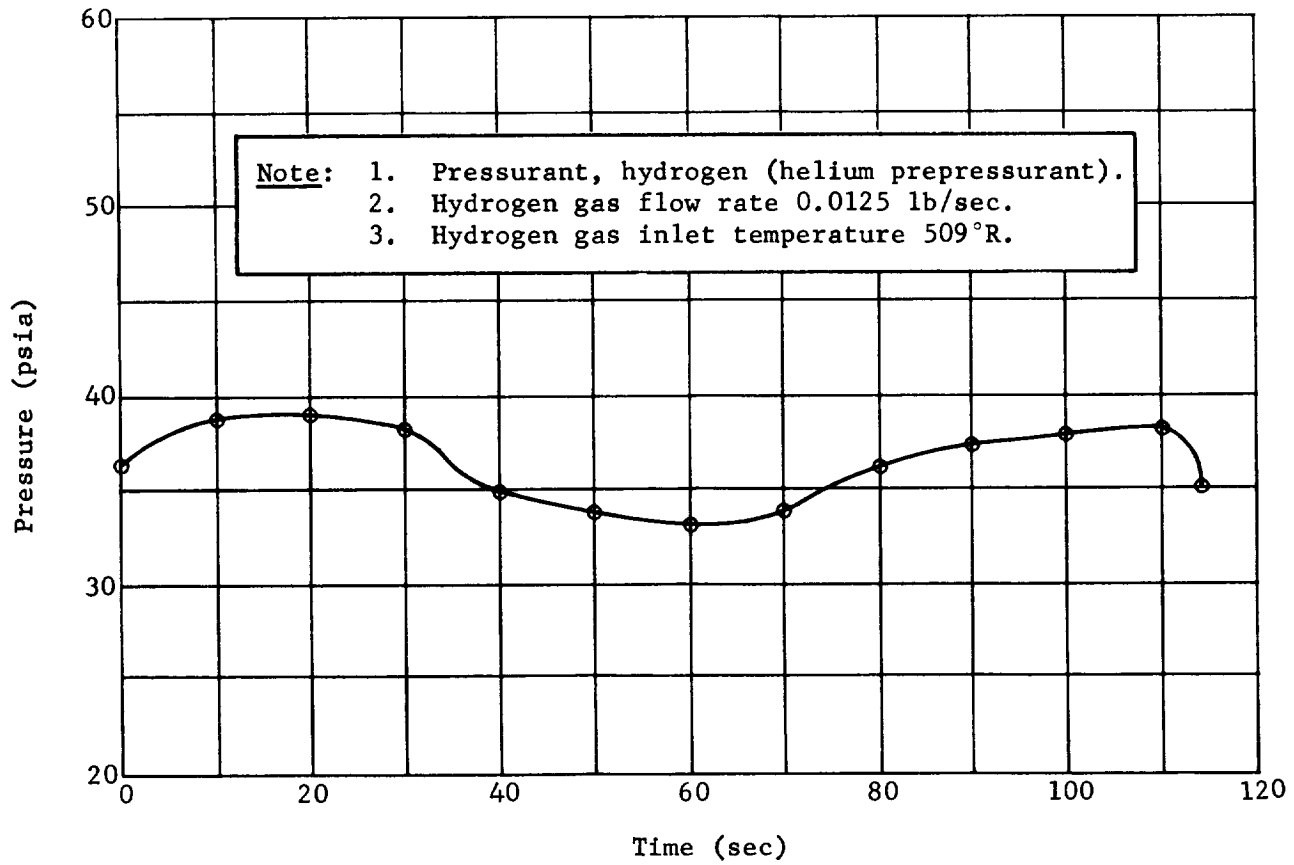


Fig. 65 Tank Top Pressure, Test No. 21

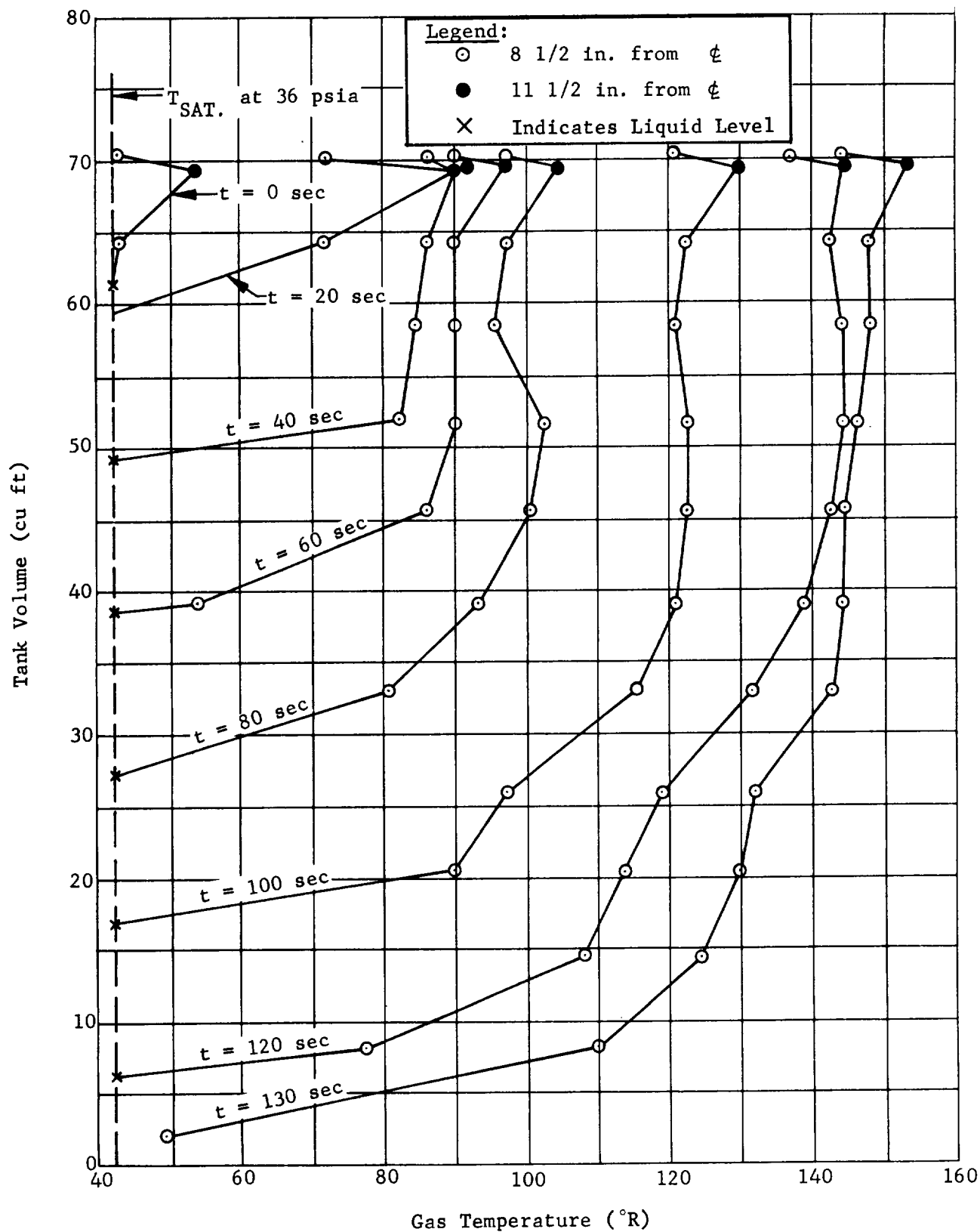


Fig. 66 Ullage Gas Temperature Profiles, Test No. 18

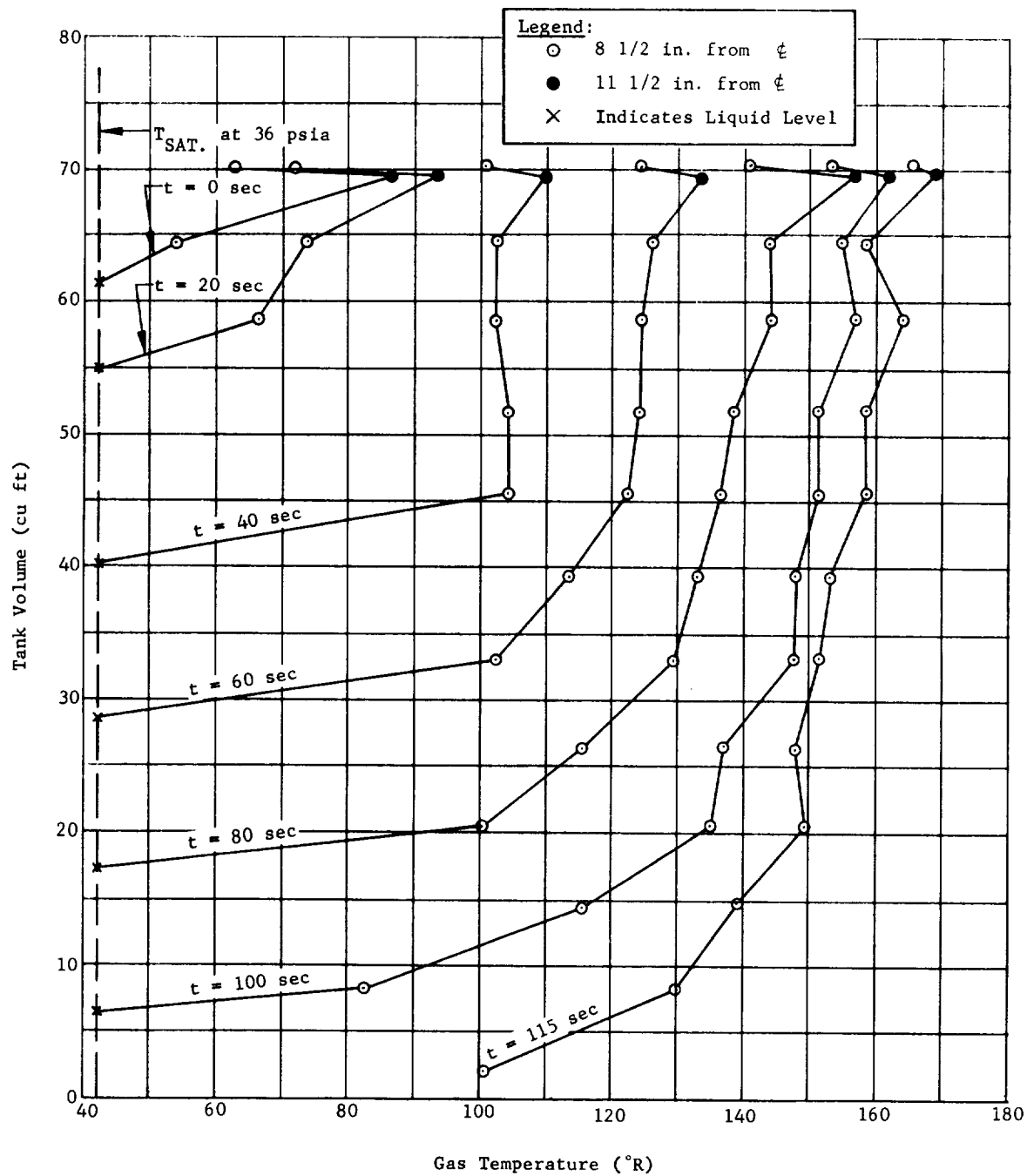


Fig. 67 Ullage Gas Temperature Profiles, Test No. 19

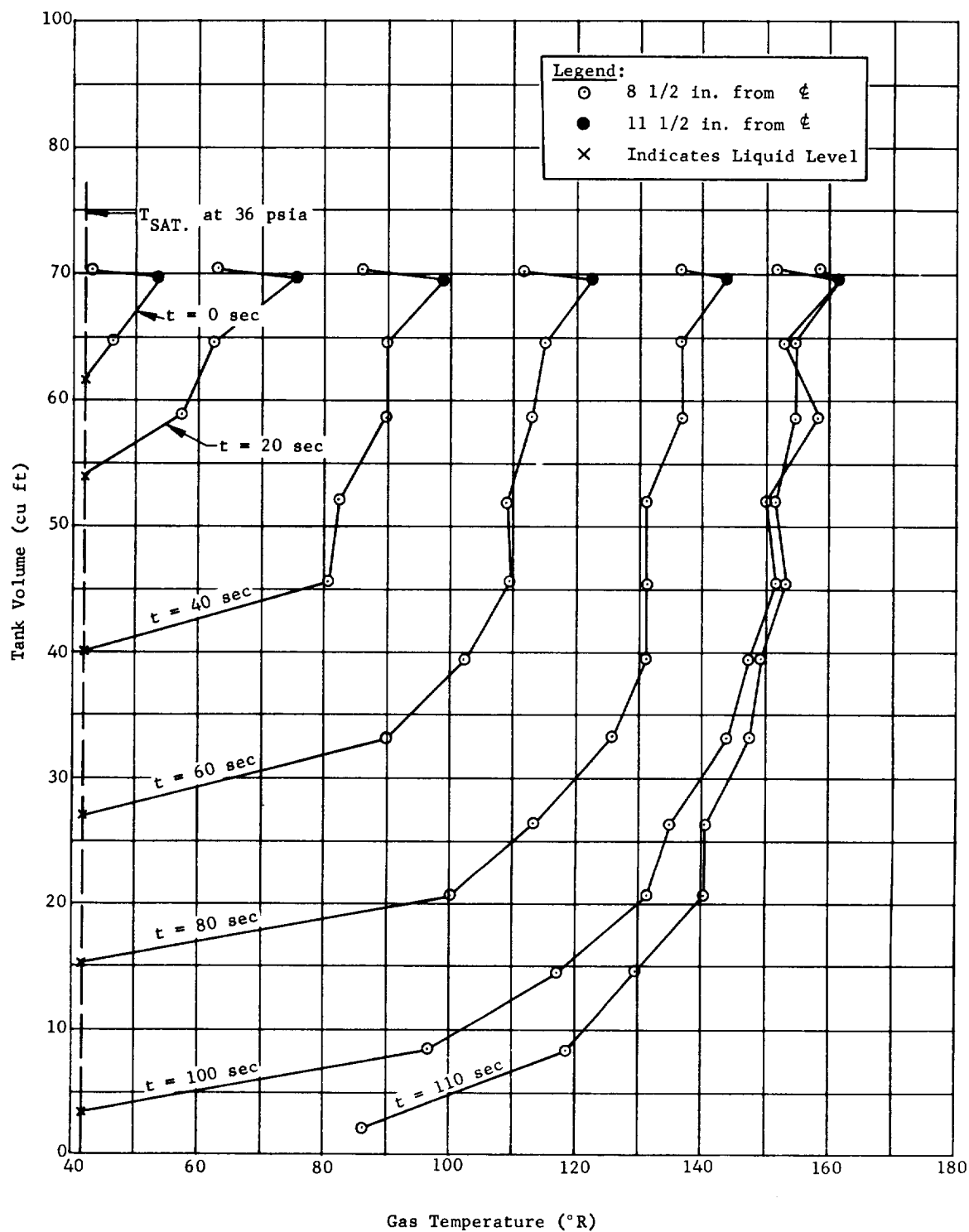


Fig. 68 Ullage Gas Temperature Profiles, Test No. 20

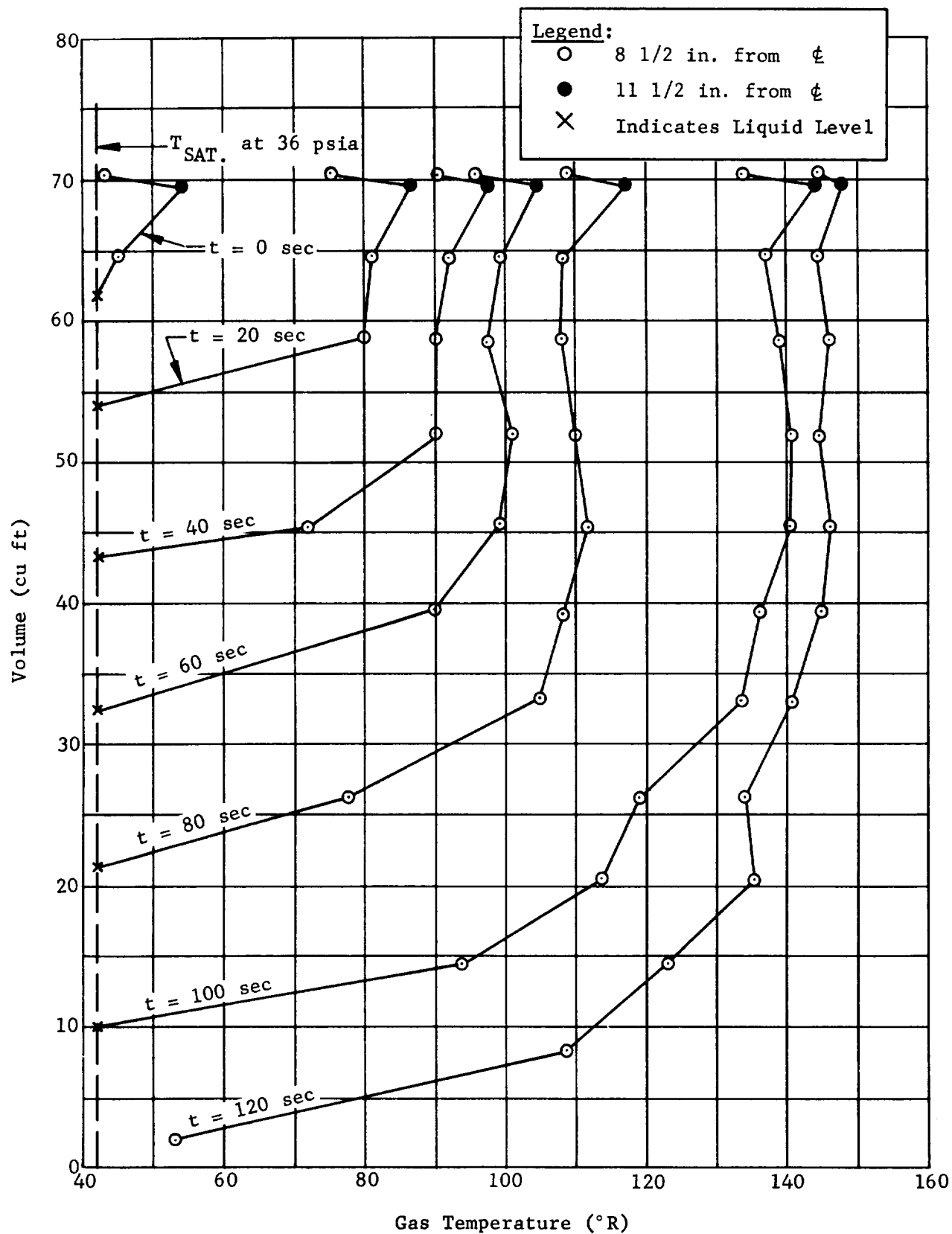


Fig. 69 Ullage Gas Temperature Profiles, Test No. 21

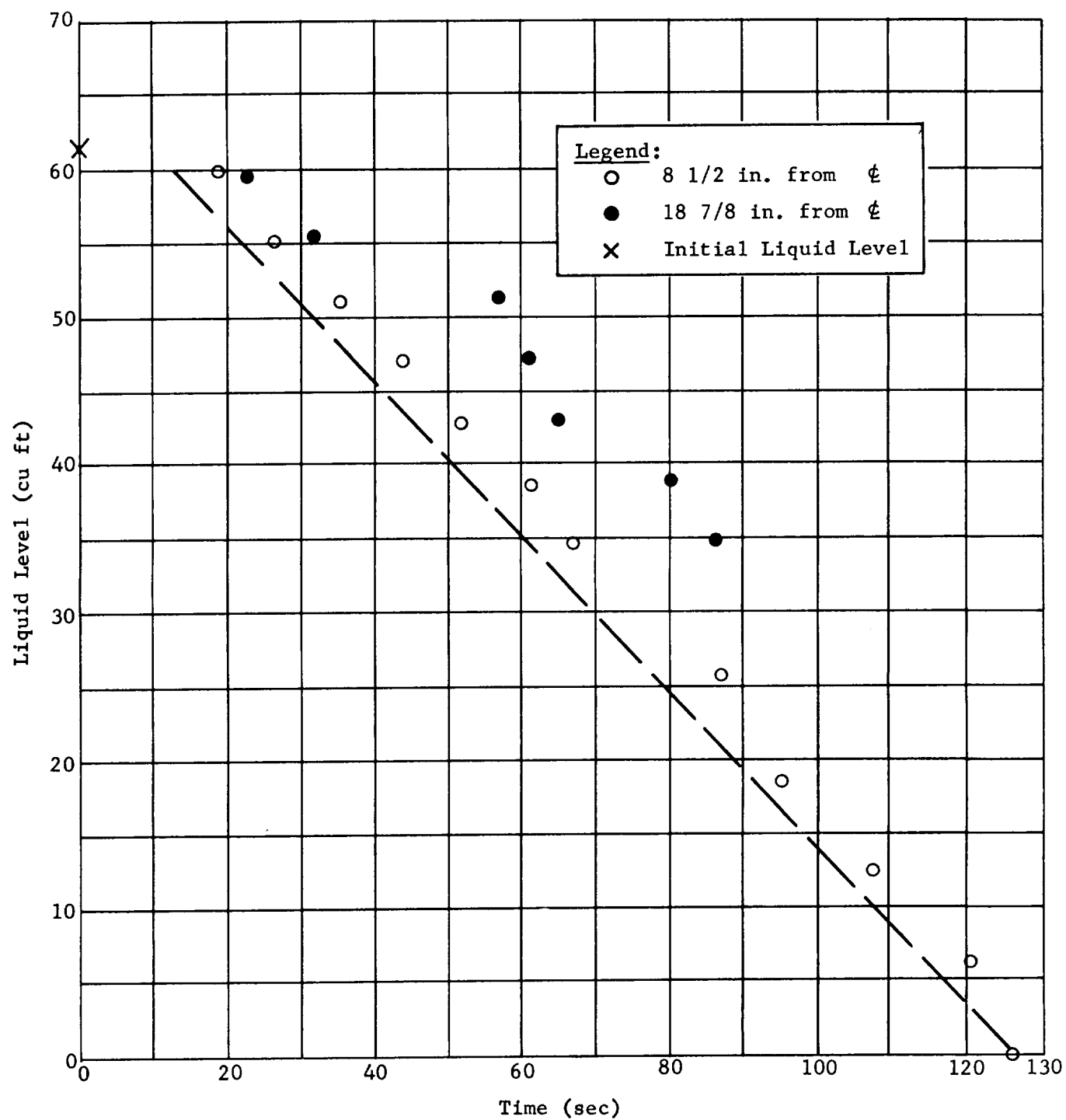


Fig. 70 Liquid Outflow Rate, Test No. 18

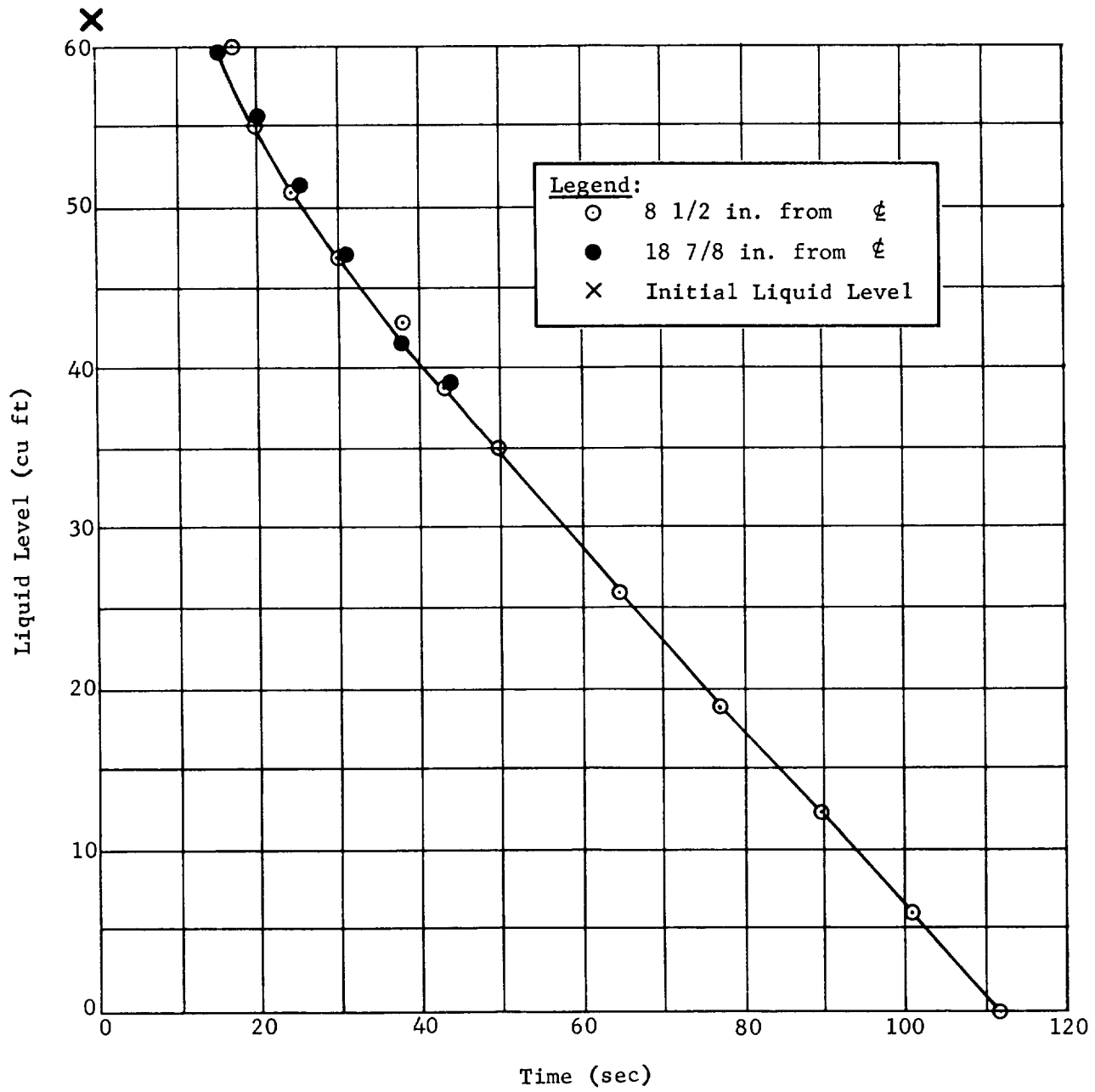


Fig. 71 Liquid Outflow Rate, Test No. 19

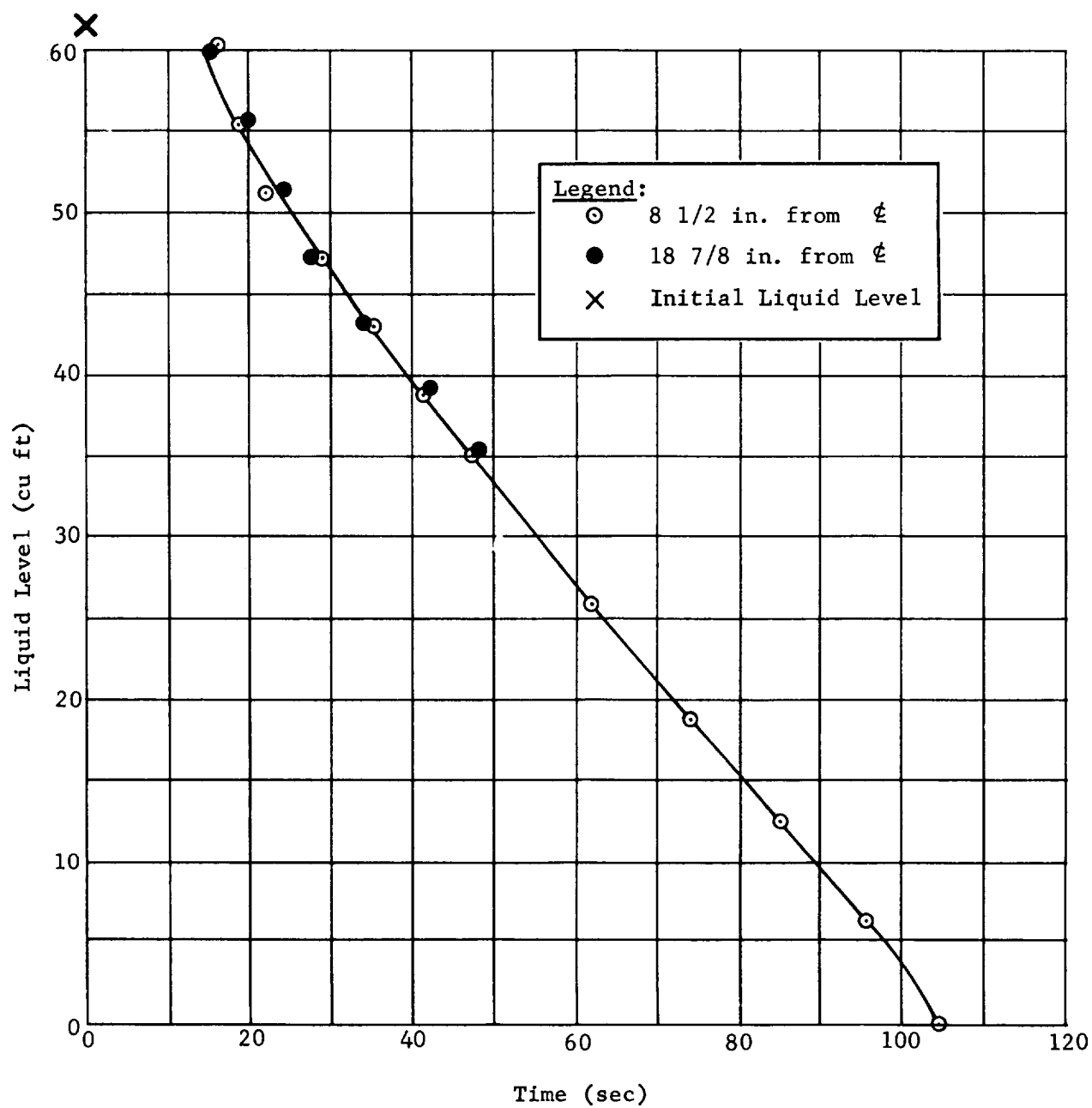


Fig. 72 Liquid Outflow Rate, Test No. 20

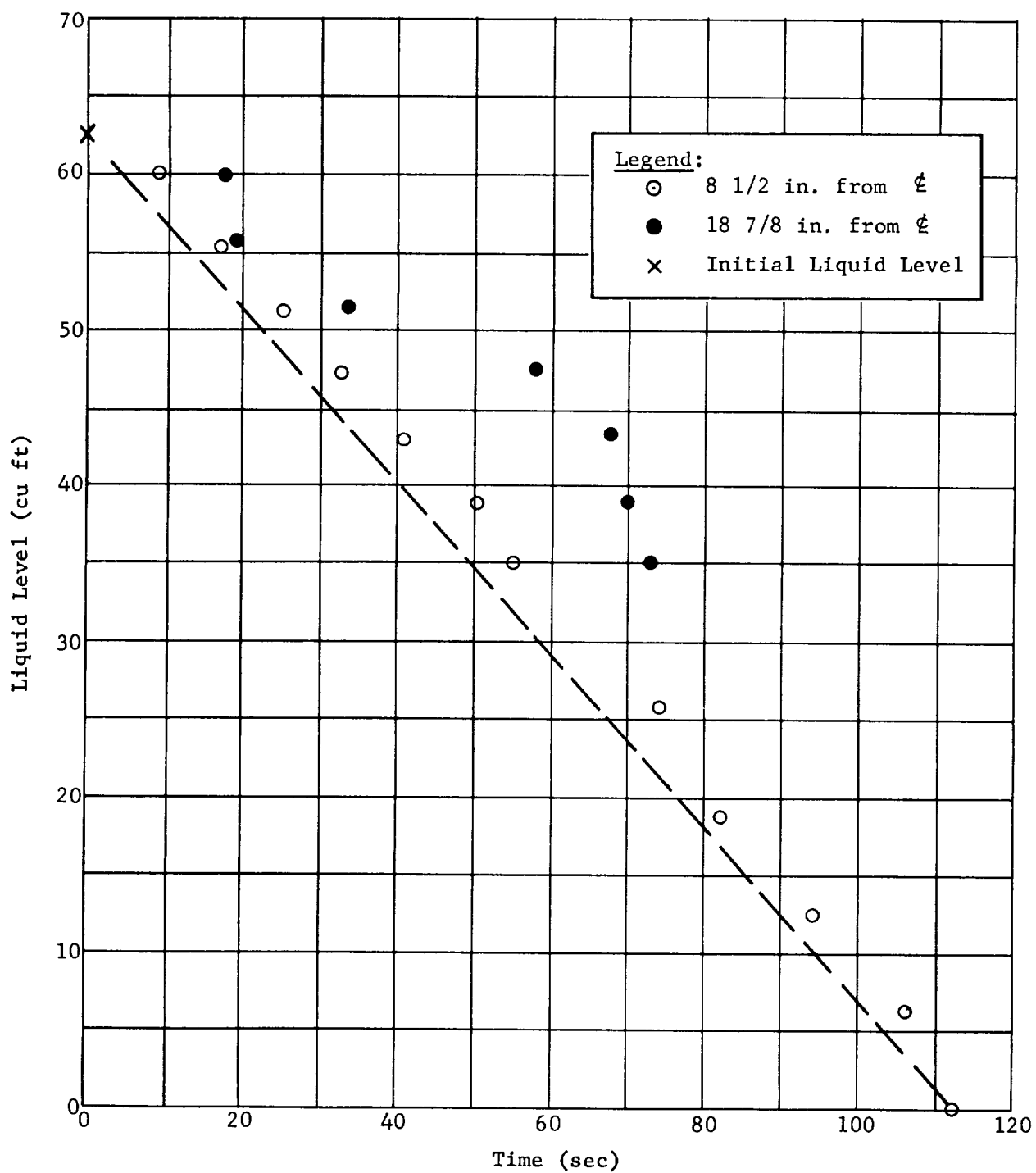


Fig. 73 Liquid Outflow Rate, Test No. 21

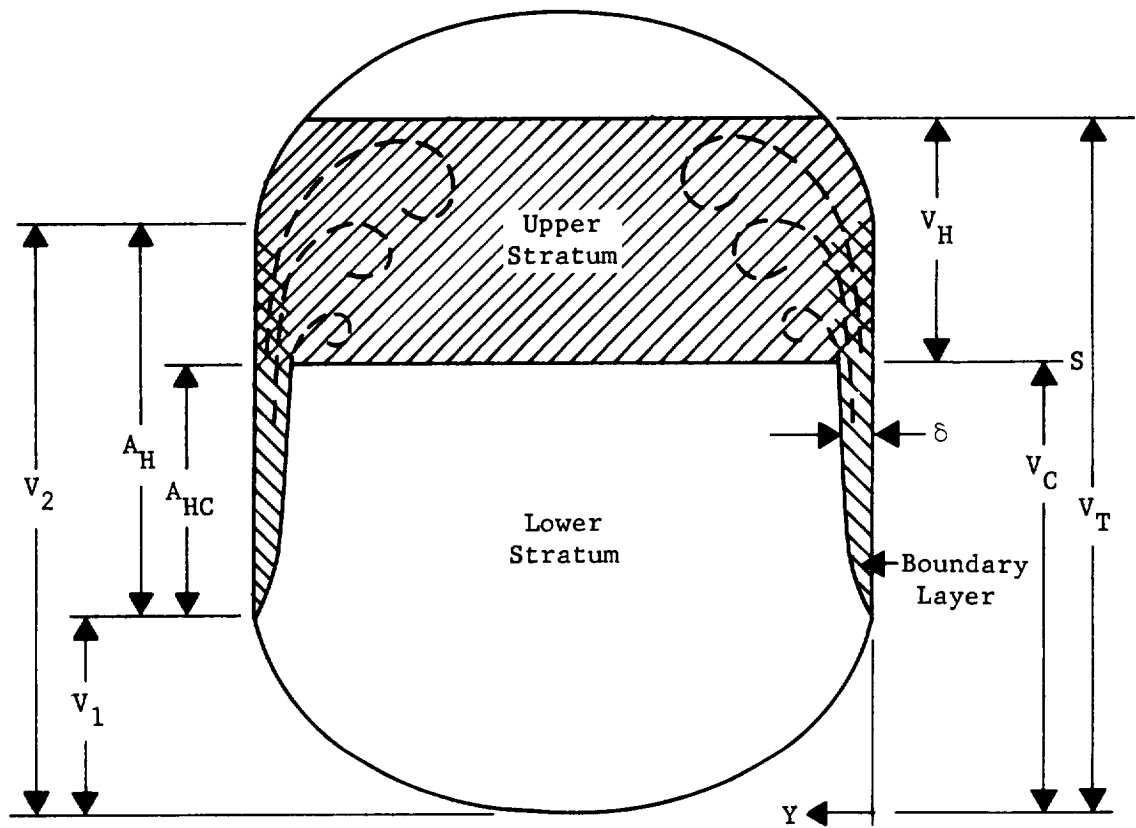


Fig. 74 Two-Layer Model

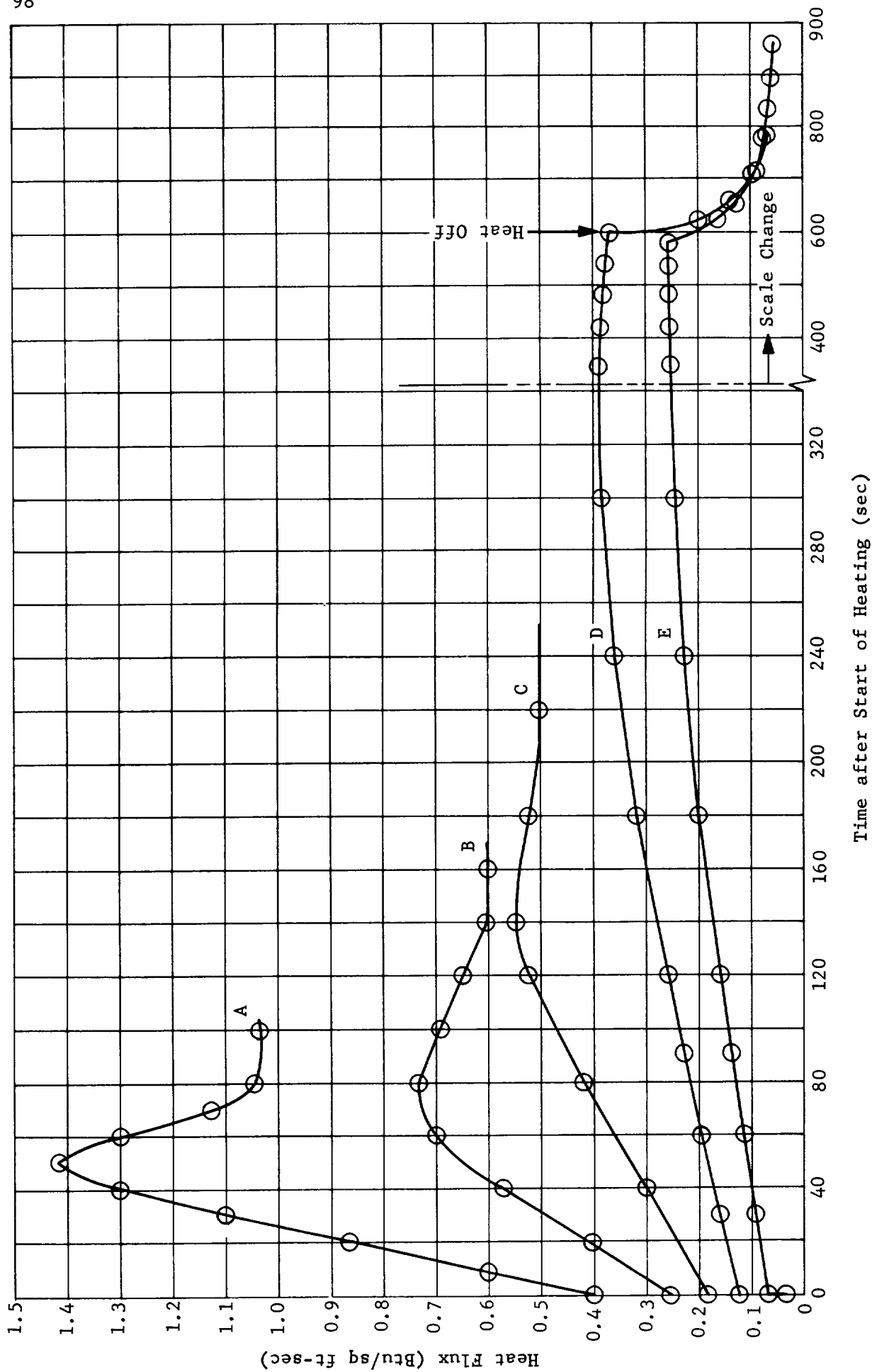
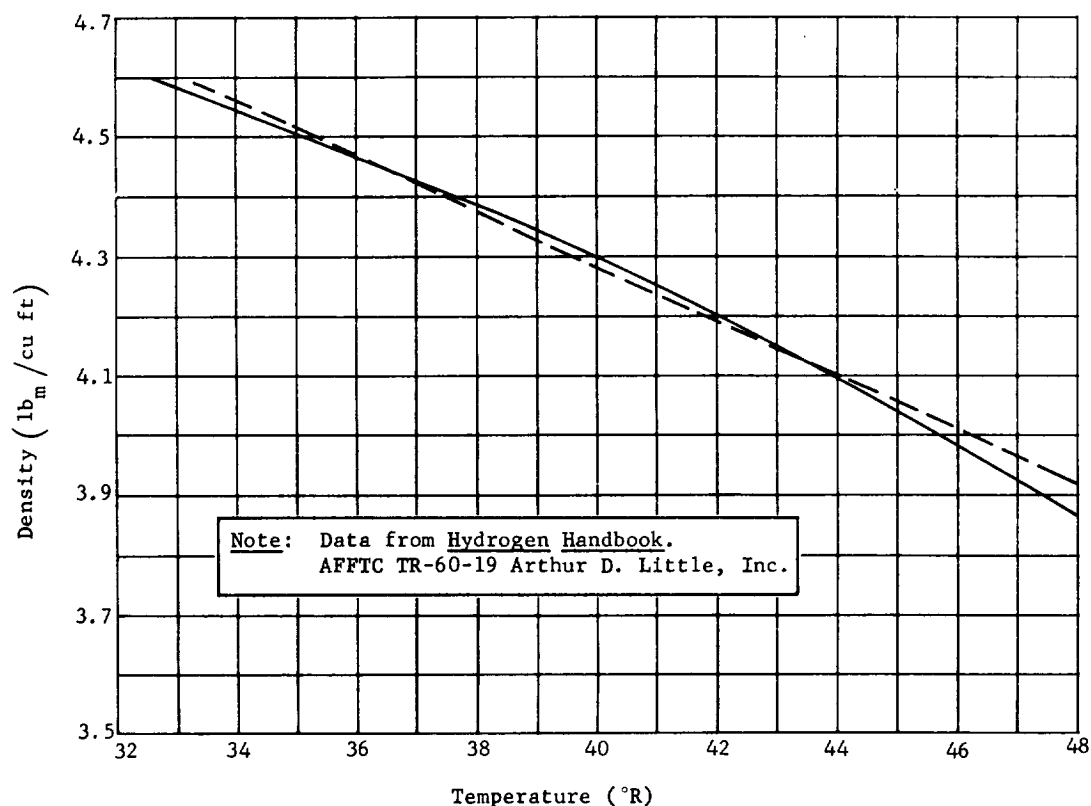


Fig. 75 Heat Flux vs Time for Different Heat Chamber Connections



a. Density of Saturated Liquid Normal Hydrogen

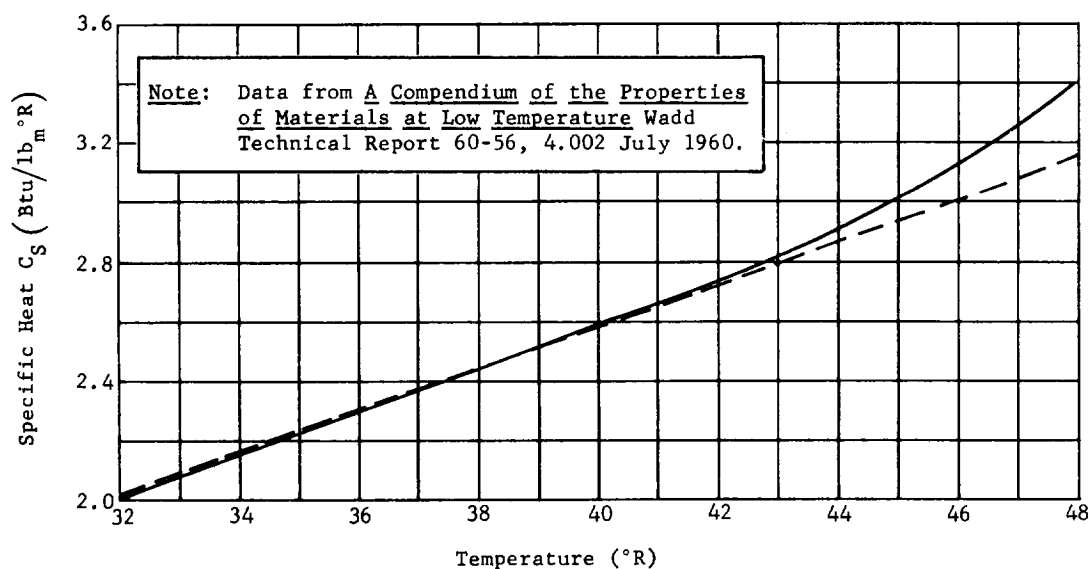
b. Specific Heat of Parahydrogen at Saturation (C_S)

Fig. 76 Density of Hydrogen and Specific Heat of Parahydrogen vs Temperature

VI. ANALYTICAL MODEL

A. NOMENCLATURE

<u>Symbol</u>	<u>Description</u>
A	Area
A_{HC}	Heated area adjacent to cold liquid
A_{HT}	Total heated area adjacent to liquid
a_1, a_2, a_3, a_4	Terms in Rung Kutta solution of stratification equation
b_1, b_2, b_3	Terms in solution of Δq equation
C_4, C_5	Constants used in heat convection equation
C_6, C_7	Constants used in boiling heat transfer equation
C_p	Specific heat of liquid
C_{Po}	Constant in specific heat as a function of temperature equation
D	Tank diameter
D_{CP}	Constant in equation for specific heat as a function of temperature
D_ρ	Constant in equation for density as a function of temperature
g	Acceleration field acting on system
h	Liquid film heat transfer coefficient
h_C	Specific enthalpy of cold liquid
h_H	Specific enthalpy of hot liquid

<u>Symbol</u>	<u>Description</u>
h_w	Specific enthalpy of liquid in contact with tank wall
M_C	Mass of the cold liquid
\dot{M}_H	Mass flow rate of liquid into hot layer
N_{Gr}	Grashof modulus
N_{Pr}	Prandtl modulus
N_{Nu}	Nusselt modulus
(q/A)	Heat transfer rate through unit area of tank wall
t	Time
t_n	Time after n time increments
T	Temperature
T_w	Temperature at tank wall
T_C	Temperature of cold liquid
T_H	Temperature of hot liquid
u	Velocity of fluid in boundary layer
V_C	Volume of cold liquid
V_H	Volume of hot liquid
V_{HC}	Volume of cold liquid adjacent to heated area
V_T	Total liquid volume
V_1	Liquid volume below bottom of heated area
V_2	Liquid volume below top of heated area
y	Distance in boundary layer measured from wall

<u>Symbol</u>	<u>Description</u>
Δh_H	Increase of specific enthalpy of hot liquid during time increment Δt
ΔM_H	Increase of mass of hot liquid during time increment Δt
Δq	Heat transfer from wall to liquid during time increment Δt
Δt	Time increment
δ	Boundary layer thickness
θ	Temperature excess (actual temperature minus liquid bulk temperature)
θ_w	Wall temperature minus liquid bulk temperature
ρ	Liquid density
ρ_o	Constant in equation for liquid density as a function of temperature
ρ_C	Density of cold liquid
ρ_H	Density of hot liquid
$\bar{\theta}$	Mean temperature of liquid flowing in boundary layer, defined in Eq [6].
ξ	Ratio of θ_w to $\bar{\theta}$

B. ANALYTICAL MODEL DERIVATION

The stratification analysis is based on integration of liquid mass flow in the natural convection boundary layer along the heated tank wall. The primary assumptions of the analysis are: (1) the initial temperature of the liquid is uniform, (2) the heat flux is uniform, (3) all the heat input to the tank wall appears as sensible heat in the boundary layer, (4) all the flow in this boundary layer goes into a warm upper stratum and remains there, (5) this warm stratum is uniformly mixed, and (6) there is no mixing between the warm stratum and the lower unheated stratum.

Consider the horizontal plane S separating the two strata, as shown in Fig. 74. The growth of the upper stratum results from the flow in the boundary layer that crosses S. This flow is confined to the annular ring in S, of width δ , inside the tank wall. Applying an energy balance to that portion of the boundary layer below S and assuming that the thermal energy stored in the boundary layer is negligible, there results the equation,

$$(q/A)A_{HC} = \pi D \int_0^{\delta} \rho [h(y) - h_C] u(y) dy. \quad [1]$$

Assuming constant specific heat and density, this can be written

$$(q/A)A_{HC} = \pi D C_P \rho \int_0^{\delta} \theta(y) u(y) dy. \quad [2]$$

The mass flow rate through S, and hence the rate of increase of the warm stratum mass, is given by the equation,

$$\dot{M}_H = \pi D \rho \int_0^{\delta} u(y) dy. \quad [3]$$

Multiplying both sides of Eq [3] by qA_{HC} and dividing by Eq [2] gives the result,

$$\dot{M}_H = \frac{(q/A)A_{HC}}{C_P} \frac{\int_0^{\delta} u(y) dy}{\int_0^{\delta} \theta(y) u(y) dy}. \quad [4]$$

This can be written

$$\dot{M}_H = \frac{(q/A)A_{HC}}{C_p \bar{\theta}} \quad [5]$$

where

$$\bar{\theta} = \frac{\int_0^\delta \theta(y) u(y) dy}{\int_0^\delta u(y) dy} \quad [6]$$

For rockets using cryogenic propellants, the propellant properties, heating rates, and tank sizes encountered are such that $N_{Gr} \gg 10^9$; and the boundary layer is, therefore, turbulent. Measurements of temperature and velocity profiles in turbulent free-convection boundary layers can be correlated with the equations (Ref 1),

$$u(y) = u_1 \left(\frac{y}{\delta} \right)^{1/7} \left(1 - \frac{y}{\delta} \right)^4 \quad [7]$$

and

$$\theta(y) = \theta_w \left[1 - \left(\frac{y}{\delta} \right)^{1/7} \right] \quad [8]$$

Introducing these into Eq [6],

$$\bar{\theta} = \frac{u_1 \theta_w \int_0^\delta \left(\frac{y}{\delta} \right)^{1/7} \left(1 - \frac{y}{\delta} \right)^4 \left[1 - \left(\frac{y}{\delta} \right)^{1/7} \right] dy}{u_1 \int_0^\delta \left(\frac{y}{\delta} \right)^{1/7} \left(1 - \frac{y}{\delta} \right)^4 dy} \quad [9]$$

Defining the ratio of the integrals,

$$\xi = \frac{\int_0^{\delta} \left(\frac{y}{\delta}\right)^{1/7} \left(1 - \frac{y}{\delta}\right)^4 dy}{\int_0^{\delta} \left(\frac{y}{\delta}\right)^{1/7} \left(1 - \frac{y}{\delta}\right)^4 \left[1 - \left(\frac{y}{\delta}\right)^{1/7}\right] dy}, \quad [10]$$

Eq [9] can be rewritten

$$\theta = \frac{\theta_w}{\xi}$$

which, when substituted into Eq [6] gives the result

$$\dot{M}_H = \frac{(q/A)A_{HC}\xi}{C_P\theta_w} \quad [11]$$

Since $q/A = h\theta_w$, this can be written

$$\dot{M}_H = \frac{hA_{HC}\xi}{C_P}. \quad [12]$$

This equation shows that the mass rate of growth of the upper stratum can be determined if the inside heat transfer coefficient, h , is known. This coefficient can be determined from the known heat input rate, together with a suitable correlation of heat transfer coefficient vs heat flux.

Performing the integrations indicated in Eq [10] gives the result

$$\xi = 4.0$$

Although this numerical value is strictly applicable only for turbulent free convection boundary layers, it is not very sensitive to the exact shape of the profiles.

In the preceding analysis, constant specific heat is assumed, and this analysis was the one used to correlate the lox and liquid nitrogen data in Ref 1. The specific heat of liquid hydrogen, however, varies considerably over the temperature range of interest, as shown in Fig. 76. To account for this variable specific heat, the quantity C_{pW} in Eq [11], which is equal to the difference between the enthalpy of the liquid at the wall and the enthalpy of the unstratified liquid, is replaced by the quantity $(h_W - h_C)$. This gives the equation

$$\dot{M}_H = \frac{(q/A)A_{HC}\xi}{h_W - h_C}. \quad [13]$$

The value of h_W is determined from the enthalpy vs temperature relationship at the wall temperature. The wall temperature is given by the equation

$$T_W = T_C + \frac{q/A}{h}. \quad [14]$$

Once the mass of the warm layer is determined by integration of Eq [13], its enthalpy is obtained from an energy balance, which gives the equation

$$M_H(h_H - h_C) = A_{HT} \int_0^t (q/A) dt. \quad [15]$$

From this equation the enthalpy (h_H) of the warm layer, and hence its temperature, may be determined. The volume of the warm layer may then be computed from its mass and density.

C. DESCRIPTION OF IBM 1620 COMPUTER PROGRAM

The principal equations used in the 1620 program are

$$\dot{M}_H = \frac{(q/A)A_{HC}\xi}{h_W - h_C} \quad [13]$$

and

$$\Delta h_H = \frac{\Delta Q - \Delta M_H(h_H - h_C)}{M_H + \Delta M_H} \quad [16]$$

Equation [13] is solved by the Runge-Kutta numerical approximation method (Ref 4), i.e.,

$$\Delta M_H = \frac{1}{6}(a_1 + 2a_2 + 2a_3 + a_4) \quad [17]$$

where

$$a_1 = \xi \Delta t \frac{q/A}{h_W - h_C} \left(t_n \right) A_{HC} \left(M_{HC}, t_n \right)$$

$$a_2 = \xi \Delta t \frac{q/A}{h_W - h_C} \left(t_n + \frac{1}{2}\Delta t \right) A_{HC} \left(M_{HC} + \frac{a_1}{2}, t_n + \frac{1}{2}\Delta t \right)$$

$$a_3 = \xi \Delta t \frac{q/A}{h_W - h_C} \left(t_n + \frac{1}{2}\Delta t \right) A_{HC} \left(M_{HC} + \frac{a_2}{2}, t_n + \frac{1}{2}\Delta t \right)$$

$$a_4 = \xi \Delta t \frac{q/A}{h_W - h_C} \left(t_n + \Delta t \right) A_{HC} \left(M_{HC} + a_3, t_n + \Delta t \right)$$

Values for (q/A) as a function of time are obtained from an input table, with a maximum capacity of 20 points, using linear interpolation.

The enthalpy of the cold layer (h_C) is a constant depending on the initial temperature of liquid, and is calculated using the equation

$$h_C = \int_0^{T_C} C_P dT. \quad [18]$$

It is assumed that $C_P = C_{Po} + T(D_{CP})$; therefore,

$$h_C = C_{Po}T_C + \frac{(D_{CP})}{2} T_C^2. \quad [19]$$

The specific enthalpy of the liquid at the wall (h_W) is obtained by using a similar equation,

$$h_W = C_{Po}T_W + \frac{(D_{CP})}{2} T_W^2. \quad [20]$$

The wall temperature (T_W) is obtained from the equation

$$\frac{q}{A} = C_4(T_W - T_C)^{C_5} g^{(C_5-1)} + C_6(T_W - T_S)^{C_7}, \quad [21]$$

which states that the heat transferred to the liquid is the sum of the convection heat transfer and the boiling heat transfer. Since T_W cannot be explicitly solved for, Newton's method of successive approximations is used to obtain T_W . The gravitational field, which affects both terms of this equation, is calculated from the equation

$$g = \frac{1}{(W/F) - (\dot{W}/F)t}, \quad [22]$$

which assumes an idealized constant thrust, and zero drag trajectory. Since gravity has a small effect, this idealization is a sufficiently good approximation. The saturation temperature (T_S) is calculated from the equation

$$T_S = \frac{C_2}{C_3 - \ln P_S}, \quad [23]$$

where P_S is the total pressure calculated for a point half way up the cold layer:

$$P_S = P_T + \frac{\rho_C g}{\frac{\pi D^2}{4}} \left(\frac{V_T + V_H}{2} \right). \quad [24]$$

The values for tank pressure (P_T) as a function of time are obtained from an input table, with a maximum of 20 points, using linear interpolation.

The heated wall area adjacent to the cold liquid layer (A_{HC}) is a function of the volume of cold liquid (V_C) and the tank geometry (see Fig. 74) and, assuming a circular cylindrical tank, can be written as

$$\begin{aligned} A_{HC} &= \left(V_2 - V_1 \right) \frac{4}{D} && \text{when } V_C \geq V_2 \\ A_{HC} &= \left(V_C - V_1 \right) \frac{4}{D} && \text{when } V_2 > V_C > V_1 \\ A_{HC} &= 0 && \text{when } V_C \leq V_1 \end{aligned} \quad [25]$$

These three equations can be combined into one equation, which is

$$A_{HC} = \frac{2}{D} \left(V_2 - V_1 + \left| V_C - V_1 \right| - \left| V_C - V_2 \right| \right). \quad [26]$$

In Eq [16], ΔQ is a function of the heated area adjacent to the liquid, and time. Combining the area with the q/A vs time curve and using Simpson's rule,

$$\Delta Q = \frac{\Delta t}{6} \left(b_1 + 4b_2 + b_3 \right) \quad [27]$$

where

$$\begin{aligned} b_1 &= (q/A)(t_n) A_{HT}(t_n) \\ b_2 &= (q/A)(t_n + \frac{1}{2}\Delta t) A_{HT}(t_n + \frac{1}{2}\Delta t) \\ b_3 &= (q/A)(t_n + \Delta t) A_{HT}(t_n + \Delta t) \end{aligned}$$

The total heated area (A_{HT}) is obtained similarly to A_{HC} :

$$A_{HT} = \frac{2}{D} \left(v_2 - v_1 + \left| v_T - v_1 \right| - \left| v_T - v_2 \right| \right). \quad [28]$$

Finally, the temperature of the hot liquid is obtained by rearranging the enthalpy equation to obtain

$$T_H = \frac{-C_{Po} + \sqrt{C_{Po}^2 + 2h_H D_{CP}}}{D_{CP}}. \quad [29]$$

The program was written in Format Fortran for an IBM 1620 computer. The definition of the Fortran symbols, a listing of the Fortran statements, a simplified flow diagram, and sample input and output data are contained in the Appendix.

D. COMPARISON OF ANALYTICAL MODEL WITH TEST DATA

The IBM 1620 computer program described previously was used to simulate, as closely as possible, each of the tests in this program. The input data for the computer runs were, in general, those actually measured in the experimental tests. Some adjustments were made, however, particularly in the initial liquid volume when the volume measured using the liquid level manometer did not agree with the thermistor indications. The thermistors serve as accurate point level sensors since their self-heating is sufficient, when the thermistor is not submerged in liquid, to drive the galvanometer trace off scale. In some tests the initial liquid volume was slightly below the top level of thermistors, although the manometer indicated otherwise. In other cases the manometer measured a level below the top level of thermistors when these gave an indication of being covered. When such discrepancies occurred, the manometer reading was ignored and an estimate of the liquid level was made from the thermistor indications.

The heat flux vs time curves used in the computer runs are shown in Fig. 75. Curves D and E were obtained from measurement of boiloff rate, as described in Chapter IV. Curves A and B were obtained from calculations of enthalpy gain of the liquid for tests No. 12 and 1, respectively. Curve C was obtained by interpolation. Curve B corresponds to the original heat chamber configuration with 320 lamps; all others correspond to the modified configuration with 304 lamps. Another curve B', not shown, was also used. This curve corresponds to the B curve for the modified configuration, and was obtained by multiplying the ordinates of the B curve by 95 percent. The explanation for the peaks appearing in these curves is not known.

For calculating heat transfer by free convection, the equation used is

$$(q/A)_C = 0.0116 (T_W - T_C)^{4/3} \text{ Btu/sq ft-sec.} \quad [30]$$

This equation was obtained from a conventional correlation (Ref 5)

$$N_{Nu} = 0.13 (N_{Gr} N_{Pr})^{1/3}. \quad [31]$$

The temperatures used in Eq [29] and [31] are in degrees Rankine.

The equation used for nucleate boiling is

$$(q/A)_B = 0.738 (T_W - T_{SAT})^{2.5} \text{ Btu/sq ft-sec.} \quad [32]$$

This equation was obtained from measurements made at the Martin-Denver liquid hydrogen laboratory, and agrees well with data shown in Ref 6.

The vapor pressure vs temperature relationship used is the equation

$$T_{SAT} = \frac{223.2}{8.804 - \ln P \text{ (psia)}} \text{ } ^\circ\text{R.} \quad [33]$$

Density and specific heat variations with temperature are approximated with the linear functions

$$\rho = 6.079 - 0.045T(^{\circ}\text{R}) \quad \frac{\text{lb}_m}{\text{cu ft}} \quad [34]$$

and

$$C_p = -0.28 + 0.071T(^{\circ}\text{R}) \quad \frac{\text{B}}{\text{lb}_m \cdot ^{\circ}\text{R}} \quad [35]$$

These approximations, together with the actual values, are shown in Fig. 76. In the case of specific heat, the data shown are for the specific heat at saturation (C_s). However, because of the low compressibility of the liquid, this is nearly equal to the specific heat at constant pressure (C_p).

The results of the computer runs are superimposed on the test data graphs, (Fig. 32 thru 61). (No computer simulation was made for run No. 18, since no wall heating was used in this test.) The computer simulation results are shown for the same times as the test data to facilitate a direct comparison. The total liquid volume at each time is shown as a short vertical bar terminating the computed temperature profile line. The initial liquid volume was an input datum; the succeeding volumes were computed by the program.

Three tests (No. 2, 7, and 12) that show a well defined two-layer stratification pattern, also are in good agreement with the computer results. In the remainder of the tests, which generally show a tendency toward a more continuous temperature gradient rather than a step function, the agreement with the model is, of course, less satisfactory. The trend, which is rather consistent, is that the model predicts a warm layer temperature that is lower than the maximum measured temperature near the liquid surface. This difference is small near the beginning of the heating period and tends to increase with time.

It is obvious that the two-layer model cannot adequately describe the temperature profiles typical of most of the tests performed in this series. However, this model may be successful in predicting the maximum temperature (excluding, of course, the sharp temperature rise in the top inch or so of liquid that is a result of heat transfer from the pressurization gas). In an attempt to get a closer agreement between the model prediction and the measured maximum temperature, the value of the parameter ξ was reduced from its theoretical value of 4.0 to 3.0, and also to 2.0 for runs No. 1 and 1A. The results, superimposed on the test data graphs (Fig. 32 and 33), show that reduction of the value of ξ does indeed increase the predicted warm layer temperature. However, the effect is large near the beginning of the heating period, but decreases with time, a trend opposite to that desired. It is apparent, therefore, that adjustment of the parameter ξ is not the proper approach toward making the model predict the maximum temperature more closely.

Although the model does not, in general, adequately describe the measured temperature profiles, it does correctly predict the trends with variations of tank pressure, heat flux, and heating duration. There is no obvious explanation for the good agreement shown in tests No. 2, 7, and 12, since these tests do not seem to have anything in common with each other and differ from the remainder of the tests. A possible explanation for these peculiarities might be the existence of residual circulation currents at the beginning of the tests. These circulation current could be the result of filling or topping operations, or from boiling that occurred before pressurization, while the tank was vented to the atmosphere. The time intervals between the completion of filling or topping operations and the start of the tests, or between the start of pressurization and the commencing of heating, were not controlled in this test program. Thus, there is a possibility of erratic effects.

Another factor that might have contributed to some of the observed discrepancies, particularly in tests where the measured total enthalpy gain does not correspond to the predicted value (No. 3), is the nonrepeatability of the heat flux input. This heat flux input is somewhat affected by the history of the heat chamber, because of residual heat in components within the heat chamber from a previous test. Evidence of this is shown in Fig. 75 by the gradual tailoff in heat flux after the power input to the chamber was turned off for curves D and E. Presumably, this tail-off would be even more significant at the heat chamber configurations corresponding to curves A, B, and C. In any future tests of this type, the above factors should be controlled more closely.

VII. CONCLUSIONS

In several respects the results of this test program fulfilled the objectives and were quite conclusive:

- 1) The stratification tendency was definitely established;
- 2) The trends in the stratification patterns with respect to variations in tank pressure, heat flux, and heat duration were found to be as predicted by the analytical model, indicating the basic correctness of the model;
- 3) The stratification pattern was found to be practically unaffected by liquid oscillation, sloshing, or outflow.

In other respects, however, the results were inconclusive. The failure of the model to accurately predict the maximum warm layer temperature, in contrast to the good agreement previously obtained between the model and lox or liquid nitrogen data, has not been explained. Also, there is no conclusive explanation for the formation of the rather well-defined two-layer pattern observed in some of the tests, in contrast to the tendency toward a more nearly linear temperature gradient observed in most of the other tests.

In the pressurization area, it may be concluded that:

- 1) Sloshing of the liquid induced significant condensation of the hydrogen gas pressurant;
- 2) The ullage gas during the outflow tests was well mixed, probably indicating an ineffective gas inlet distributor.

Quantitative analyses of pressurization data were not performed; however, it may be concluded that the test apparatus used in this program could readily be used to obtain much valuable pressurization data.

REFERENCES

1. "Cryogenic Propellant Stratification Analysis and Test Data Correlation." Technical Memorandum 431-265, Martin Company, Denver, Colorado, 19 May 1960.
2. Analytical and Experimental Determination of Liquid Hydrogen Temperature Stratification. P-61-11 (Rev 1) (Vol I), Martin Company, Denver, Colorado, April 1962, pp. 1-11.
3. "Low Temperature Thermocouples, Table II." NBS Publication R-188. (Reprint from Cryogenics Vol I, No. 3; Haywood & Co. Ltd., 1961).
4. F. B. Hildebrand: Advanced Calculus for Engineers, Prentice Hall, 1949, pp 103-107.
5. W. H. McAdams: Heat Transmission, 3rd Ed, McGraw Hill Book Co., Inc., 1954, p 172.
6. C. R. Class, J. R. DeHaan, M. Piccone, and R. B. Cost: Pool Boiling Heat Transfer to a Cryogenic Liquid. WADC Technical Report 58-528, Beechcraft Research and Development, Inc., Boulder, Colorado, October 1958.

APPENDIX

IBM 1620 DIGITAL COMPUTER PROGRAM

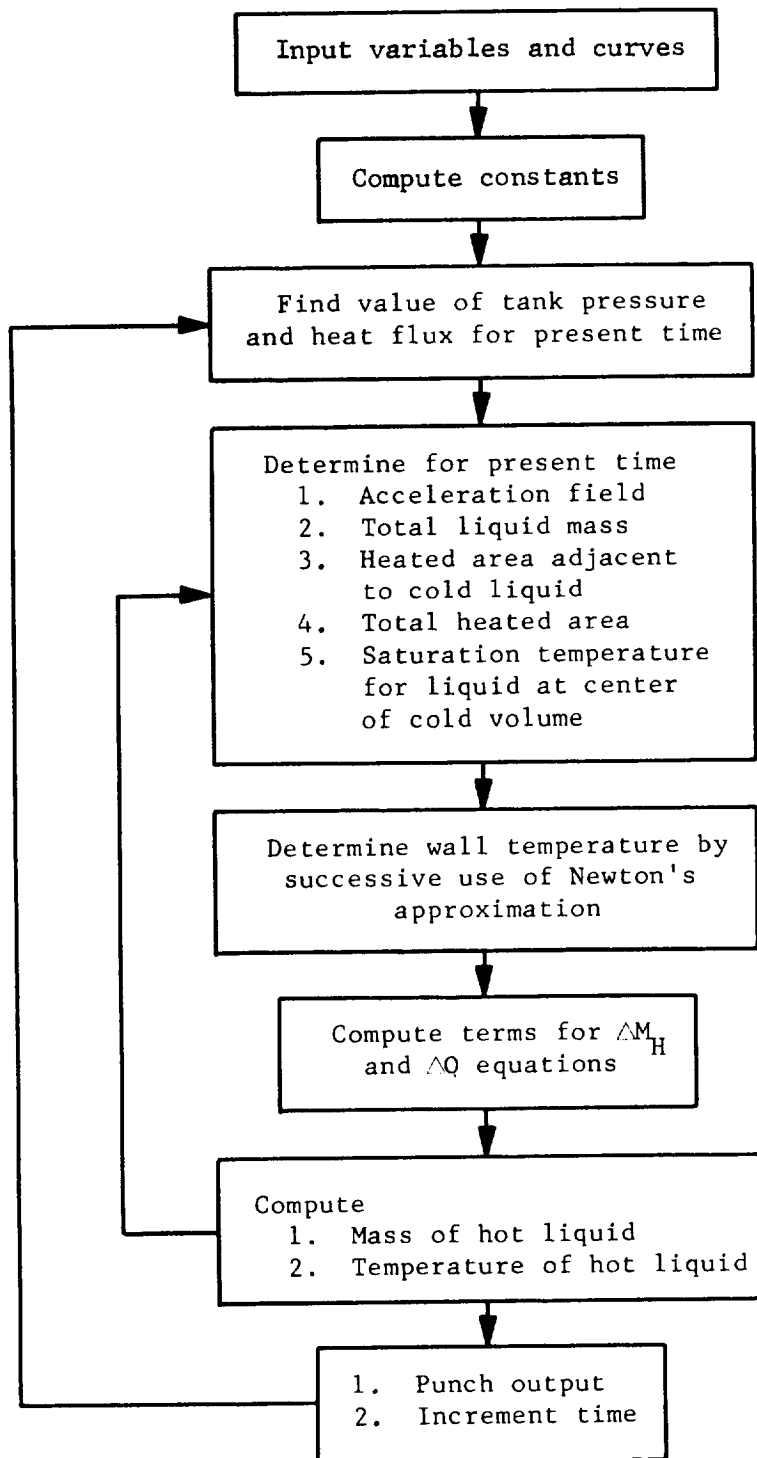
DEFINITION OF FORTRAN SYMBOLS

<u>Symbol</u>	<u>Definition</u>	<u>Units</u>
AC	$A_{HC}(D/2)$	cu ft
AH	$A_{HT}(D/2)$	cu ft
A1, A2, A3	a_1, a_2, a_3	lb _m
B	$(q/A)A_{HT}(D/2)$	Btu-ft/sec
B1, B2, B3	$b_1(D/2), b_2(D/2), b_3(D/2)$	Btu-ft/sec
CPZ	C_{p_o}	B/lb _m -R
C1	$2\xi/D$	1/ft
C2	C_2	°R
C3	C_3	--
C4	C_4	Btu/sq ft-sec-R ^{C5}
C5	C_5	--
C6	C_6	Btu/sq ft-sec-R ^{C7}
C7	C_7	--
C8	$\Delta t/3D$	sec/ft
D	D	ft
DCP	D_{cp}	B/lb _m -R ²
DQ	ΔQ	B
DRHO	D	lb _m /cu ft-R
DT	Δt	sec
DT2	$\Delta t/2$	sec
F1	$(dM_H/dt)\Delta t$	lb _m /sec

<u>Symbol</u>	<u>Definition</u>	<u>Units</u>
G	g	lb _f /lb _m
HC	h _c	Btu/lb _m
HH	h _H	Btu/lb _m
HW	h _w	Btu/lb _m
PA	Initial pressure at which all the liquid is saturated	lb _f /sq in. (abs)
P(I)	P _T at time TP(I)	lb _f /sq in. (abs)
PS	P _S	lb _f /sq in. (abs)
PT	P _T	lb _f /sq in. (abs)
Q(J)	(q/A) at time TQ(J)	Btu/sq ft-sec
QB	(q/A) resulting from boiling	Btu/sq ft-sec
QC	(q/A) resulting from free convection	Btu/sq ft-sec
QT	Total (q/A)	Btu/sq ft-sec
RHOC	ρ _c	lb _m /cu ft
RHOH	ρ _H	lb _m /cu ft
RHOZ	ρ _o	lb _m /cu ft
T	t	sec
TC	T _c	°R
TF	Time at which run is terminated	sec
TH	T _H	°R
TS	T _S	°R
TW	T _w	°R

<u>Symbol</u>	<u>Definition</u>	<u>Units</u>
TZ	Time at which run is started	sec
VC	V_c	cu ft
VH	V_H	cu ft
VT	V_T	cu ft
V1	V_1 (see Fig. 74)	cu ft
V2	V_2 (see Fig. 74)	cu ft
WDOF	\dot{W}/F	$lb_m/lb_f\text{-sec}$
WDOT	\dot{M}	lb_m/sec
WH	M_H	lb_m
WHT	Temporary value of M_H used in Runge Kutta method	lb_m
WOF	W/F	lb_m/lb_f
WT	W_T	lb_m
WZ	W_o	lb_m
XI	ξ	--

Simplified Flow Diagram for
IBM 1620 Stratification Program



FORMAT FORTRAN STATEMENTS FOR IBM 1620 COMPUTER PROGRAM

```

C      STRATIFICATION PROGRAM, VAR. RHO + CP, INPUT Q/A
2  FORMAT(7E10.4)
3  FORMAT(8F10.4)
4  FORMAT(I4)
5  FORMAT(40X39X1H+)
6  FORMAT(7F10.2)
7  FORMAT(/ / 3X4HTIME8X2HVT8X2HVVH8X2HVC8X2HTH7X3HQ/A9X1HP/)
   DIMENSION TP(20),P(20),TQ(20),Q(20)
8  PUNCH 5
   READ 3,VZ,V1,V2,WDOT,RHOZ,DRHO,CPZ,DCP
   READ 3,DT,TF,TZ,WOF,WDOF,PA,XI,D
   READ 2,C2,C3,C4,C5,C6,C7
   PUNCH 3,VZ,V1,V2,WDOT,RHOZ,DRHO,CPZ,DCP
   PUNCH 3,DT,TF,TZ,WOF,WDOF,PA,XI,D
   PUNCH 2,C2,C3,C4,C5,C6,C7
   PUNCH 7
   READ 4,IMAX
   DO22I=1,IMAX,4
22  READ 3,TP(I),P(I),TP(I+1),P(I+1),TP(I+2),P(I+2),TP(I+3),P(I+3)
   READ 4,JMAX
   DO23J=1,JMAX,4
23  READ 3,TQ(J),Q(J),TQ(J+1),Q(J+1),TQ(J+2),Q(J+2),TQ(J+3),Q(J+3)
   TC=C2/(C3-LOG(PA))
   RHOC=RHOZ+TC*DRHO
   WZ=RHOC*VZ
   WT=WZ
   C10=RHOC/(226.*D**2)
   T=TZ
   DT2=DT*.5
   HC=CPZ*TC+.5*DCP*TC**2
   HH=HC
   C1=2.*XI/D
   I=1
   J=1
   G=1.
   C8=DT/(3.*D)
   TH=TC
   TW=TC+10.
   WH=0
24  WHT=WH
   K=0
   GO TO 50
25  A1=DT*F1
26  B1=B
   PUNCH 6,T,VT,VH,VC,TH,QT,PT
   T=T+DT2
   WHT=WHT+.5*A1
   GO TO 50
27  A2=DT*F1
28  B2=B
   WHT=WHT+.5*A2
   GO TO 50
29  A3=DT*F1
   WHT=WHT+A3
   T=T+DT2
   GO TO 50
30  A4=DT*F1
   B3=B

```

```

DWH=(A1+A2+A2+A3+A3+A4)/6.
DQ=C8*(B1+4.*B2+B3)
WH=WH+DWH
WH=(WT+WH-ABS(WT-WH))*0.5
HH=HH+(DQ-DWH*(HH-HC))/WH
IF(DCP)31,32,31
31 TH=((CPZ**2+2.*HH*DCP)**0.5-CPZ)/DCP
GO TO 33
32 TH=HH/CPZ
33 IF(TH-TS)35,35,34
34 TH=TS
35 IF(T-TF)24,24,8
50 IF(T-TP(I))51,51,52
51 PT=P(I)
GO TO 55
52 IF(T-TP(I+1))54,54,53
53 I=I+1
IF(I-IMAX)52,52,8
54 PT=P(I)+(P(I+1)-P(I))*(T-TP(I))/(TP(I+1)-TP(I))
55 IF(T-TQ(J))56,56,57
56 QT=Q(J)
GO TO 60
57 IF(T-TQ(J+1))59,59,58
58 J=J+1
IF(J-JMAX)57,57,8
59 QT=Q(J)+(Q(J+1)-Q(J))*(T-TQ(J))/(TQ(J+1)-TQ(J))
60 IF(T)62,61,61
61 G=1./(WOF-WDOF*T)
WT=WZ-WDOT*T
62 RHOH=RHOZ+DRHO*TH
VH=(WT+WHT-ABS(WT-WHT))/(2.*RHOH)
VC=(WT-WHT+ABS(WT-WHT))/(2.*RHOC)
VT=VC+VH
AC=V2-V1+ABS(VC-V1)-ABS(VC-V2)
AH=V2-V1+ABS(VT-V1)-ABS(VT-V2)
PS=PT+C10*G*(VT+VH)
TS=C2/(C3-LOG(PS))
63 QC=C4*(TW-TC)**C5*G**(C5-1.)
IF(TW-TS)71,71,72
71 DTP=-(QC-QT)/(C5*QC/(TW-TC))
GO TO 73
72 QB=C6*((TW-TS+ABS(TW-TS))/2.)*C7
DTP=-(QC+QB-QT)/(C5*QC/(TW-TC)+C7*QB/(TW-TS))
73 IF(ABS(DTP)-0.01)65,65,64
64 TW=TW+DTP
GO TO 63
65 HW=CPZ*TW+0.5*DCP*TW**2
F1=C1*AC*QT/(HW-HC)
80 B=QT*AH
K=K+1
GO TO(25,27,29,30),K
END

```

SAMPLE INPUT DATA (RUN NO. 1)

63.3	6.6	62.	0.	6.079	-0.045	-0.28	0.0712
10.	180.	0.	1.	0.	12.6	4.	3.96
223.26E00	8.8046E00	.0116	E0013333333-02.738	E00	2.5E00		
4							
.	52.9	60.	55.6	120.	68.1	180.	94.2
4							
.	.25	60.	.72	80.	.72	200.	.55

SAMPLE OUTPUT DATA (RUN NO. 1)

63.3000	6.6000	62.0000	.0000	6.0790	-0.0450	-0.2800	0.071
10.0000	180.0000	.0000	1.0000	.0000	12.6000	4.0000	3.960
.2232E+03	.8804E+01	.1160E-01	.1333E+01	.7380E-00	.2500E+01		

TIME	VT	VH	VC	TH	Q/A	P
.00	63.29	-0.00	63.29	35.60	.25	52.90
10.00	63.45	5.14	58.31	38.67	.32	53.35
20.00	63.65	10.85	52.80	38.90	.40	53.80
30.00	63.90	16.88	47.02	39.15	.48	54.25
40.00	64.18	22.95	41.23	39.45	.56	54.70
50.00	64.51	28.84	35.67	39.79	.64	55.15
60.00	64.88	34.35	30.52	40.19	.72	55.60
70.00	65.27	39.11	26.16	40.62	.72	57.68
80.00	65.66	42.95	22.70	41.07	.72	59.76
90.00	66.04	46.08	19.95	41.52	.70	61.85
100.00	66.41	48.63	17.77	41.97	.69	63.93
110.00	66.78	50.74	16.03	42.42	.67	66.01
120.00	67.13	52.51	14.62	42.87	.66	68.10
130.00	67.48	53.99	13.49	43.31	.64	72.45
140.00	67.82	55.24	12.58	43.75	.63	76.80
150.00	68.15	56.31	11.84	44.18	.62	81.15
160.00	68.47	57.24	11.23	44.60	.60	85.50
170.00	68.79	58.06	10.72	45.01	.59	89.85
180.00	69.10	58.80	10.30	45.42	.57	94.20

DISTRIBUTION

Copies

To

1 thru 12

Director
George C. Marshall Space Flight Center
National Aeronautics and Space Administration
Huntsville, Alabama
Attn: M-P&C-CA
Contract: NAS8-5046
Control No.: TP2-85304

Remaining
Copies

Martin Company
Denver Division
Denver 1, Colorado
Attn: Libraries Section

